WRDC-TR-89-2125   **AD-A223 487**

EVALUATION OF PLANE-OF-LIGHT NONINTERFERENCE STRESS
MEASUREMENT SYSTEMS FOR MEASURING BLADED DISK VIBRATIONS

Swaminadham Midturi and Robert J. Dominic
Aerospace Mechanics Division
University of Dayton Research Institute
Dayton, Ohio 45469

December 1989

Interim Report for Period September 1987 - August 1988

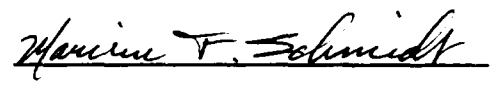Approved for public release; distribution is unlimited

NOTICE

When Government drawings, specifications, or other data are used for any purpose other than in connection with a definitely Government-related procurement, the United States Government incurs no responsibility or any obligation whatsoever. The fact that the government may have formulated or in any way supplied the said drawings, specifications, or other data, is not to be regarded by implication, or otherwise in any manner construed, as licensing the holder, or any other person or corporation; or as conveying any rights or permission to manufacture, use, or sell any patented invention that may in any way be related thereto.

This report is releasable to the National Technical Information Service (NTIS). At NTIS, it will be available to the general public, including foreign nations.

This technical report has been reviewed and is approved for publication.

JOHN D. REED, Aerospace Engineer
Propulsion Integration
Engine Integration & Assessment Branch

MARVIN F. SCHMIDT, Chief
Engine Integration & Assessment Branch

FOR THE COMMANDER

JAMES S. PETTY, PhD
Acting Deputy for Technology
Turbine Engine Division
Aero Propulsion & Power Laboratory

If your address has changed, if you wish to be removed from our mailing list, or if the addressee is no longer employed by your organization please notify WRDC/ POTC, WPAFB, OH 45433- 6563 to help us maintain a current mailing list.

Copies of this report should not be returned unless return is required by security considerations, contractual obligations, or notice on a specific document.

REPORT DOCUMENTATION PAGE

Form Approved
OMB No. 0704-0188

1a. REPORT SECURITY CLASSIFICATION Unclassified	1b. RESTRICTIVE MARKINGS

2a. SECURITY CLASSIFICATION AUTHORITY	3. DISTRIBUTION/AVAILABILITY OF REPORT Approved for public release. Distribution is limited.
2b. DECLASSIFICATION/DOWNGRADING SCHEDULE	

4. PERFORMING ORGANIZATION REPORT NUMBER(S) UDR-TR-89-18	5. MONITORING ORGANIZATION REPORT NUMBER(S) WRDC-TR-89-2125

6a. NAME OF PERFORMING ORGANIZATION University of Dayton Research Institute	6b. OFFICE SYMBOL (If applicable)	7a. NAME OF MONITORING ORGANIZATION Aero Propulsion & Power Lab (WRDC/POTC) Wright Research & Development Center

6c. ADDRESS (City, State, and ZIP Code) 300 College Park Dayton Ohio 45469	7b. ADDRESS (City, State, and ZIP Code) Wright-Patterson Air Force Base Ohio 45433-6563

8a. NAME OF FUNDING/SPONSORING ORGANIZATION WRDC/POTC	8b. OFFICE SYMBOL (If applicable) POTC	9. PROCUREMENT INSTRUMENT IDENTIFICATION NUMBER F33615-85-C-2585

9c. ADDRESS (City, State, and ZIP Code) WPAFB OH 45433-6563	10. SOURCE OF FUNDING NUMBERS

PROGRAM ELEMENT NO.	PROJECT NO.	TASK NO	WORK UNIT ACCESSION NO.
62203F	3066	12	21

11. TITLE (Include Security Classification)
Evaluation of Plane-of-Light Noninterference Stress Measurement Systems for Measuring Bladed Disk Vibrations

12. PERSONAL AUTHOR(S)
Swaminadham, M.   Dominic, R. J.

13a. TYPE OF REPORT Interim	13b. TIME COVERED FROM Sept 87 TO Aug 88	14. DATE OF REPORT (Year, Month, Day) 1989 December 24	15. PAGE COUNT 121

16. SUPPLEMENTARY NOTATION

17. COSATI CODES

FIELD	GROUP	SUB-GROUP
20	11	
21	05	

18. SUBJECT TERMS (Continue on reverse if necessary and identify by block number)
Structural Dynamics   Optical Sensors,
Noncontacting Stress Measurement System   Vibration
Plane-of-Light

19. ABSTRACT (Continue on reverse if necessary and identify by block number)
This report describes techniques for the measurement of traveling-mode vibrations of rotating bladed disks using a nonintrusive optical instrumentation system. This system incorporates a circumferentially-mounted plane-of-light sensor to detect time of arrival of blades on a rotating disk. These time of arrivals are compared to a 1-per-rev signal to determine the amount of relative displacement. This displacement is fed into a model-generating algorithm to determine frequencies of vibration; and mode shape. This system was compared to a separate noncontacting system to compare their measuring capability and accuracy.

20. DISTRIBUTION/AVAILABILITY OF ABSTRACT ☒ UNCLASSIFIED/UNLIMITED ☐ SAME AS RPT. ☐ DTIC USERS	21. ABSTRACT SECURITY CLASSIFICATION Unclassified
22a. NAME OF RESPONSIBLE INDIVIDUAL JOHN D. REED	22b. TELEPHONE (Include Area Code) 513-255-5308	22c. OFFICE SYMBOL WRDC/POTC

DD Form 1473, JUN 86   Previous editions are obsolete.

SECURITY CLASSIFICATION OF THIS PAGE
UNCLASSIFIED

TABLE OF CONTENTS

TABLE OF CONTENTS (cont.)

TABLE OF CONTENTS (cont.)

v

LIST OF ILLUSTRATIONS

LIST OF ILLUSTRATIONS (cont.)

LIST OF ILLUSTRATIONS (cont.)

LIST OF TABLES

ACKNOWLEDGEMENTS

SUMMARY

This research task has been performed as an extension to the present contract the University of Dayton Research Institute (UDRI) has with the Aero Propulsion Laboratory for bladed disk dynamics research. This contract extension applied noncontact optical instrumentation systems to measure traveling wave vibrations of rotating bladed disks. Two noninterference Stress Measurement Systems (NSMS) - one developed by the United Technologies Research Center (UTRC) for Arnold Engineering Development Center (AEDC) and the other developed by the University of Dayton for Innovative Structures Research laboratory (ISRL) of the Aero Propulsion Laboratory were evaluated concurrently to compare their vibration measuring capability and accuracy. The two systems were compared against each other and against deflection measurements obtained by multipulse interferometric holography.

This combined research and test effort had four-fold objectives: first, the development of an excitation system that would cause a simple bladed disk to vibrate in a traveling wave mode; second, the comparison of UTRC and UD NSMS systems for blade tip vibration measurement; third, recording of the double and triple pulse interferograms for the diametral modes of a test disk; and fourth, comparison of the disk modal parameters obtained from plane-of-light sensor systems and interferometric methods.

SECTION 1
INTRODUCTION

1.1 IMPORTANCE OF TURBINE DISK VIBRATIONS

Modern aircraft engines have several hundred rotating blades in their compressor and turbine sections. These components are designed to withstand high temperatures in a vibration environment because a single blade failure due to vibration induced fatigue could threaten the safety of the entire aircraft. To ensure the safe operation of aeroengines, we recommend continuous monitoring of vibration amplitudes by techniques like those described in this report.

Many flow related phenomena - self-excited oscillations due to flutter, rotating stall, and distorted-flow-induced standing waves - are often the major sources of vibration in aero engine blades. In addition, recent advances in materials and structures technology have increased the prospect of using lightweight, high performance airfoils. These design approaches have increased component susceptibility to vibrations. These vibrations, if continued for long operating periods of the machine, would reduce the safe operational life of blades. Consequently, we must use real-time monitoring devices to ensure the safe operation of turbines and compressors.

1.2 NONINTERFERENCE MEASUREMENT METHODS AND THEIR RELEVANCE

Measurement methods involving strain gage-slip ring, strain gage-telemetry, and laser interferometry systems have been used to monitor blade vibrations. These methods have disadvantages like (a) limited survivability in high temperature and high speed environments (b) required disassembly of parts for sensor installation and repair (c) location of sensors and transmitting elements on the rotor and (d) nonaccessibility to viewing optics except for the front stage of the compressor. The drawbacks associated with the strain gage and interferometry methods have

1

led to the development of noncontacting deflection measurement systems for rotating turbine/compressor blades.

1.3 PAST WORK ON THE DISK DYNAMICS AND NONINTERFERENCE METHODS

Tobias and Arnold (1) conducted the first comprehensive study of the vibratory response of imperfect disks. Extending the work of Tobias and Arnold, Ewins (2) developed a generalized force model for coupled bladed disk response and used it to perform a numerical study on a simple mistuned bladed disk. Stetson (3) and MacBain, et al., (4) used double and triple pulse laser interferometric experiments to record mode shapes of rotating turbofan bladed disks. Stange and MacBain (5) studied dual modes and their dependence on mistuning masses and recorded resonant disk modes.

The idea of measuring compressor blade vibrations by a remote optical sensor was proposed and implemented by Hohenberg (6) and Zablofskiy, et al. (7). Nieberding and Pollack (8) of NASA Lewis and McCarty and Thompson of AEDC (9) measured compressor blade tip vibrations by a single spot sensor. Roth (10) and Endoh (11) developed multiprobe spot sensor methods to measure rotating blade vibrations. Spot sensors cannot always measure the same location on the blade tip cross section. This leads to gross measurement errors. The use of multiple plane-of-light sensors to look at blade tip corners was proposed by Chi and Jones (12, 13, 14). These researchers, besides implementing the plane-of-light sensor concept, also developed hardware and software specifications for a real-time Noninterference Stress Measurement System (NSMS). United Technologies Research Center (UTRC) assembled a test model of this system for AEDC. Concurrently, UDRI designed and assembled, for ISRL, a NSMS using the same technological basis, but implemented in different hardware and software systems.

1.4 SCOPE OF THE PRESENT WORK

Although the existence of standing wave vibrations in the turbine engine environment has been recognized by engine disk designers, the quantitative effects of such are seldom completely measured and interpreted. In the present task, plane-of-light optical sensors were used to measure the standing wave (traveling wave on the disk) vibrations of a disk due to a stationary static force field. The test object was a simple version of a turbine disk which had coupled disk and blade motions. Blade tip deflections were measured by the AEDC and ISRL plane-of-light sensors, and wholefield disk deflection patterns were measured by laser interferometry. The rotating bladed disk 2, 3, and 4 diametral modes were measured by each system and compared.

UDRI performed (a) design and fabrication of a test disk, according to the specifications set forth by UTRC; (b) design and assembly of excitation magnets, optical probe-magnet-mounting ring and the instrumentation of the bladed disk; (c) setup, recording and processing of the ISRL NSMS data; (d) recording and interpreting laser interferograms; and (e) coordination of AEDC equipment shipments, setup requirements, and everyday test activity.

The program started in September 1987 and was completed in August 1988. Technical developments related to the task during this period were documented in contractual bimonthly reports to the Air Force.

SECTION 2
TEST DISK CRITICAL SPEED ANALYSIS

Discussions with the Arnold Engineering Development Center (AEDC) and the United Technology Research Center (UTRC) on the evaluation of their NSMS led to the design of a suitable test specimen and test setup.

The test specimen had to meet three requirements: first, UTRC preferred a 38-bladed disk with modal frequencies in the frequency range of 100-250 Hz for the lower order modes; second, the disk should show large deflection at blade tips so that UTRC optical probes could capture these deflections with ease; third, the size of the test specimen was not to exceed 12-inch diameter, a size that was acceptable for optical holography.

2.1 FINITE ELEMENT FREQUENCY ANALYSIS OF STATIC BLADED DISKS

Prior experience with disk dynamics guided us to select the approximate diameter and thickness for the proposed test disk. NASTRAN based finite element methods were used to design the test disk to satisfy frequency-amplitude-size requirements. Four possible test disk configurations were analyzed. Their natural frequencies are summarized in Table 1. The two 12-inch-diameter

TABLE 1

NATURAL FREQUENCIES OF FOUR 62.5-MIL-THICK TEST DISKS (HZ)

Disk Dia(in)	12.0	12.0	10.0	11.0
Blade Length (in)	1.5	3.0	1.0	2.0
Mode				
1D	59.29	57.04	90.82	72.56
0C	71.45	63.83	107.89	83.99
2D	87.16	68.92	133.98	96.34
3D	168.98	101.86	269.17	166.16
4D	--	125.59	434.17	231.26

disks produced low frequencies, whereas a 10-inch disk yielded higher frequencies. The 11-inch-diameter disk with 2-inch blades was selected because it yielded frequencies close to UTRC specifications. Considering the size of excitation magnets, blade length was later changed to 1 1/2 inch. Disks of 62.5- and 50-mil thickness were analyzed, and their natural frequencies are presented in Table 2. The 62.5-mil-thick disk had a 4D frequency of 294 Hz at zero speed and would have required much larger excitation force to produce acceptable blade tip deflections. The disk of 50-mil thickness then was selected and was analyzed in greater detail.

TABLE 2

NATURAL FREQUENCIES (HZ) OF 62.5- AND 50-MIL-THICK
DISKS, EACH 11 INCH DIA. WITH 38 BLADES OF
1.5-INCH LENGTH

Mode	62.5-Mil Thickness	50-Mil Thickness
1D	72.5	58.2
0C	85.8	69.6
2D	103.3	84.4
3D	195.0	161.8
4D	294.1	244.0

A reasonable number (38x8) membrane and bending, constant thickness plate elements were used to model a 38-bladed, 11-inch diameter, 50-mil-thick disk. The finite-element geometric model of the disk is shown in Figure 1. The normal mode method (Rigid Format 3) of analysis was used to determine the natural frequencies and modes of the centrally clamped, nonrotating bladed disk. The centrally clamped model was used because a 2-
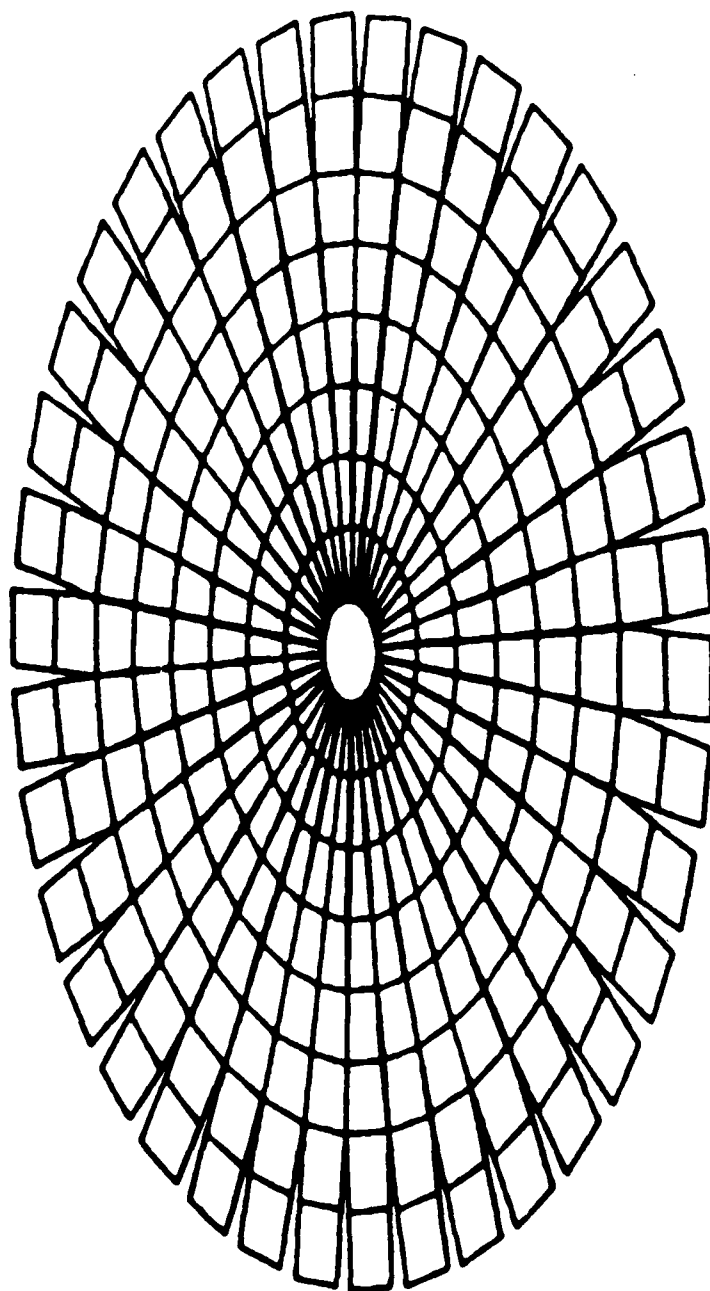
Figure 1. Finite Element Model of the Bladed Disk.

inch-diameter, ten-channel slip ring assembly was directly mounted to the disk center to connect disk response monitoring accelerometers and piezocrystals to a frequency analyzer. Two cases of hub-clamping, one without a slip ring but centrally clamped over a 1-inch diameter and the other with a slip ring assembly rigidly fixed at the 2-inch diameter, were analyzed with the results shown in Table 3.

To reduce computational effort, a simple assumption of infinite rigidity was assumed for the 1- or 2-inch diametral surface at the disk hub. Details of the slip ring are shown in Figure 2. Natural frequencies of the 11-inch-diameter,

TABLE 3

HUB-SLIP RING EFFECT ON NATURAL FREQUENCIES
AT ZERO RPM OF 50-MIL-THICK DISK OF 11-INCH DIAMETER
WITH 1.5-INCH-LONG BLADES

Mode	Without Slip Ring	With Slip Ring
1D	58.2	80.5
0C	69.6	83.9
2D	84.4	100.4
3D	161.8	165.1
4D	244.0	244.6

50-mil-thick surface at the disk hub. Details of the slip ring are shown in Figure 2. Natural frequencies of the 11-inch-diameter, 50-mil-thick disk with the slip ring were within acceptable limits. Out of plane normalized vibration contours of the disk diametral modes were determined analytically.

Static bench tests to establish modal characteristics were performed for fabricated 50-mil and 62.5-mil-thick steel disks. Time-average holography was used to record mode shapes of these disks. Verification of analytical frequencies and modes helped us to continue the disk analysis for the rotational effects.
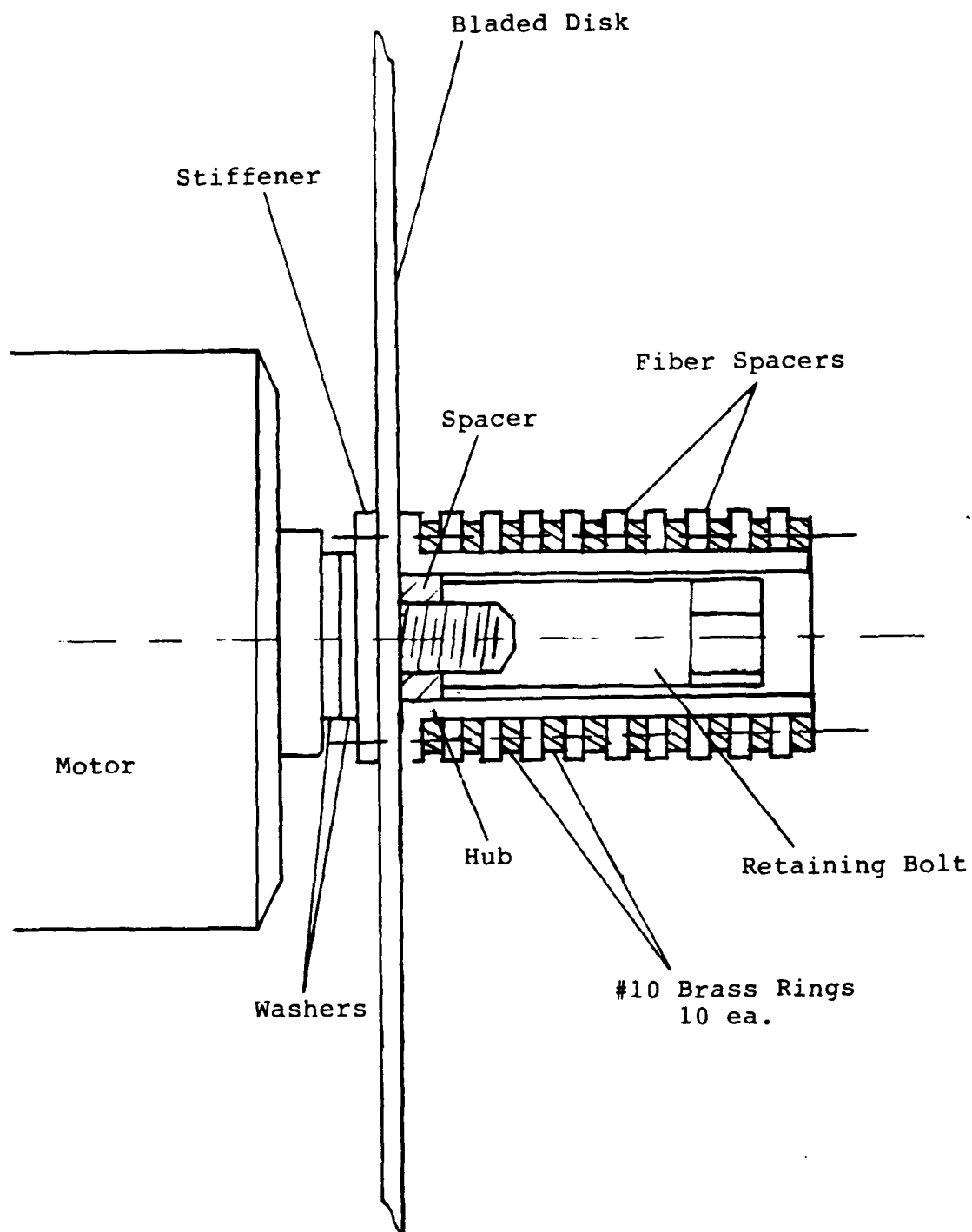
Figure 2. Slip Ring Mounting to the Disk.

2.2 ROTATIONAL EFFECTS ON THE TEST DISK FREQUENCIES

NASTRAN's differential stiffness feature, Rigid Format 13, was used to analyze the disk rotational effects. Modal frequency increases due to centrifugal stiffening during rotation were determined, and the resulting frequencies are shown in Table 4. Information from this table was used to construct the frequency-speed diagram to determine the critical speeds of the test disk.

TABLE 4

ROTATIONAL EFFECT ON DISK NATURAL FREQUENCIES (HZ)
DISK GEOMETRY: 11-INCH-DIA., 50-MIL-THICK 38 EACH OF 1.5-INCH-LONG BLADES
2-INCH-DIA. HUB SLIP RING UNIT

	SPEED IN RPM					
Mode	0	1000	2000	3000	4000	5000
2D	100	103	109	115	130	148
3D	155	158	163	170	185	201
4D	225	227	234	241	250	264

2.3 EXCITATION OF A ROTATING DISK DUE TO A STATIC FORCE FIELD

To explain the disk vibrations due to a static force, consider a point force F_o acting on the disk at $\theta = \theta_r$. This point force can be represented by the Fourier series as

$$F(\theta) = \frac{F_o}{2\pi} + \frac{F_o}{\pi} \sum_{m=1}^{\infty} \cos\, m(\theta - \theta_r) \qquad (1)$$

The generalized force in each mode can be determined from the relation

$$Q_i = \int F(\theta)\ \phi_i(\theta)d\theta, \quad i = 1,\, 2 \qquad (2)$$

9

and
$$Q_i = \frac{F_o}{2\pi} \int_0^{2\pi} \left|\begin{matrix} \cos \\ \sin \end{matrix}\right| n\theta d\theta + \frac{F_o}{\pi} \int_0^{2\pi} \sum_{m=1}^{\infty} \cos m(\theta - \theta_r) \qquad (3)$$

$$\left|\begin{matrix} \cos \\ \sin \end{matrix}\right| n\theta d\theta, \quad i = 1,2$$

Resonance condition occurs when $Q_i \neq 0$ and $m = n$ and

$$Q_i = F_o \left|\begin{matrix} \cos \\ \sin \end{matrix}\right| n\theta_r \qquad (4)$$

θ_r, the position of static force is time variant due to the disk rotation at speed Ω. Therefore,

$$\theta_r = \theta + \Omega t \qquad (5)$$

and letting $\theta = 0$ and for any time, t, eq. (5) becomes

$$Q_i = F_o \left|\begin{matrix} \cos \\ \sin \end{matrix}\right| n\Omega t \qquad (6)$$

From this equation, it is evident that a disk rotating past a static force is stimulated for a specific mode of vibration at speed Ω.

Considering only one mode of vibration, the generalized excitation force is $Q = F_o \cos n\Omega t$.

The vibration of an axisymmetric disk due to a stationary concentrated harmonic force $P \cos \omega t$ can be written as

$$\phi_i = A_i \left|\begin{matrix} \cos \\ \sin \end{matrix}\right| n\theta \cos \omega t \quad , \quad i = 1, 2 \qquad (7)$$

where ϕ_i is the solution of the equation of motion of disk in generalized coordinates; A_i is the amplitude of vibration and a function of radius, excitation force and magnification factor; θ is the angular coordinate of the disk relative to inertial frame; cos $n\theta$ and sin $n\theta$ are the shapes of vibrations of two dual modes; and t is the time.

Letting $\theta_r = 0$ in eq. (5), we get the instantaneous position of excitation force as

$$\theta = \Omega t \tag{8}$$

Substituting eq. (8) into eq. (7) and from the trigonometric identities $\cos \omega t \cos n\Omega t = \frac{1}{2}[\cos(\omega+n\Omega)t + \cos(\omega-n\Omega t)]$

and $\cos \omega t \sin n\Omega t = \frac{1}{2}[\sin(\omega+n\Omega)t - \sin(\omega-n\Omega t)]$

Eq. (7) becomes

$$\phi_i = \frac{A_i}{2} \begin{vmatrix} \cos \\ \sin \end{vmatrix} n\theta \begin{vmatrix} \cos (\omega \pm n\Omega)t \\ \sin (\omega \pm n\Omega)t \end{vmatrix} \tag{9}$$

From Eq. (9), four conditions for resonance are possible for an imperfect disk. These are

$$\cos (\omega+n\Omega)t \text{ and } \sin (\omega+n\Omega)t \tag{10a}$$
$$\text{and} \quad \cos (\omega-n\Omega)t \text{ and } \sin (\omega-n\Omega)t \tag{10b}$$

Eq. (10a) represents two forward traveling waves whereas Eq. (10b) represents two backward traveling waves. These are shown in the frequency-speed diagram (Figure 3a), of the test disk.

But in the present analysis, the disk is treated as perfect and hence, only two resonance conditions are possible.

Also, by extending backward traveling wave branches of Eq. (10b) to intersect the speed (Ω) axis, we obtain critical speeds of the rotating disk.
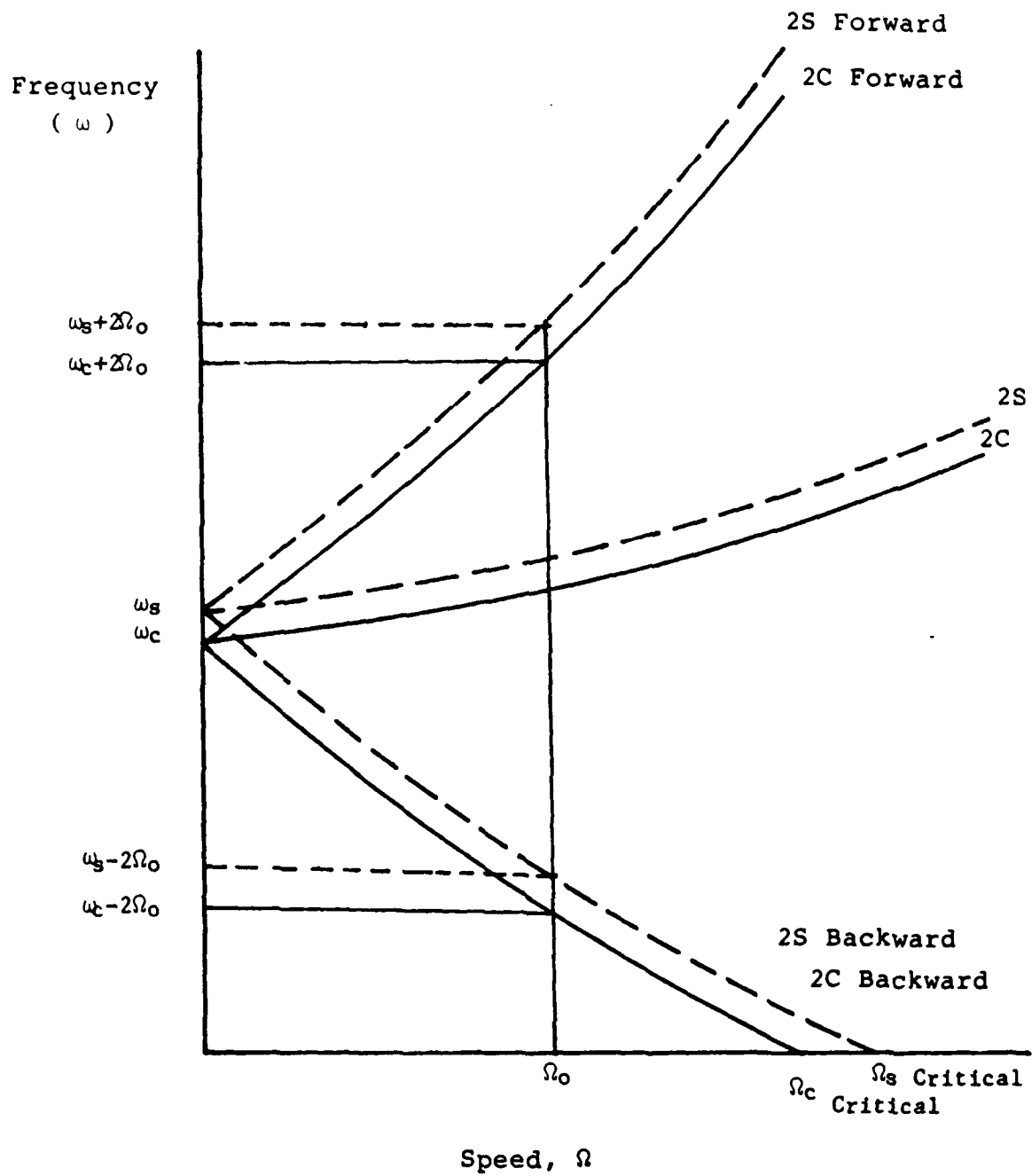
Figure 3a. Frequency - Speed Diagram of an Imperfect Disk.

Using the information in Table 4 and the conditions in Eq. (10b), the critical speeds for our test disk have been determined from Figure 3b. These speeds are 3,950 rpm for 2D, 3,640 rpm for 3D, and 3,700 for 4D. At these speeds, an excitation force with zero excitation frequency would set the disk in resonance.

Assuming nonpreferential modes for the disk, its vibration can be written as

$$\phi = a_1 \cos n\Omega t \sin \omega t + a_2 \sin n\omega t \sin(\omega t + \epsilon) \tag{11}$$

and letting $a_1 = a_2 = a$ and $\epsilon = \frac{\pi}{2}$ by the assumption of one mode being orthogonal to the other, Eq. (11) becomes

$$\phi = a \sin (\omega - n\Omega)t \tag{12}$$

This is a backward traveling wave at speed $n\Omega$. This wave appears stationary to a stationary observer in space.

The experiments were designed to define the backward traveling wave on the disk due to a static force field in space.

11" DIA., 0.05" THICK DISK WITH 38-1.5" LONG
BLADES AND 2" DIA. HUB SLIPRING
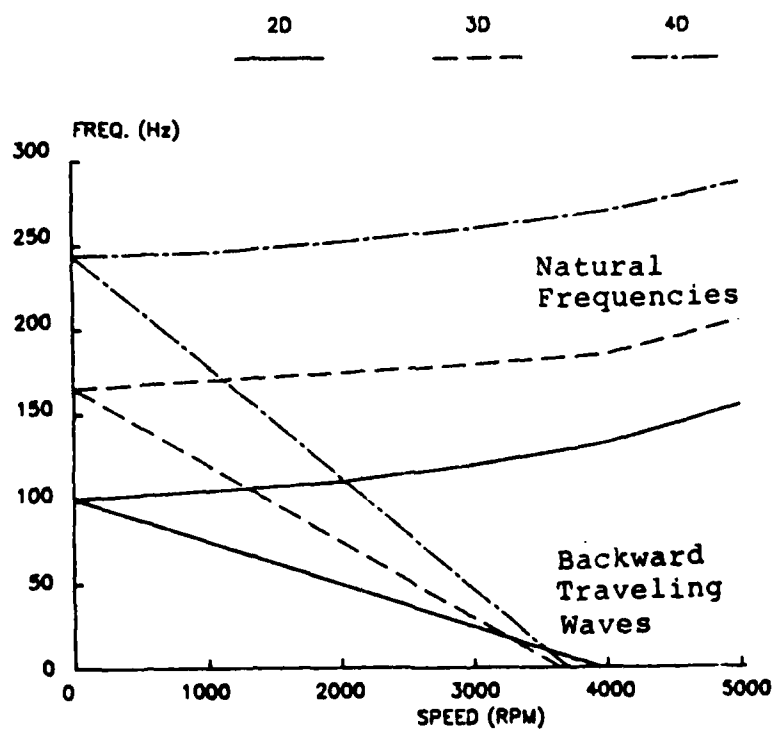
Figure 3b.   Frequency - Speed Diagram of the Test Disk.

14

SECTION 3
TEST SETUP DESIGN, FABRICATION AND PRELIMINARY TESTING

3.1 DEVELOPMENT OF EXCITATION SYSTEM

As agreed by APL-UDRI, AEDC-UTRC, we designed an excitation system to excite the disk in its 2-, 3-, and 4-diametral modes and measure its response.

Stimulus to form a pure mode was provided by placing permanent magnets at desired sine wave response peaks. Magnets (4 for 2D, 6 for 3D, and 8 for 4D) were positioned on both sides of the disk at wavelength intervals of the desired mode-pattern but offset by half a wavelength on the front and back sides. Aluminum bars, shown in Figure 4, were used to support the front magnets from a circular yoke. The back magnets were held by a plate fixed to the test chamber floor and motor support frame behind the disk. The front magnet holder mounting locations are shown in Figure 5 for the three test modes.

3.2 NSMS OPTICAL PROBE POSITIONS

Plane-of-light sensors were used to measure blade tip deflections of the rotating disk. Since the speed of the rotating disk and the speed of the response wave were the same, a stationary probe measured nearly constant amplitude as the disk-blades passed the probe. In effect, one probe provides only a constant amplitude, masking the dynamic response of the disk. Therefore, more than one probe is necessary to define the blade traveling wave vibrations in integral order modes.

In this investigation, four AEDC and three UDRI plane of light sensors were used to define modal deformation of the test disk. The following paragraphs describe some considerations for probe locations to monitor three diametral modes of the disk.

Positioning of three UDRI probes to measure 2D, 3D, and 4D mode shapes is shown in Figure 6. For 2D mode excitation, probes were spaced 60 degrees apart in space around the perimeter of the
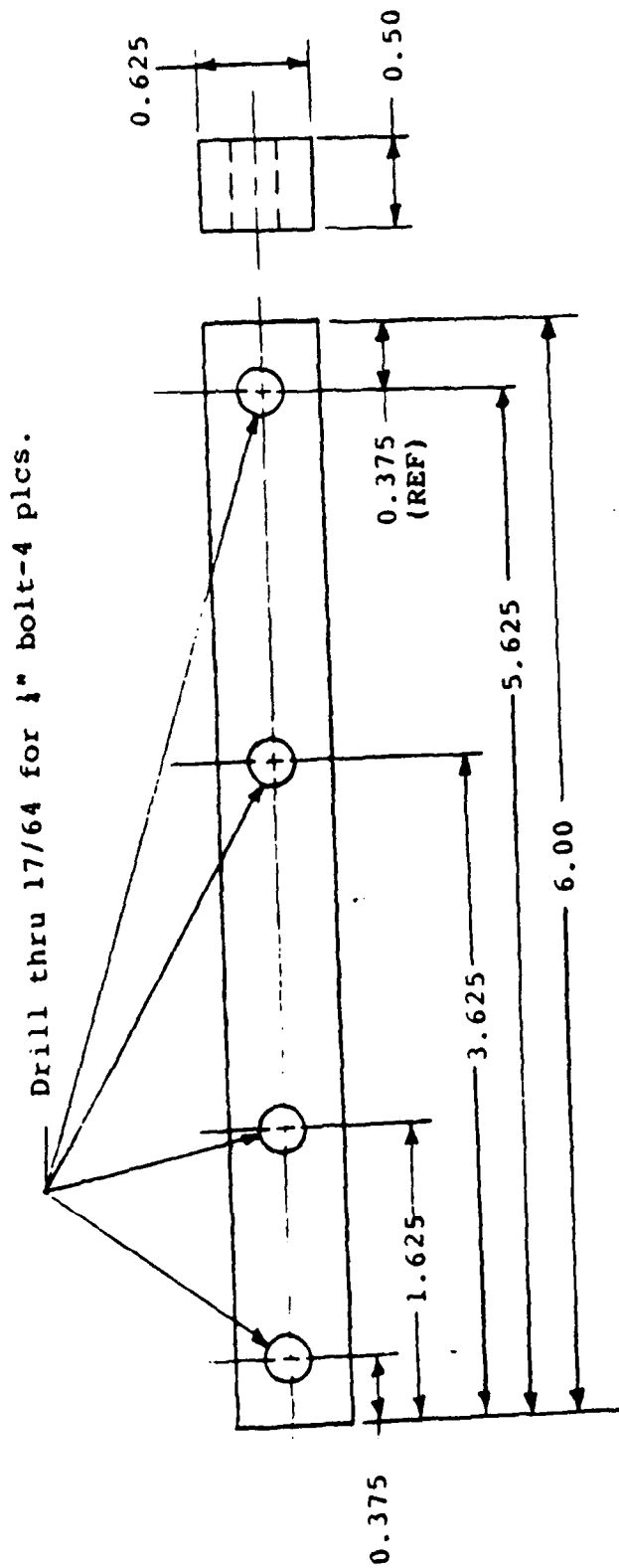
Figure 4. Support Bars for the Excitation Magnets.

16
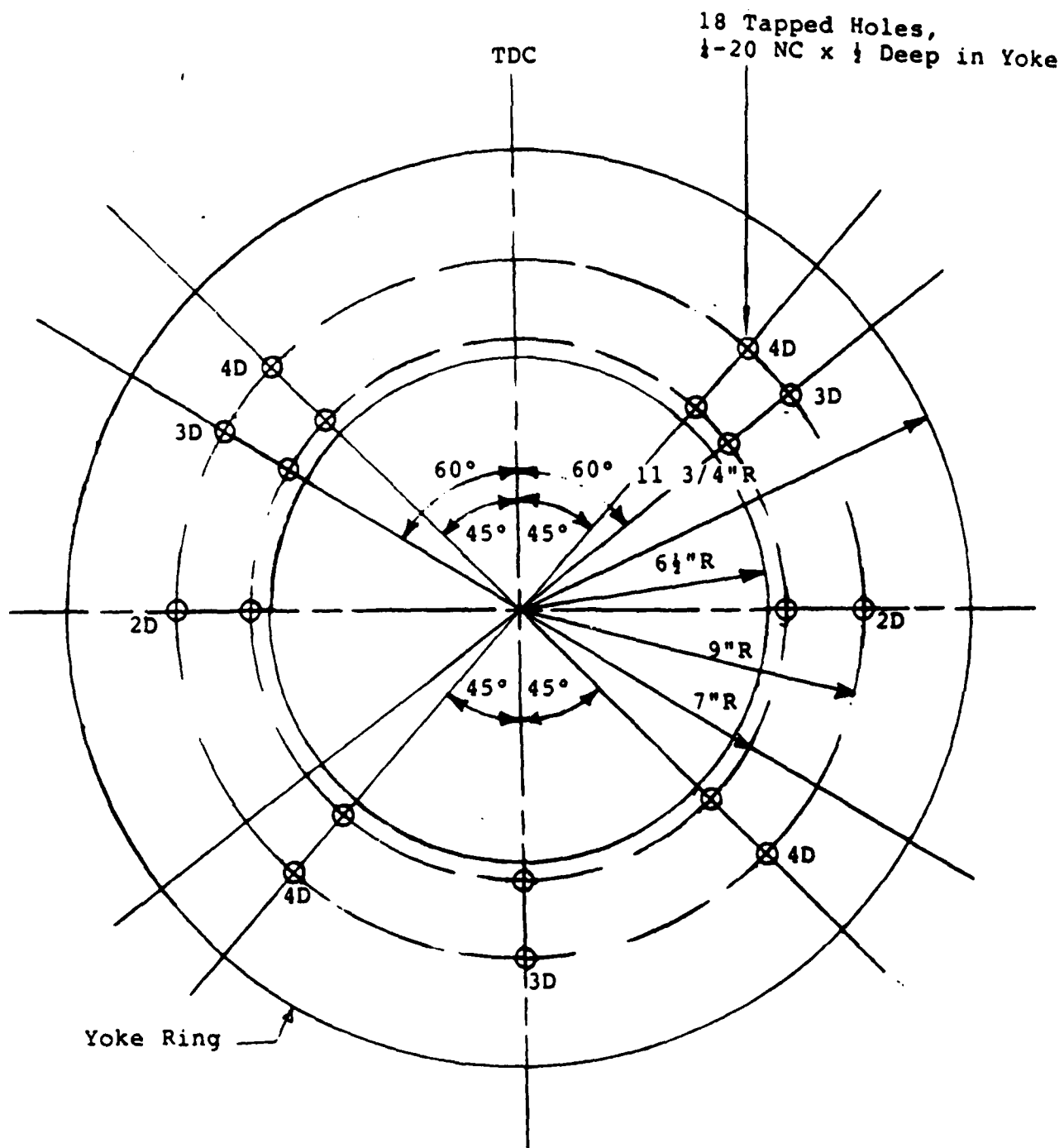
Figure 5. Excitation Magnet Positions.

Probe Locations on Mounting Ring (Looking Aft)
      ◯=2D, x=3D, △=4D Probe Locations
       1/4" Mounting Holes at 7" Rad.
Angular Spacing for 2D Probes, 60°
Angular Spacing for 3D Probes, 40°
Angular Spacing for 4D Probes, 30°
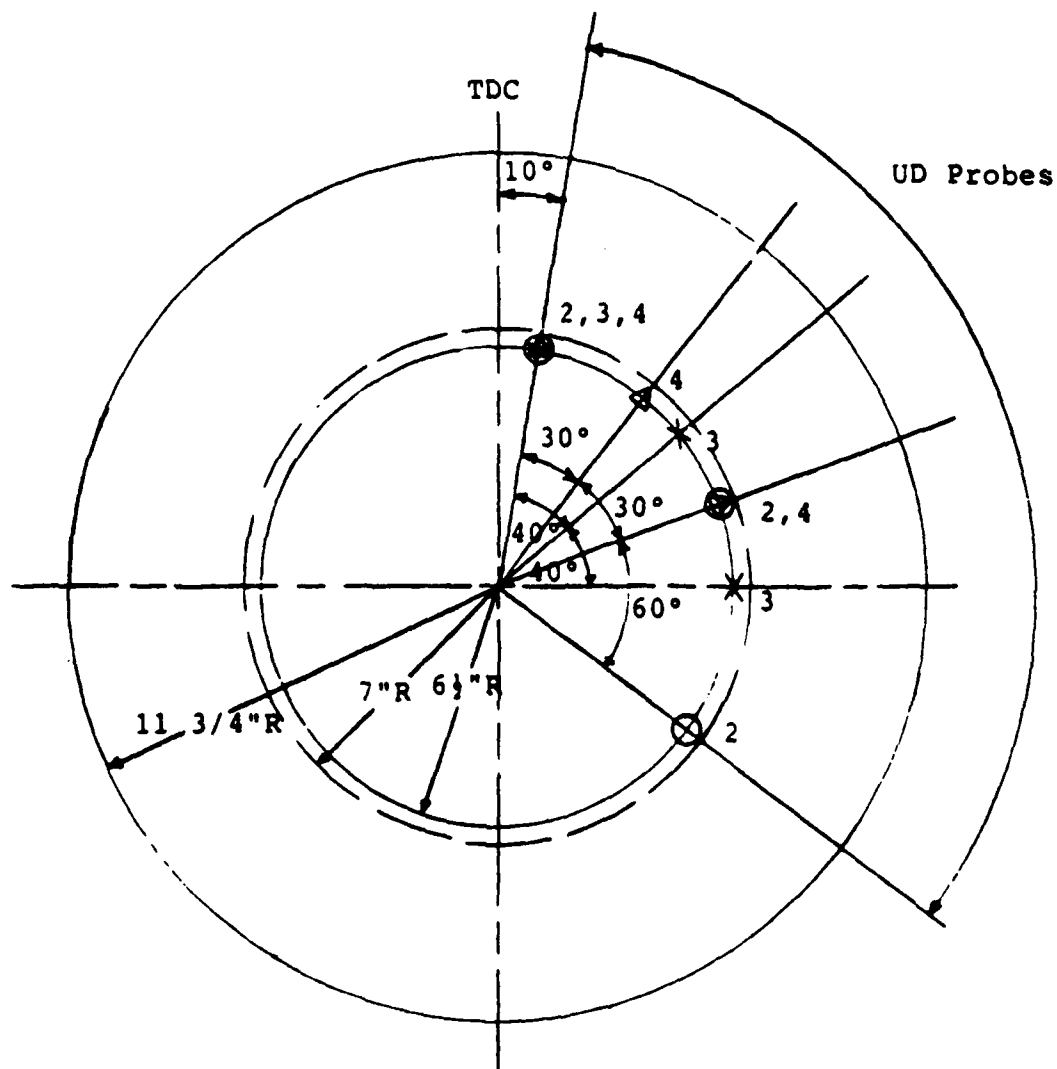
Figure 6.   Plane-of-Light Probe Locations.

18

test disk, while for the 3D and 4D modes the probes were spaced at 40 and 30 degrees, respectively. The probe location requirement was to space the three probes 120 degrees apart within the modal pattern of each response so a standard Fourier transform routine based on uniformly spaced time samples could be used to analyze the optical data.

The AEDC NSMS measuring system requires four blade deflection measurements within a modal wavelength. The transducer locations need not be symmetrically spaced within the wavelength, but the locations must be known relative to each other. The four deflection amplitude readings are used to define the blade response equation of the known mode shape to yield the modal amplitude and frequency.

3.3 INSTRUMENTATION RING (YOKE) DESIGN, FABRICATION AND ASSEMBLY

A yoke was used for mounting the UD and UTRC optical probes and the front excitation magnets. The yoke, shown in Figure 7, was designed by UTRC to mount their sensors and modifications for the other purposes were added by UDRI. After the yoke was fabricated by the Air Force machine shop, it was mounted within the test chamber as shown in Figure 8. Mounting brackets, shown in Figure 9, held the yoke in position. Tolerances provided in the holes of these mounting brackets allowed the yoke to be positioned concentrically with the test disk. Concentricity within three mils was established, using a dial gage mounted directly on the test disk, by slowly rotating the disk and adjusting the position of the yoke with respect to the disk.

3.4 TEST DISK VIBRATION MONITORING INSTRUMENTATION, EXCITATION SYSTEM AND PRELIMINARY TESTS

The test disk was instrumented with three miniature accelerometers and two piezocrystals. The instrumented disk with its sensing elements and their slip-ring connections is shown in Figure 10. The specimen and test monitoring system consisted of
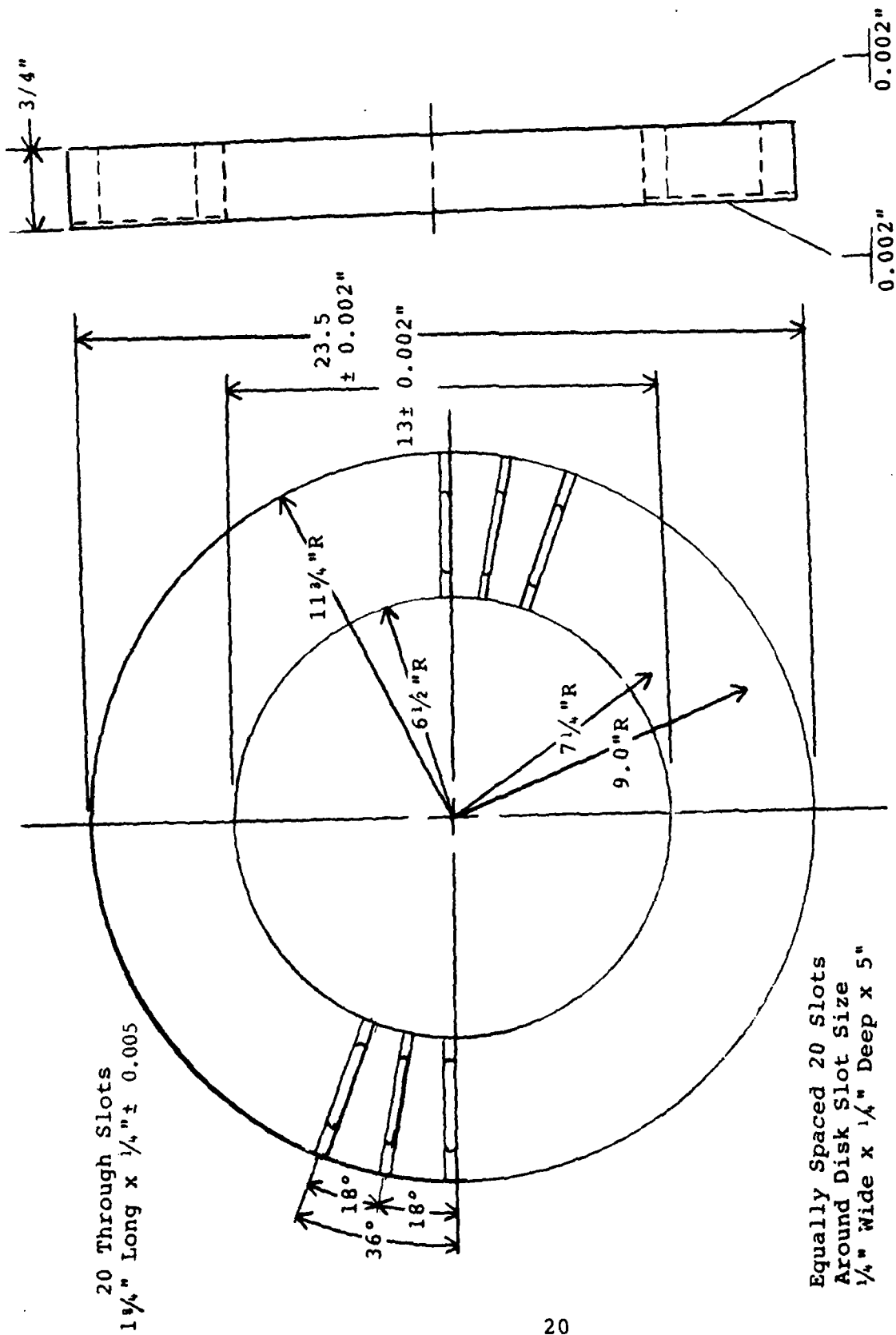
Figure 7. Instrumentation Ring (Yoke).

3/4"

0.002"

0.002"

23.5 ± 0.002"

13± 0.002"

11³/₄"R

6¹/₂"R

7¹/₄"R

9.0"R

20 Through Slots
1³/₄" Long x ¹/₄"± 0.005

18°
18°
36°

Equally Spaced 20 Slots
Around Disk Slot Size
¹/₄" Wide x ¹/₄" Deep x 5"

20
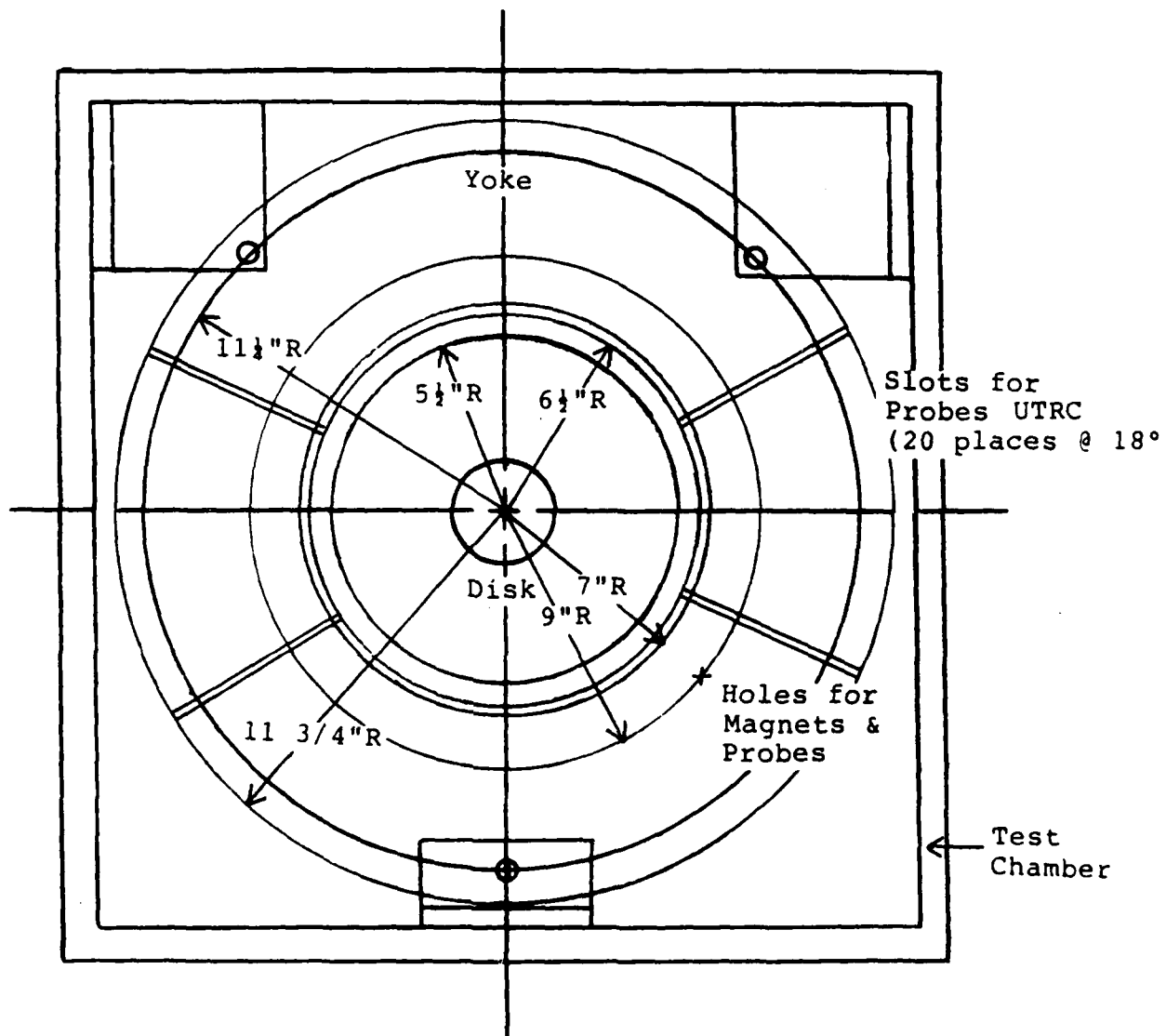
Figure 8.   Assembly of Instrumentation Ring in the Test Chamber.
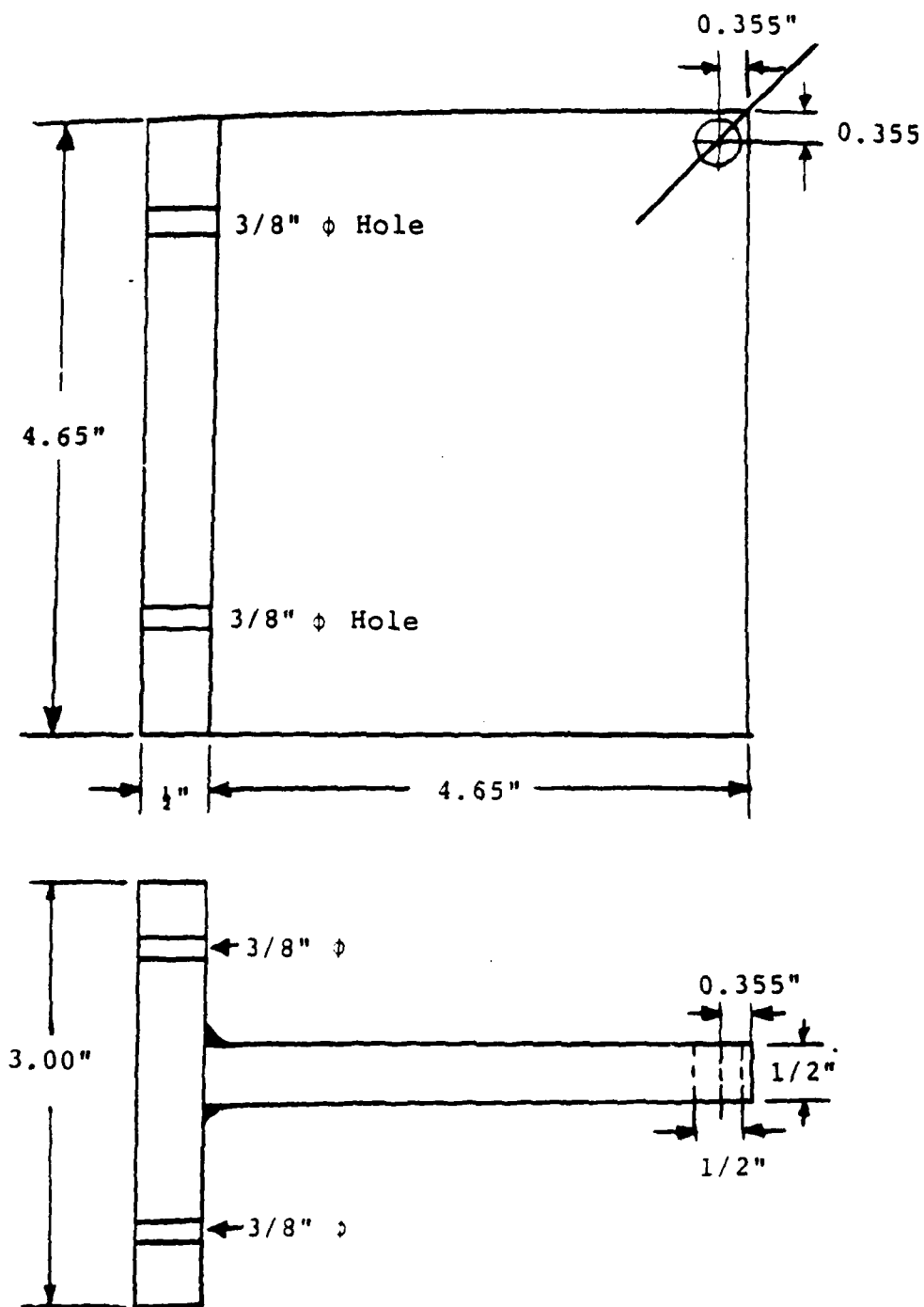
Figure 9.   Mounting Brackets for the Yoke.
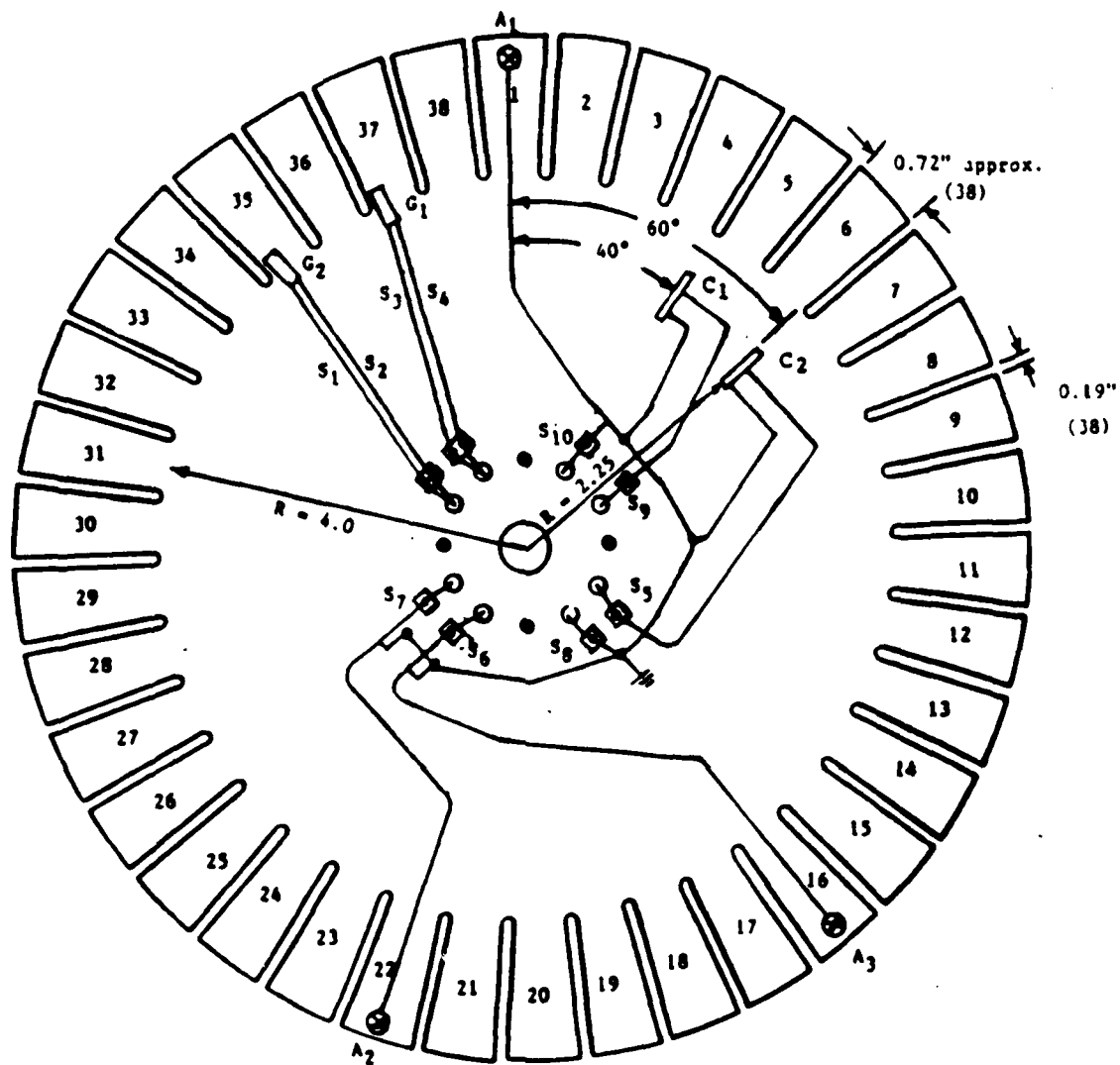
A = Accelerometer
C = Crystal
G = Strain Gage
S = Slip Ring Number
● = Slip Ring Hub Mount Holes
○ = Slip Ring Leadwire Holes

Figure 10.   Disk Instrumentation.

the instrumented disk, the slip ring unit, preamplifiers, a spectrum analyzer, and several oscilloscopes.

Preliminary tests were conducted to excite the test disk by permanent magnets at the disk critical speeds. Half-inch diameter Samarium-Cobalt permanent magnets were installed to an existing mounting plate and were positioned perpendicular to the aft disk surface only at a 3.75-inch radius from the spin axis.

Spin tests were conducted with four magnets mounted at 90-degree spacing, two magnets mounted at 180-degree spacing, and with a single magnet installed. The accelerometer signal spectra for three typical runs are shown in Figure 11. The magnets were widely spaced in comparison to their diameter, and tended to excite all the lower order modes of the bladed disk test specimen. Figure 12 shows, from top to bottom, vibration spectra generated by four, two, and one magnets. The 4-D disk system mode is marked by the bright spot at the top of the spectral peak in the range of 260 to 293 Hz for the three spectra shown.

It can be seen in the spectra: that all magnet configurations excite the lower four modes of the system; that a single magnet excites all modes of the system, much like an impact, but the odd-order modes are excited relatively more strongly than the even-order modes; and that for excitation by two or four evenly spaced magnets, the even-order modes are excited more strongly then the odd-order modes, except for the 1-D mode. In addition to the characteristics shown in the spectral plots, holographic interferograms were produced which showed that a particular mode could be emphasized by rotating the specimen in the magnetic field configuration at a speed where that mode became dominant. This test series showed that we could excite backward traveling vibration waves on our test disk with the magnets on hand. We observed from these tests that a fine speed control was required to generate a pure stationary wave. To circumvent this difficulty and to excite a selected mode with ease, we decided to install excitation magnets on both sides of the disk.

24
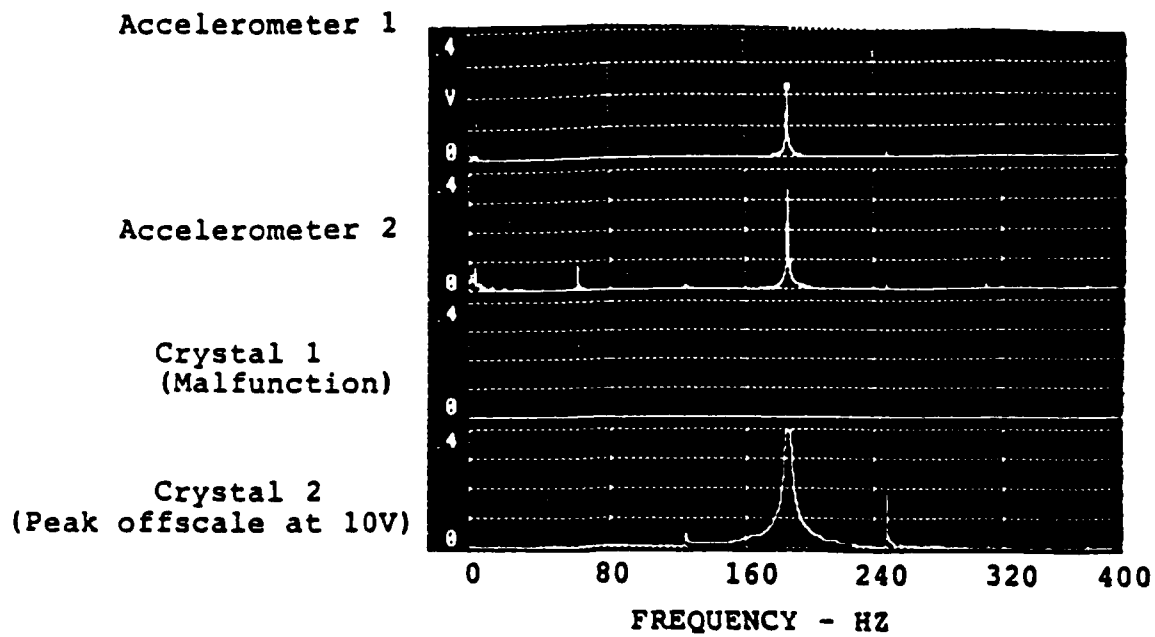
Figure 11. Accelerometer Output Signals.
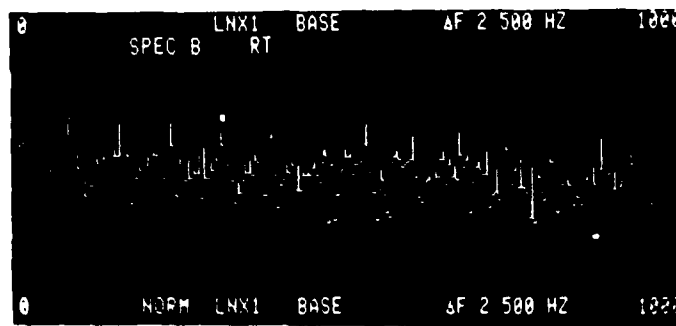
4 Magnets - 4400 RPM
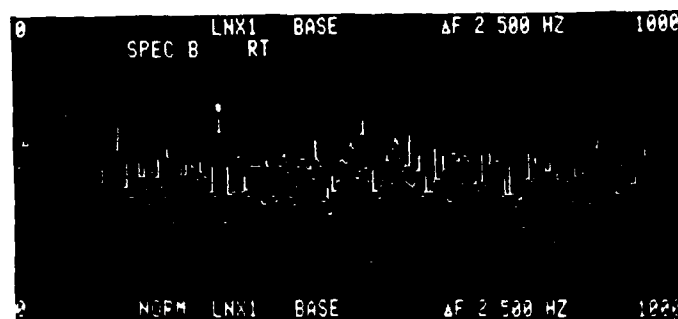
2 Magnets - 3900 RPM
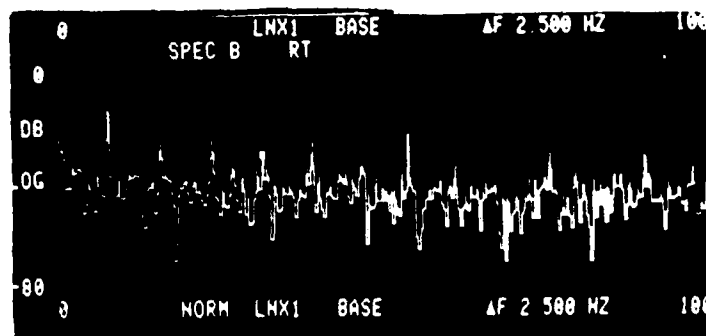
1 Magnet - 4405 RPM

Figure 12. Response Spectra Due to Magnetic Excitation by Permanent Magnet Excitation Systems.

SECTION 4
NONINTERFERENCE DEFLECTION MEASUREMENT SYSTEMS

Two optical methods were used to measure the test disk blade deflections in resonance. The two plane-of-light systems designed by AEDC and UDRI and the inhouse double- and triple-pulse interferometry system were employed to provide the frequency and modal deflection patterns of the test disk.

The following paragraphs describe the concepts and system details of these measurement techniques.

4.1 PRINCIPLE OF OPERATION OF THE FIBER OPTIC PLANE-OF-LIGHT SENSOR METHOD

The method measures the time of arrival of the rotatin. blade tips and the differential arrival time for a vibrating blade as compared to an unexcited blade is a direct indication of the blade tip deflection.

To express the idea in basic mathematics, let a blade tip travel with constant velocity, $v(=\omega R)$, where ω is the angular velocity and R is the radius of blade tip. The distance, y, traveled by blade tip in time, t, is

$$y = VT \tag{13}$$

Introducing variations in variables y and t, we obtain

$$\Delta y = V(\Delta t). \tag{14}$$

Obviously from this equation, the differential time measurements (Δt) will yield changes in positions or deflections (Δy) of the blade tip.

The schematic diagram in Figure 13 explains the concept application to a rotating bladed disk. Let a plane-of-light sensor be mounted in a stationary case, surrounding a constant speed, four bladed rotor. The sensor receives evenly spaced

REFERENCE PULSES--SOLID LINES
VIBRATION PULSES--DOTTED LINES
ΔT IS A MEASURE OF THE BLADE TIP DEFLECTION
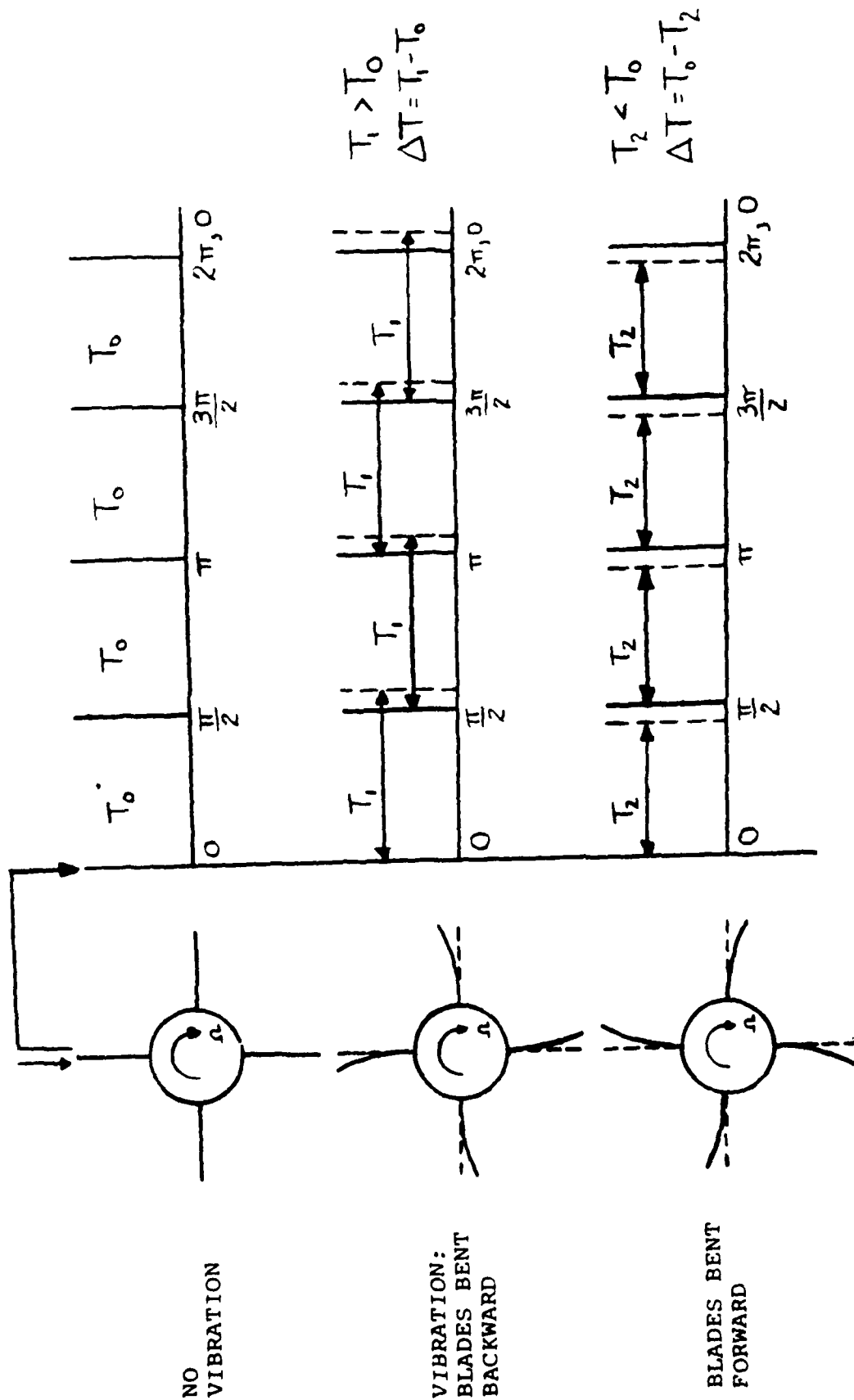
Figure 13. Differential Time Measurement Concept for the NSMS.

28

reflected light pulses off the blade tips when blades are in the undeformed state. Time interval (T_o) is digitally measured. If the blades are deflected to the left, the light pulses occur at a later time (T_1) and $T_1 > T_0$. Similarly, for the blades deflected right, $T_2 < T_0$. The time differential in either case, $T_1 - T_0$ or $T_2 - T_0$ is the direct measurement of the deflection of blade tips of a rotating bladed disk. In our system, the probes monitor the vibration of 38 blades.

4.2 UDRI PLANE-OF-LIGHT SENSOR PROBE CONSTRUCTION DETAILS

Each probe has a layer of 75 glass fibers, each of 125 micron core diameter, for emitting a 1/2 x 1/100 plane of white light. Another layer of similar fibers receives the light reflected back from the blade tips. A 5-mil-thick shim separates the emitter and sensor fiber layers. This emitter-sensor unit is housed in an aluminum casing of 5 x 20 x 50 mm (0.2 x 0.75 x 2 inch) size. The optical probe integration with a fast response (5 to 10μs) preamplifier-photodetector assembly is shown in Figure 14.

4.3 UDRI ELECTRONICS-OPTICS SYSTEM OPERATION

The electro-optic system has four major components: the 1-pulse-per-rev (1PPR) system, the signal processing unit, the computer console and the videographic terminal. These key components are shown in block diagram, Figure 15.

A 10-MHz clock in the signal processor drives five latch cards, one for the 1PPR system and one each for four probes. On receiving a 1PPR pulse, the system stores the clock digital counts and resets the counter. When a blade passes a probe, the light pulse latches the clock count value to the card corresponding to that probe. This time value is digitally stored in the computer. The data from the other four probes are referenced in time to the 1PPR value at the end of the set of

Input

Output

2"

0.2"

$\frac{3}{4}$"

ROTATING TEST OBJECT

OPTICAL
SENSOR

LIGHT
SOURCE

DIFFUSER

LENS SYSTEM

DETECTOR
AND
PHOTOMULTIPLIER
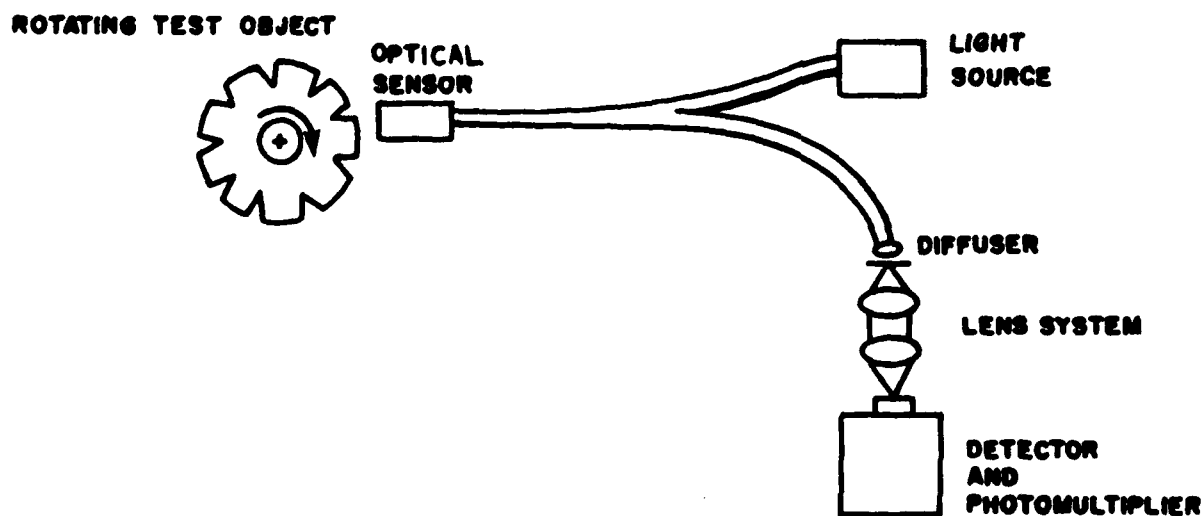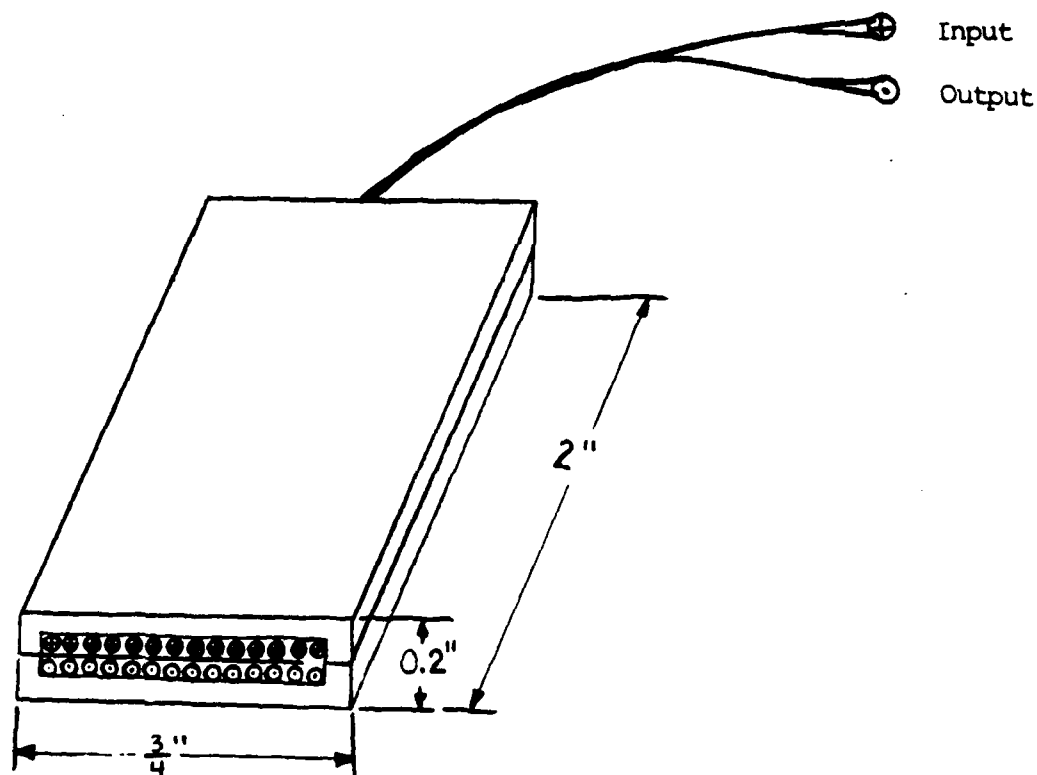
**OPTICAL ARRANGEMENT USING
DIFFUSING PLATE TO IMPROVE SIGNAL QUALITY.**

Figure 14.   UDRI - Optical Probes and System.

30

1-4 OPTICAL PROBES

DETECTOR OPTICS
AND
ELECTRONICS CHASSIS

1PPR Amp

CONTROL
AND
DISPLAY TERMINAL

DATA
ACQUISITION
COMPUTER SYSTEM
AND
TAPE RECORDER
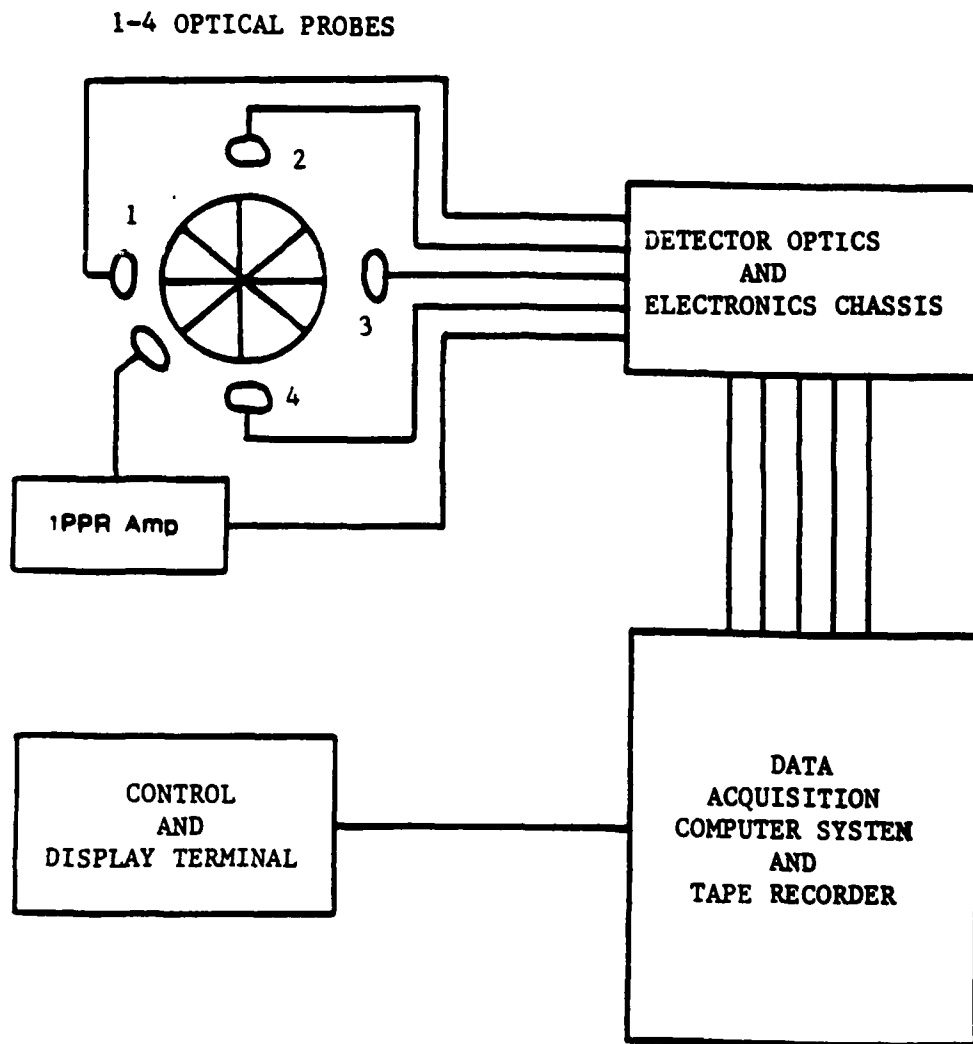
Figure 15.   Block Digram of UDRI NSMS System.

31

readings for one test disk revolution when the 1PPR reset occurs. A nine track tape unit stores the data set for off-line analysis.

In addition to recording blade arrival data, the system can generate and display a histogram of all the blade arrival time data of a particular probe. Alternatively, time history display of blade arrival time counts for up to five blades for a specific probe can be shown on the videographic terminal.

4.4 UTRC OPTICAL SYSTEM

Four sensors are located on an axial plane, common to the rotating disk and the probe mounting ring. These sensors project a narrow 0.005 x 0.5 inch plane of Argon-ion laser light (4880 A°) radially inward onto the blade tips. Each sensor has a 1.5-inch diameter and can be focused within the range of 0.1 to 1.0 inch from its lens. These probes are mounted in radial slots in the yoke as shown in Figure 16.

These sensors are designed to operate under engine environment-temperatures up to 2,000°F and are provided with cooling and lens purging passages. They are also designed to withstand severe vibrating and shock conditions.

The UTRC-AEDC NSMS system is designed to measure the vibration of a 38 bladed disk within the speed range 2,000-10,000 rpm. The data acquisition and data processing hardware integrate five (four vibration sensors and a one-per-rev sensor) data channels with a computer controlled data acquisition system.

AEDC probes, probe-mounts, and system electronics hardware are shown in Figures 16 through 18.

4.5 OPTICAL INTERFEROMETRY

For the quantitative determination of the vibration amplitude of a rotating disk, two whole-field interferometric methods were used. First, the sequential double pulse method (two pulse pairs of a triplet) in conjunction with optical image

32
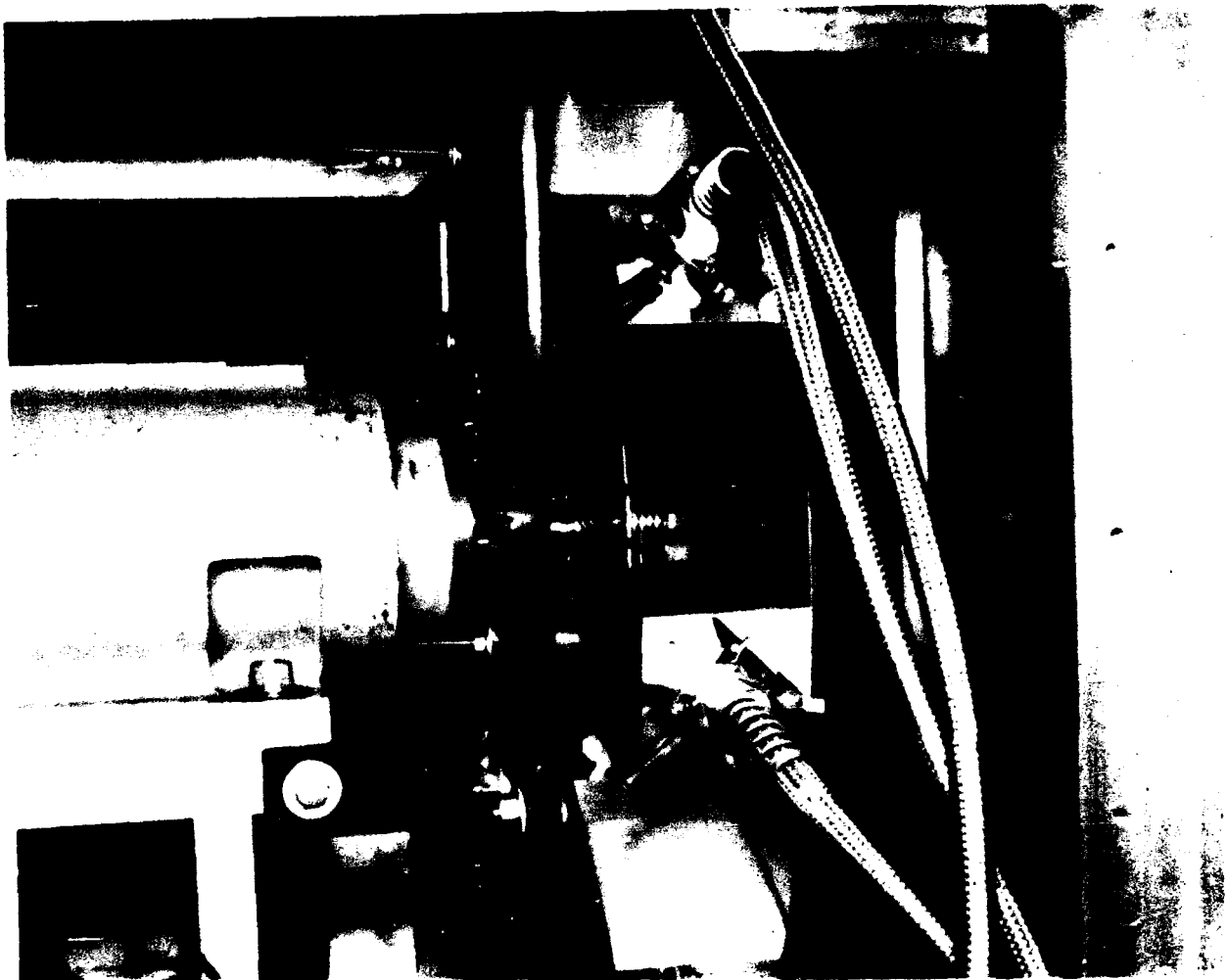
Figure 16. UTRC Plane-of-Light Sensor Probes
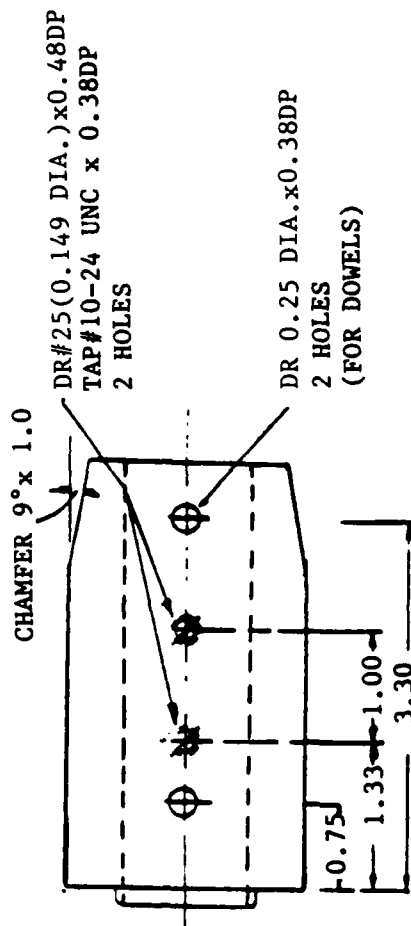
Figure 17. UTRC Probe Mounting Blocks.

Material 6061-T6 ALUM

CHAMFER 9°x 1.0

DR#25(0.149 DIA.)x0.48DP
TAP#10-24 UNC x 0.38DP
2 HOLES

DR 0.25 DIA.x0.38DP
2 HOLES
(FOR DOWELS)

DR#25(0.149 DIA.)x0.50DP
TAP#10-24 UNC-2x0.38DP
8 HOLES EQ. SP.

34

Figure 18.   UTRC NSMS System.

derotation was intended to provide not only the amplitude of
vibration but also the phase angle change over a finite time
interval. This method is well suited for analysis of traveling
or stationary modes of a disk. The second method is conventional
double pulse interferometry through the derotator in which fringe
counts show the disk vibration amplitude.

4.5.1 Triple Pulsed Holography Using a Triple Pulse Ruby Laser

        The triple pulse holographic system was designed to
yield the traveling wave shape and frequency on a spinning disk.
A Q-switched triple pulsed ruby laser (Apollo Laser Model 22HT)
was used for these experiments. Three pulses are emitted during
one lasing of the ruby rod by adjusting voltage levels to each of
three thyratron tubes that provide high voltage pulses to Pockels
cells beam switches. The sequence of triple pulse action in
conjunction with a vibrating disk is shown in Figure 19. This
optical setup is configured to shutter three laser pulses using
two external Pockels cells. Voltage applied to each Pockels cell
achieve the necessary switching of the ruby light pulses. The
three laser pulses are split into three beams using a glass
wedge, W. The object beam (0) and two reference beams, R_{12} and

R_{23} interfere at the hologram plane. Two Pockels cells (PC) in
synchronism with three laser pulses allow sequential emission of
two pulses. When PC_1 is switched on, it allows only the pulses

P_1 and P_2 to pass. Similarly the Pockels cell PC_2 allows only

the P_2 and P_3 pulses to pass. It is important that vertically
polarized light beams reach the holographic recording medium to
form time-sequential interferograms and this is achieved by a
Pockels cell - calcitepolarizer - $\lambda/2$ plate combination. If the
system operates correctly, two separate holograms are recorded -
one for the disk displacement change in the time interval between
pulses P_1 and P_2 and the other for the displacement occurring

between pulses P_2 and P_3. The first interferogram is

36
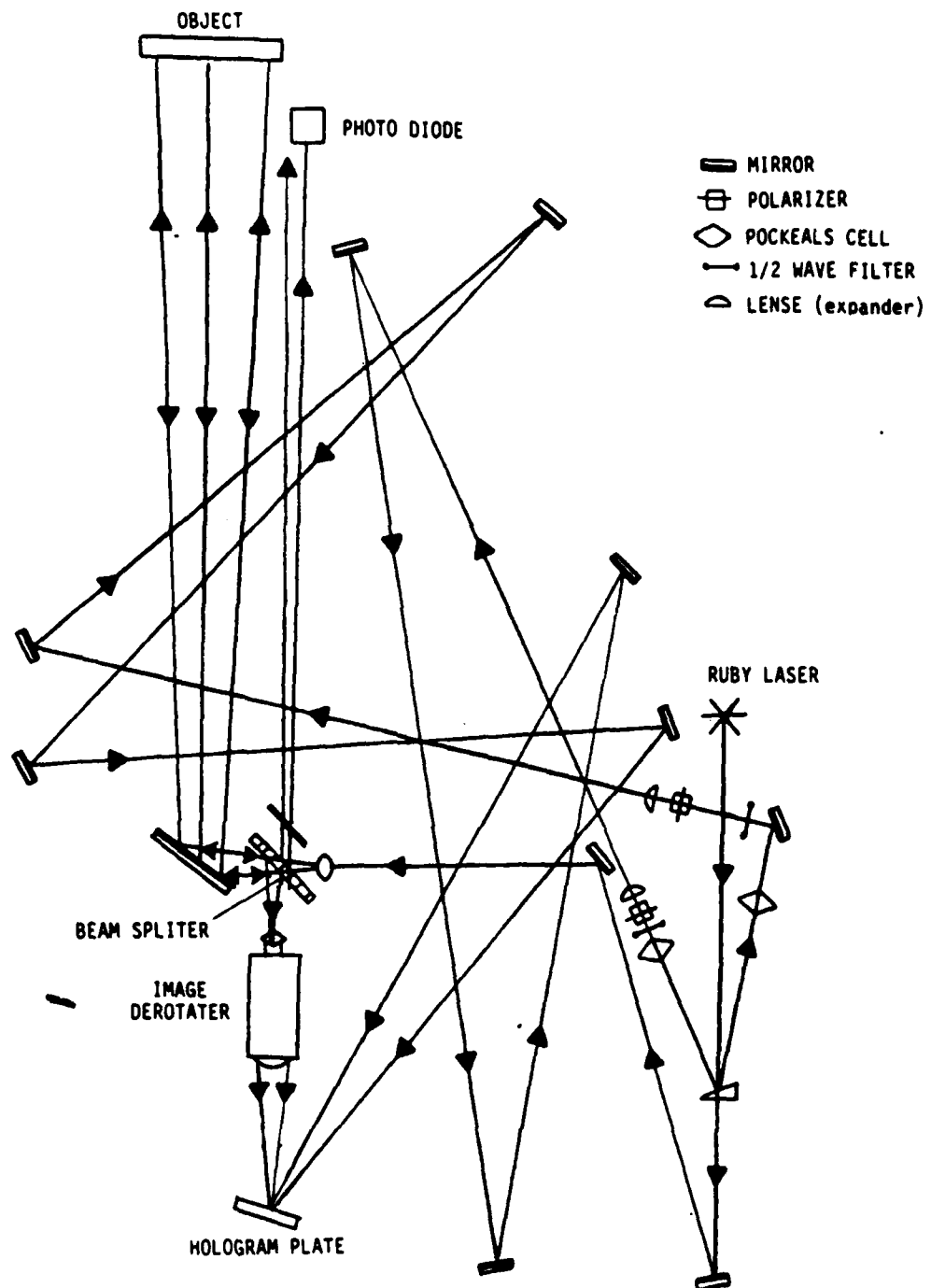
Figure 19. Optical Arrangement for Triple Pulse Interometry.

reconstructed using the reference beam R_{12} and the second is reconstructed using reference beam R_{23}.

Triple pulse interferograms were recorded for the test disk in its 2D, 3D, and 4D modes and the results are discussed in a separate section.

4.5.2   Double Pulse Interferometry

The double exposure method, involving two holographic exposures of the vibrating disk in rapid succession, also was used to record disk displacements. The resulting interference fringe patterns were interpreted to provide net displacement of the disk between the two exposures. This amplitude was used to determine the peak to peak vibration of the disk. The method of calculation is explained below.

Consider the disk vibrating sinusoidally in its normal mode when two exposures are made by pulsing the ruby laser (λ = 694 nm) at the time t_1 and t_2, as shown on the sinusoidal signal of Figure 20. The displacement at time t_1 is

$$Z_1 = A \sin \omega t_1 \tag{15}$$

where ω is the circular frequency ($\omega = 2\pi f$) and A is the half amplitude vibration. The displacement at time t_2 is

$$Z_2 = A \sin \omega t_2 \tag{16}$$

The net displacement is

$$Z_2 - Z_1 = A(\sin \omega t_2 - \sin \omega t_1) \tag{17}$$

but $t_1 = 0$, $\omega t_1 = 0$, $\sin \omega t_1 = 0$, and $z_i = 0$ for integral order traveling wave modes, and t_2 is the pulse separation time (Δt). Then

$$Z_2 - Z_1 = A \sin (\omega \Delta t) \tag{18}$$

In the double exposure method interference fringes occur when
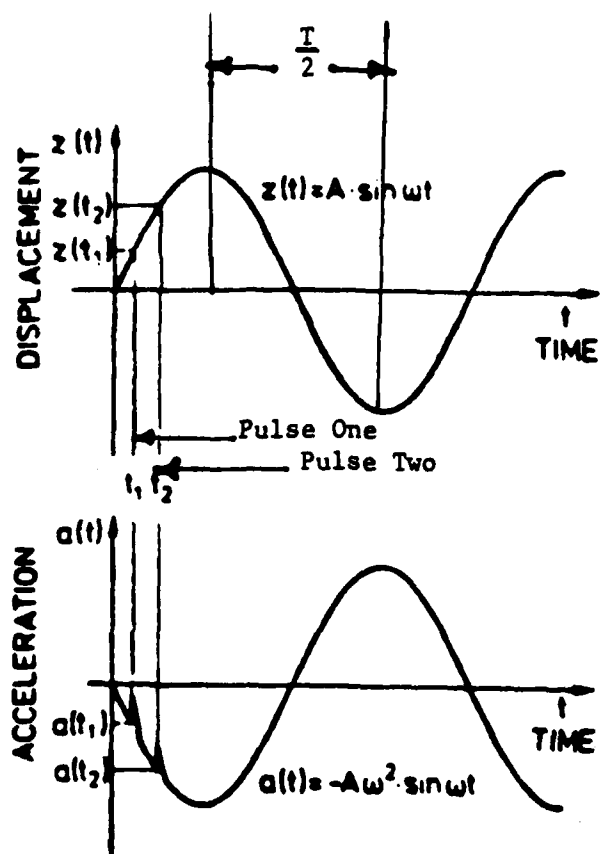
Figure 20. Pulse Locations on Sine Wave for
Double Pulse Interferometry.

39

$$z_2 - z_1 = \frac{(2n-1)\ \lambda}{4} \tag{19}$$

where n is the number of fringes and λ is the wavelength. Then from (18) and (19)

$$A = \frac{(2n-1)\ \lambda}{4\ \sin\ (2\pi f \Delta t)} \tag{20}$$

The out of plane displacement of the disk must be corrected for the beam separation angle (α of Figure 21) by $\frac{1}{\cos\ \alpha}$. Then

$$A = \frac{(2n-1)\ \lambda}{4\ \sin\ (2\pi f \Delta t)\ \cos\ \alpha} \tag{21}$$
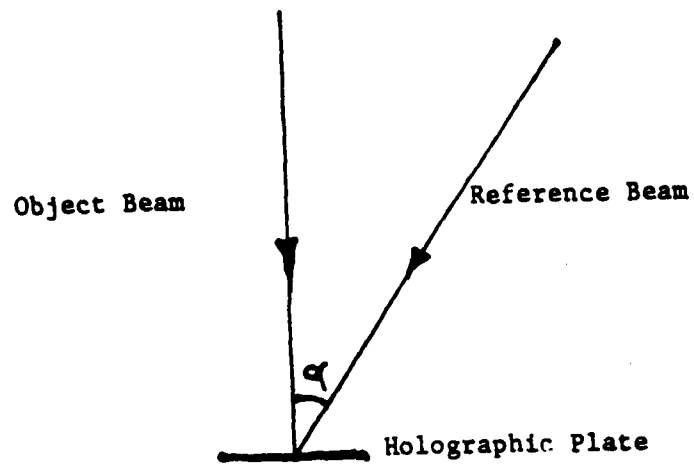
α, the setup Angle = 34.92°,
is used to modify the equation,

$$A = \frac{(2n-1) \ \lambda}{4 \ \sin \ (2\pi f \Delta t)}$$

Figure 21. Object and Reference Beam Orientation.

SECTION 5

EVALUATION TESTS

The AEDC NSMS evaluation test efforts started early in April
of 1988. Trial runs were made to (1) determine the rotational
speeds required to resonate the test disk in its 2D, 3D, and 4D
integral order modes with the permanent magnet excitation system
(2) check the response of the AEDC and ISRL optical transducer
sets in the test setup at the expected test shaft rotational
speeds and (3) setup the triple-pulse laser interferometric
holography system at the expected run speeds. Trial runs were
made first with the magnets located 0.25 inch from the test disk
blades at a 5.0-inch radius from the disk center. This produced
approximately a 0.5-inch peak-to-peak deflection of the blade
tips. The magnets then were moved to a 3.75-inch disk radius
position just below the blade root area at a 0.25-inch spacing
from the disk. This produced an estimated 0.25-inch peak-to-peak
deflection of the blade tips in the 3D integral order mode. It
was decided then to begin the test series with the magnets spaced
5/16 inch from the test disk at the 3.75-inch disk radius.

5.1 AEDC NSMS EVALUATION TESTS: FIRST TEST SERIES

An AEDC NSMS Evaluation test series was conducted during the
week 11-15 April 1988. While the disk was running at constant
speed with peak response of each modal pattern, indicated by
peaking of the signals from the accelerometers and crystals
mounted on the disk as displayed on the spectrum analyzer screen,
UDRI would record a set of blade tip deflection data on the ISRL
NSMS data system; United Technologies Research Corporation
(UTRC), as the AEDC NSMS contractor, would record a set of blade
tip deflection data on the AEDC NSMS data system; and a triple-
pulse holographic interferogram would be recorded on film from
the ISRL optical instrumentation system. UDRI planned to reduce
the ISRL NSMS data and compare it later to the AEDC NSMS data and

the holographic data, which would be reduced and compared to each other by UTRC.

The first test run was conducted on 12 April 1988. Excitation was by six permanent magnets spaced at 60-degree intervals on alternating sides of the disk at the 3.75-inch disk radius and spaced 5/16 inch from each each surface. This produced a 3D mode fixed in space (a backward traveling 3D mode on the disk at the disk rotational speed) with peak disk response occurring at 3732 rpm. The test run was recorded by UDRI with zero response reference runs recorded first at 1,500 and 3,000 rpm for use in the data reduction programs. UTRC recorded a resonance data set and then asked to record spin-up and spin-down runs through resonance as additional data sets. When these runs were made, we found that a broad resonance peak occurred more or less continuously from 3,700 to 3,850 rpm with a normal onset at the lower speed but an abrupt dropoff at the higher speed. Resonance onset then could not be achieved until the rotational speed was reduced to about the midpoint of the resonance speed range.

With the magnet-disk gaps at 5/16 inch, a number of holograms were made of the 3D integral mode at 3,720 rpm. UTRC then recorded an AEDC NSMS data set at 3,720 rpm followed by a reference data set at 3,720 rpm with the excitation magnets removed. The hologram films were developed and were carried back to UTRC in the evening by Ray Chi of UTRC for examination the next day by Karl Stetson of UTRC.

During the morning of 14 April 1988, four magnets were installed at 90 degree intervals and 5/16-inch spacing from the test disk to excite the 2D integral mode. We found that if the disk was accelerated very slowly, the resonance could be extended from 3,600 to 4,300 rpm before it collapsed. UTRC then recorded the 2D blade deflections at 3,920 rpm on the AEDC NSMS and then recorded a reference data set at speed with the magnets removed. At that time UTRC called from Hartford, CT with recommendations from Karl Stetson for realignment of the holographic optical

system. At about the time the optical realignment was accomplished, UTRC received another call from Hartford requesting reduction of the response amplitude to reduce the number of fringes displayed in the holograms. The magnets then were set at 7/16 inch from the disk and the 2D mode was recorded on the AEDC NSMS, on the ISRL NSMS, and on a series of triple-pulse holograms at 3,780 rpm. The response amplitude was decreased nearly half by this lower excitation force, and the resonant frequency and response frequency range of the disk also were reduced, but the resonance response characteristic remained the same. Eight magnets then were installed at 7/16 inch from the disk to excite the 4D mode. Again, the same response characteristic of the disk occurred. The response peak seemed highest at 3,630 rpm, and data were taken there on the two NSMS systems and on holographic film.

On 15 April 1988, six magnets were installed at 7/16 inch from the disk to repeat the 3D mode test at the same excitation level used for the 2D and 4D modes the previous day, which had seemed to produce the desired number of fringes on the holograms. Then the hologram reference beams were readjusted according to another request from Hartford. The 3D modal data then were recorded by the three instrumentation systems. Again, we found that the resonance frequency could be sustained over a range of about 300 rpm with a sharp collapse and instantaneous phase shift of the response at the upper speed (or frequency) limit of the resonance.

During the course of this testing program, UDRI recorded response data on the ISRL NSMS for the 3D mode with 5/16-inch magnet spacing and for the 2D, 4D, and 3D modes with 7/16-inch magnet spacing. For each of those records reference data were taken immediately before or immediately after the modal data at 1,500 and 3,000 rpm where no disk response was indicated by the monitoring instruments on the disk or in the recorded reference data. The ISRL NSMS data records are listed in Table 5.

TABLE 5

AEDC NSMS EVALUATION TESTS - FIRST TEST SERIES
ISRL NSMS DATA SYSTEM TEST RECORDS
APRIL 12-15, 1988

Date	Run #	Mode	Magnet Gap (Inch)	RPM	Data Type	Remarks
4/12	1A	3D	5/16	1500	Reference Speed 1	No AEDC Data
	2A	3D		3000	Reference Speed 2	ISRL Data OK
	3A	3D		3732	Resonance Data	No Phase Records
4/14	4A	2D	7/16	3780	Resonance Data	ISRL & AEDC
	5A	2D		3000	Reference Speed 1	Data OK
	6A	2D		1500	Reference Speed 2	No Phase Records
4/14	7A	4D	7/16	1500	Reference Speed 1	ISRL & AEDC
	8A	4D		3000	Reference Speed 2	Data OK
	9A	4D		3630	Resonance Data	Small Phase Change
4/15	10A	3D	7/16	1500	Reference Speed 1	
	11A	3D		3000	Reference Speed 2	
	12A	3D		3560	Resonance Data	No Real Resonance

Similarly, data were recorded on the AEDC NSMS for these conditions but the reference data for these records were taken at the same rpm as the resonance data with the excitation magnets removed. No accel or decel data were taken on the AEDC NSMS because of the nonlinear response characteristic of the test disk. We were later informed by the project monitor that none of the holographic data were useful except that which was recorded for the 3D mode on 15 April 1988 after the last optical system alignment was made. Similarly, we were told the AEDC NSMS data were usable only for the 2D and 4D modes that were recorded on 14 April 1988.

5.1.1 Nonlinear Response Studies of the Disk

As mentioned previously, one of the plans during the April test series was that UTRC wanted to accomplish two types of data collection and data reduction with the AEDC NSMS

instrumentation system. The first of these was for steady-state data collected at the peak modal response for the 2D, 3D, and 4D resonant modes of the test disk. The second was for data collected during spin-up and spin-down through each resonance response, the so-called accel and decel test runs. However, during testing, we found that the test disk displayed nonlinear response in that a normal onset of resonance with a gradual phase shift was not displayed during spin-up to resonance, but that an abrupt collapse of response with an accompanying immediate phase shift occurred as speed was increased through the resonance response range. Then as speed was decreased back through the resonance range, an abrupt response onset with an immediate phase shift occurred at a considerably lower spin speed within the spin-up resonance response speed range. This resonance characteristic is shown in Figures 22 and 23 for 2D and 3D response modes for small magnet gap settings.

We thought that the nonlinear response of the test disk was a function of the strength of the force field of the excitation magnets. A number of test runs then were made with magnet spacing from the test disk varied from 5/16 inch to 9/16 inch, but the same nonlinear type of response was shown during all test runs. UDRI then was asked to try air-jet excitation of the test disk. This was accomplished in early May of 1988 with two small air jets supported at 3/8-inch spacing from each side of the disk to excite the 2D modal response. Figure 24 shows the results of this test and the same nonlinear response.

Subsequently, a meeting was held between UDRI and APL/POTC personnel at which it was decided to attach stiffener plates of 2.25-inch diameter and 0.115-inch thickness, as shown in Figure 25, to each side of the hub area of the instrumented test disk in the expectation that this would improve the linearity of the modal responses. UDRI fabricated the plates, removed the slip ring hub, installed the plates with high-
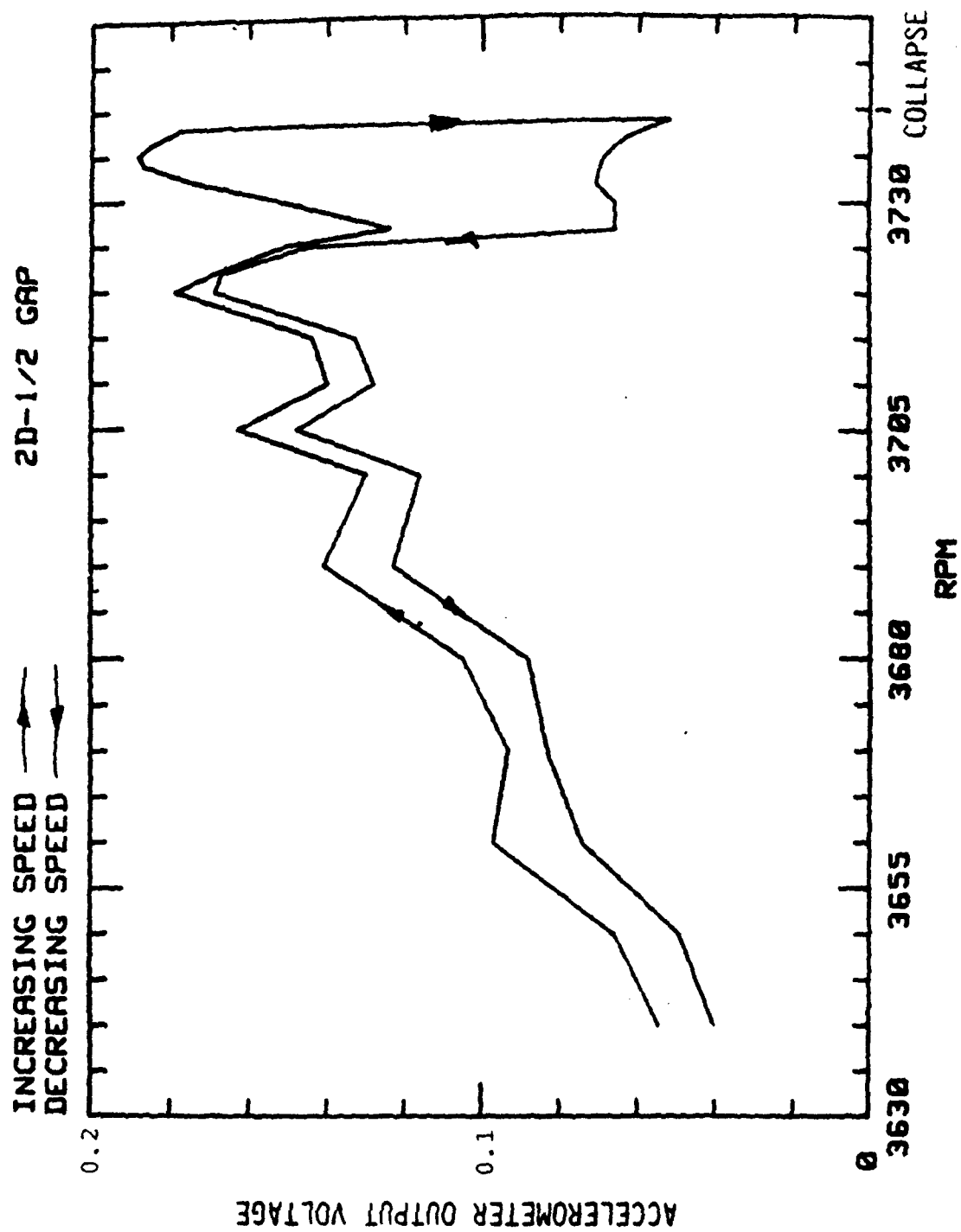
Figure 22. Nonliner Disk Response for the 2D Mode.

1/2" GAP - April 29, 1988 - 3E Excitation, 3D MODE
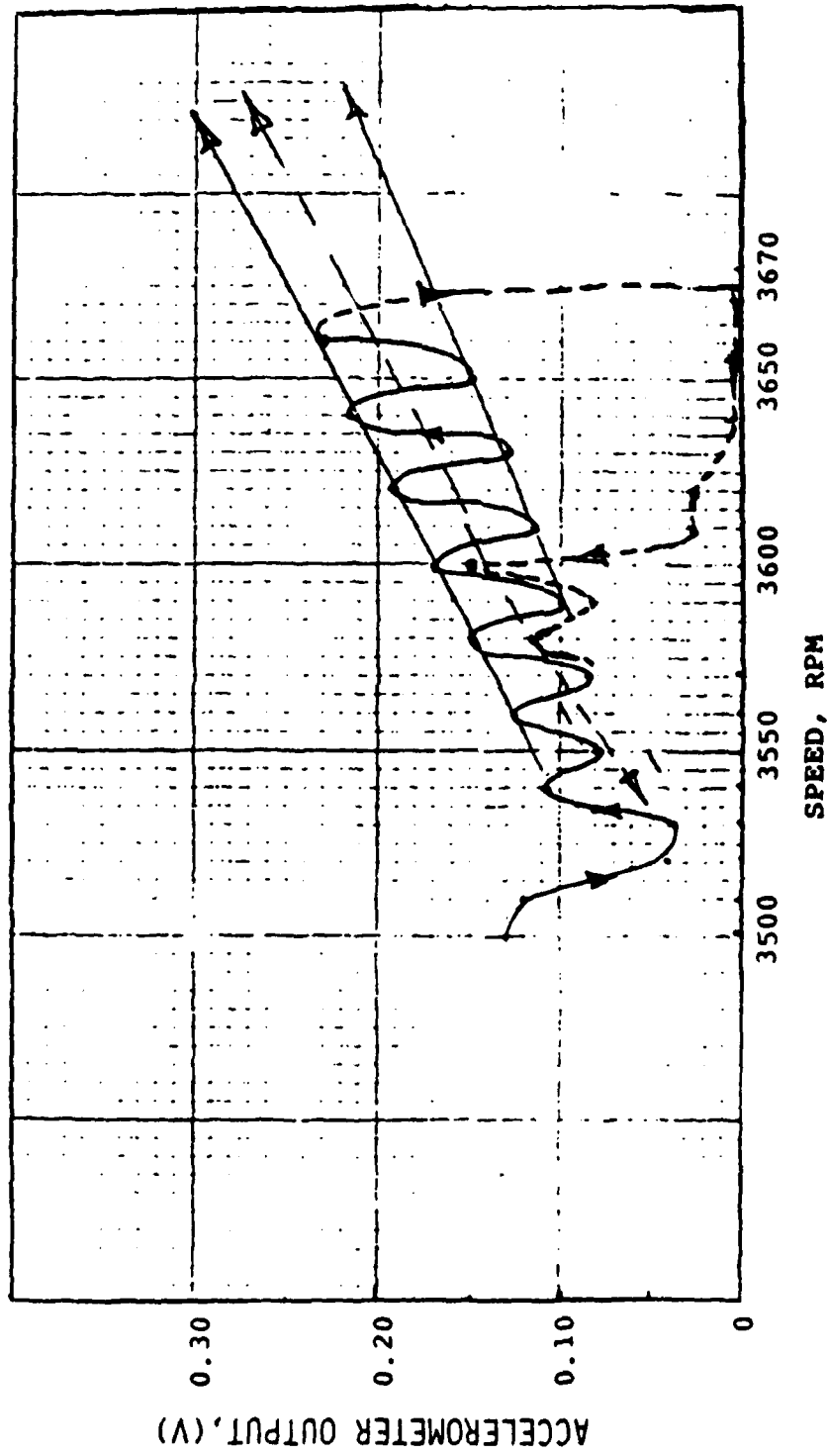
Figure 23. Nonliner Disk Response for the 3D Mode.

48

4 Airjets, 3/8" GAP, 70 PSI, 1/16" Dia Nozzles
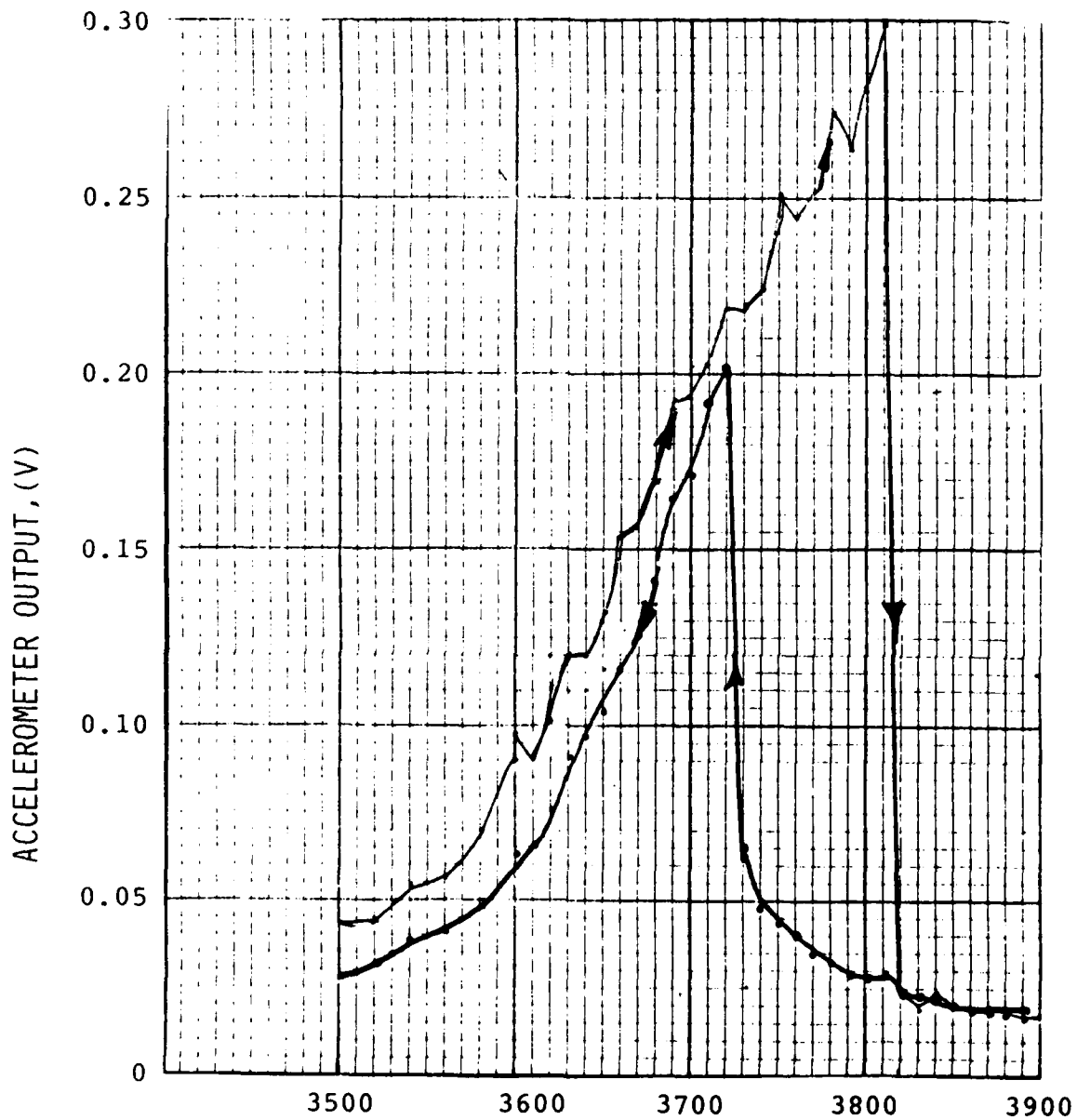
Figure 24. Airjets Excitation - Response Diagram of the Test Disk for 2D Mode.

12 Holes @ 30° on 1.70 Dia. Circle
#30 Drill

0.115

2.25

0.375
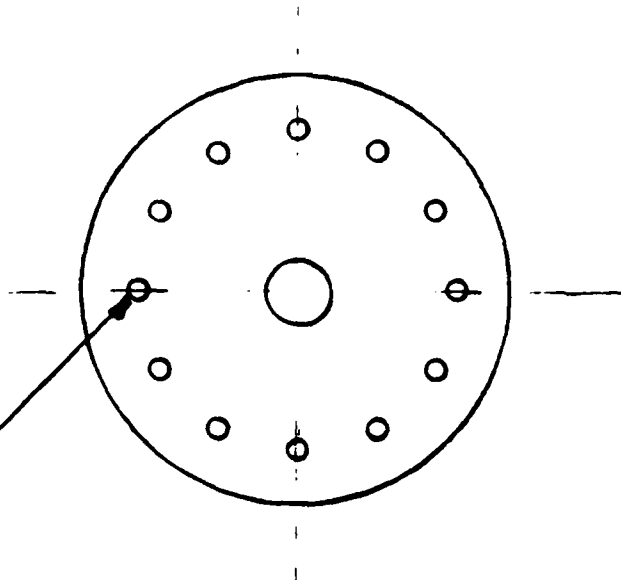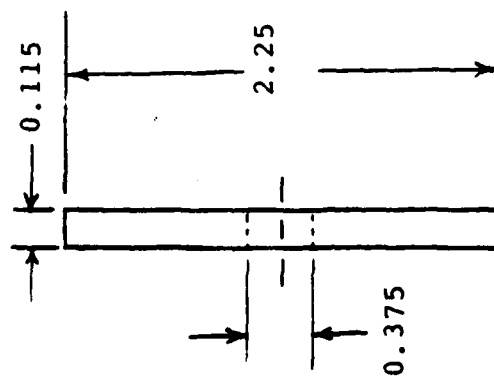
Figure 25. Disk Hub-Stiffener.

strength HySol EA934 epoxy adhesive, and reinstalled and rewired the slip ring hub set. Then tests were conducted to determine if the reinforced-hub test disk possessed nonlinear behavior in non-rotating conditions. The test disk was hard mounted and was driven by an electromagnet exciter at a constant level of excitation voltage but with different gaps between the electromagnet and the test disk. The static test results shown in Figures 26 and 27 indicated that the disk behaves like a soft spring. Variation of response frequency with amplitude of excitation force decreases with increase in the mode number of vibration. For example leftward shift of the response frequency peak with higher excitation force is more pronounced for 1D as compared to the 3D and 4D modes.

After the static vibration tests were completed, the disk was reinstalled in the spin test setup and was excited in the 2D mode at various magnet gap spacings from the disk. The results of five successive runs in which the magnet gaps were increased from 3/8 inch to 5/8 inch in 1/16-inch increments indicated that the disk now displays a linear response in the 2D mode if the magnet gaps are 9/16 inch or greater, as seen in Figure 28. The response amplitude, however, is reduced appreciably at the larger magnet gaps and the accelerometer output amplifier gain was doubled when the magnet gaps increased from 1/2 inch to 9/16 inch.

5.1.2 <u>Laser Holographic Interferometry Problems</u>

One of the requirements introduced by UTRC for the triple-pulse, double-image holograms was exact measurement of the pulse spacing between the first and second pulses, which produce the first interferogram, and the second and third pulses, which produce the second interferogram. The exact times are needed to establish the frequency and phasing of the two images. The desired time intervals were 10 μsec between the successive pulses. UDRI monitored some triple-pulse events with a high frequency oscilloscope, but pulse intervals could be measured

2-D

VOLTS

ACCELEROMETER OUTPUT, (V)

0.8
0.7
0.6
0.5
0.4
0.3
0.2
0.1
0

74 75 76 77 78 79 80 81 82 83 84 85

FREQUENCY HZ

0°
90°

DRIVER 45°
25 MIL GAP

DRIVER 90°
100 MIL

DRIVER 90°
50 MIL

DRIVER 90°
25 MIL

DRIVER 0°
100 MIL

DRIVER 0°
50 MIL
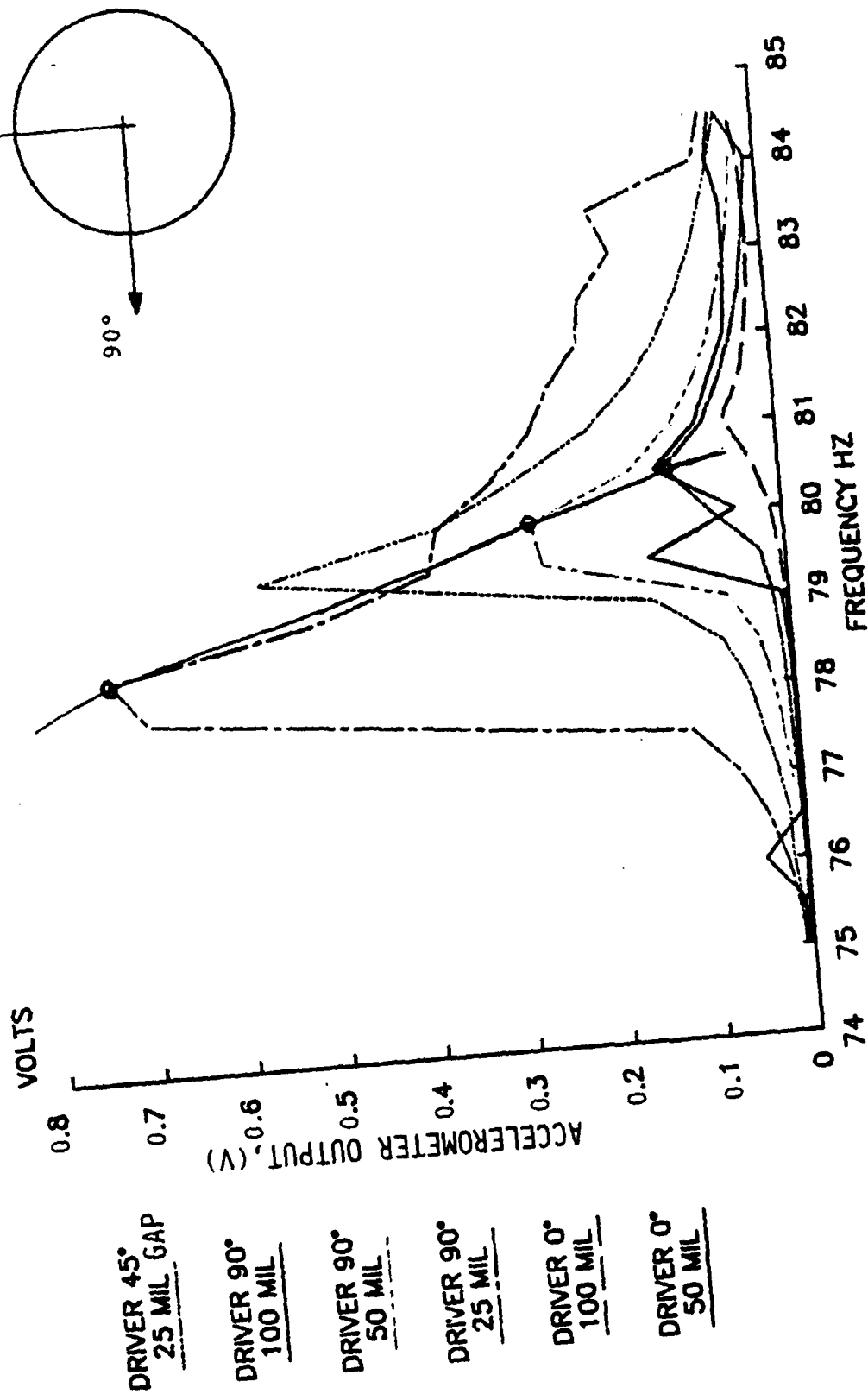
Figure 26. Static Disk Nonliner Response for 2D Mode.

52
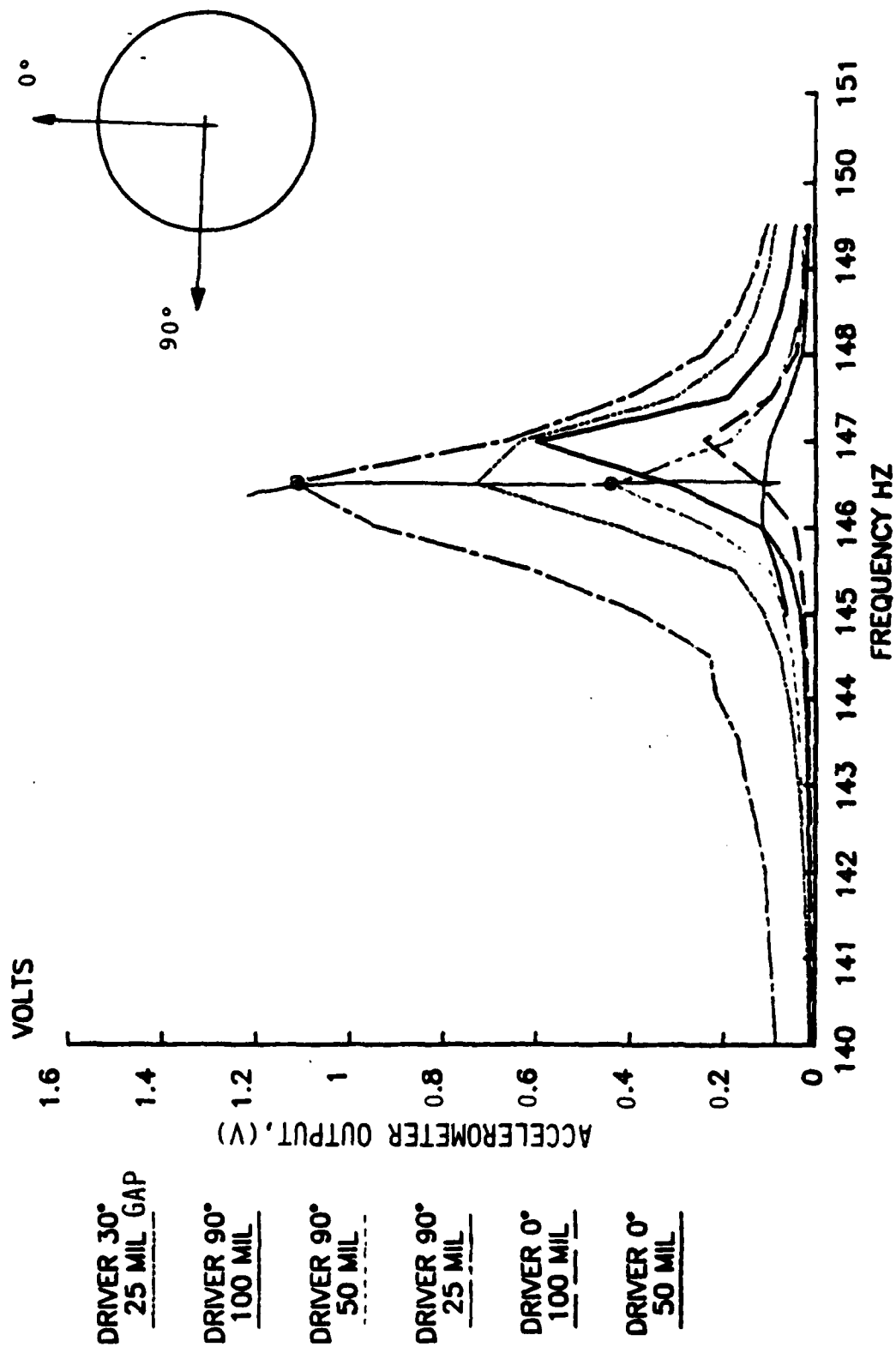
Figure 27. Static Disk Nonliner Response for 3D Mode.

53
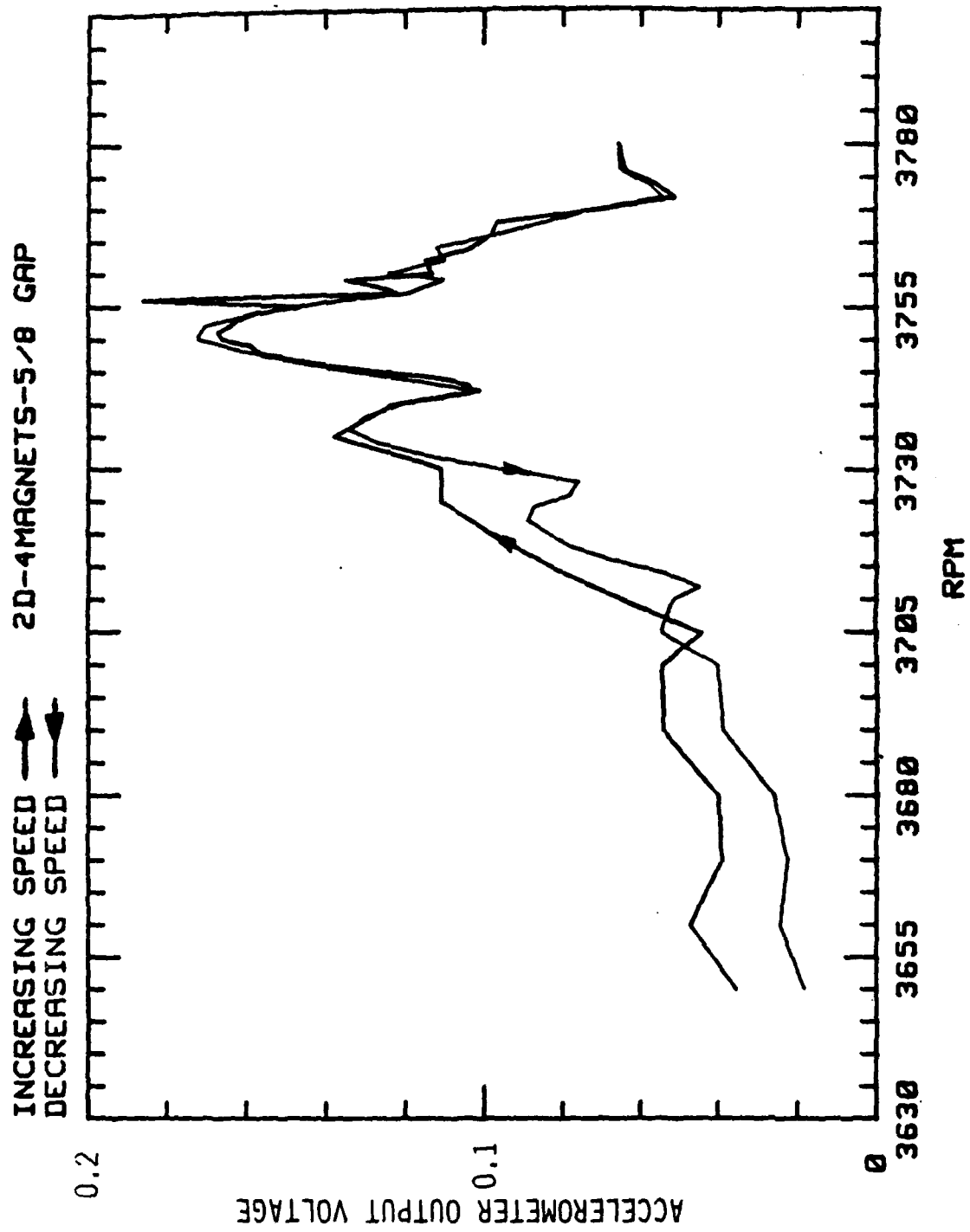
Figure 28. Linear Response of the Test Disk with Large Magnet Spacing.

54

with confidence only to 1-μsec accuracy on the oscilloscope screen.

However, during the study of the pulse interval timing problem, we found that the Appollo ruby laser often produced spurious pulses. Sometimes as many as five or six pulses occurred, as shown in the oscillograph screen pictures of Figure 29. Careful study of the three storage circuits of the triple-pulse system showed a shorted silicon controlled rectifier (SCR), a missing diode, and a thyratron that sometimes broke down spontaneously at normal operating voltage, all in the energy storage circuit for the third laser pulse. Obviously, the multipulses occurred because of the faults in that circuit. After those faults were repaired, spurious pulses did not occur but neither did triple-pulses and only double-pulse firing of the laser could be achieved.

Phone conferences then were held with Mr. Ralph Page of the Appollo Co., and he suggested that, contrary to what is prescribed in the system operations manual, triple-pulsing is more easily achieved by first adjusting the third pulse circuit, then the second and the first, instead of the specified ascending order. He also said a success rate of greater than 30 percent was not to be expected for the triple-pulse system. By following his directions, UDRI was able to achieve a triple-pulse success rate of about 25 percent for either 10- or 25-μsec pulse intervals.

After restoring the system to its triple pulse operation with pulse separation accuracy of 1μs as displayed in Figure 30, several triple-pulse (sequential double pulse) holograms were tried while the test disk was in resonance. The three pulses are achieved by sequential switching of the laser head three internal and the two external Pockels cells. But it was discovered that even when no third pulse was displayed on the pulse monitoring scope, the reconstructed image contained spurious fringes. This fact led us to believe that the external Pockels cells in the reference path had a poor extinction ratio and
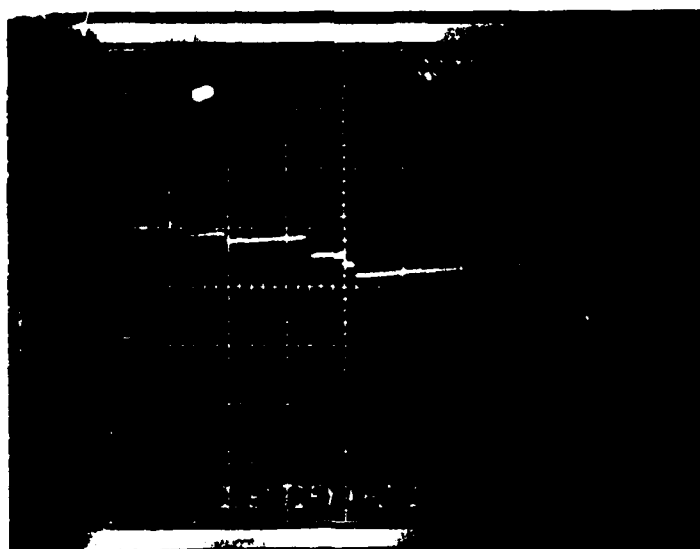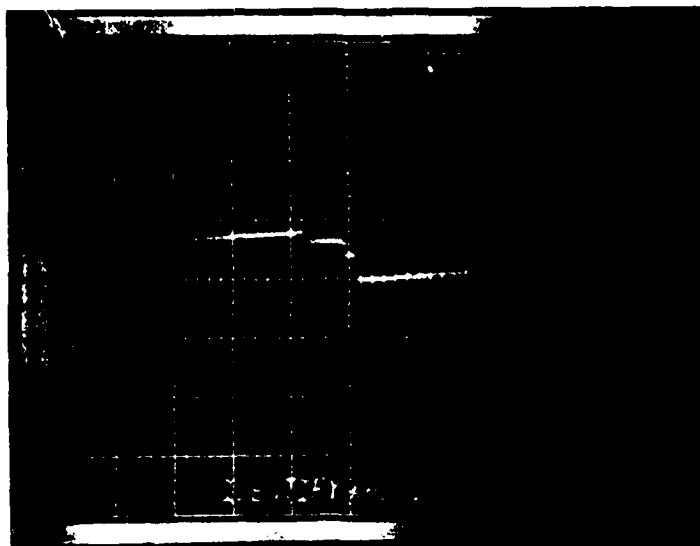
Figure 29.   Multi-Pulse Operation of the Ruby Laser.
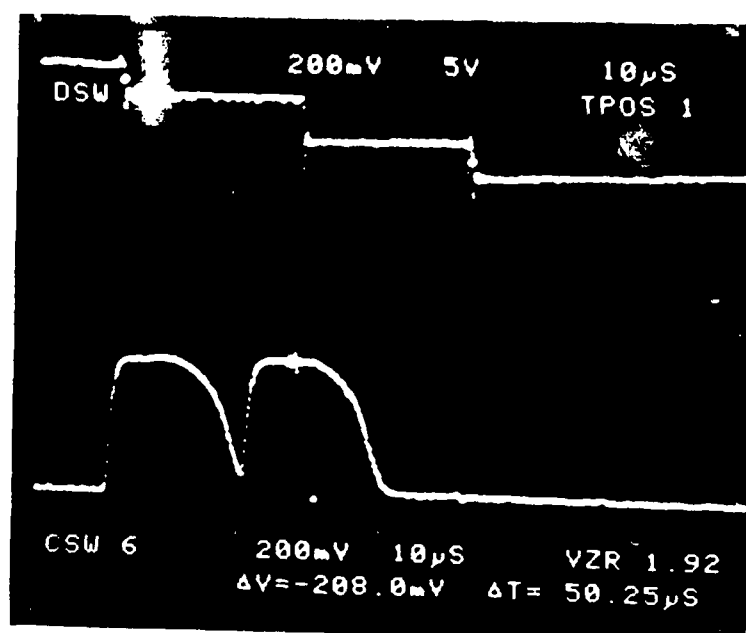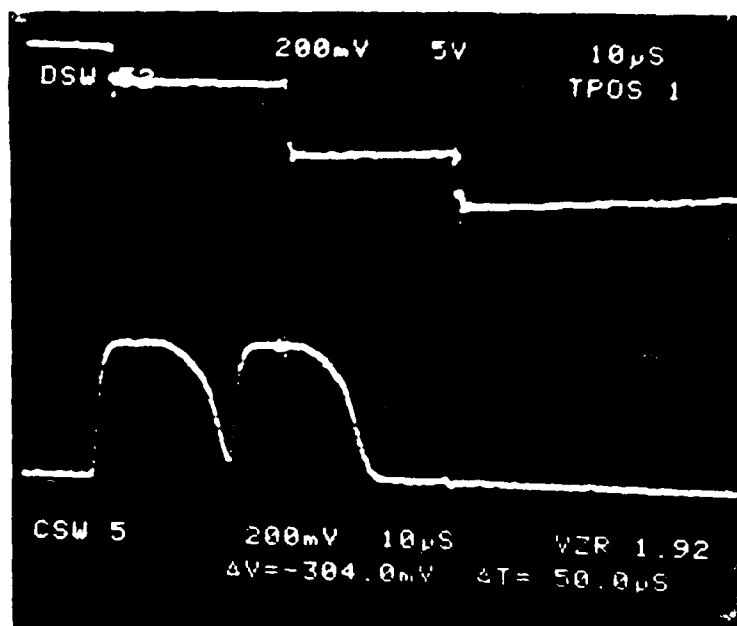
Figure 30. Pulse-Separation Measurement.

allowed light passage when it was intended to completely block a laser pulse. This leakage of laser light through one of the external Pockels cells combined with the hologram due to the two intended pulses produced an effect similar to Moire. One such sample interferogram is enclosed in Figure 31 to show the difficulty in interpreting such holograms. An attempt to quench the leakage by placing a combination polarizer-filter in front of the Pockels cells, proved to be a failure as the same effect was seen in the interferograms produced by the system. We concluded at this stage that the trouble was in the delay lines and pulse forming networks of the external Pockels cells control voltages, causing them to attain inconsistent and inadequate extinction levels, or in the Pockels cells themselves.

Meanwhile, Ray Chi and Karl Stetson of UTRC had agreed to utilize double pulse holograms to determine the modal deformation of the resonating disk and accordingly requested us to proceed to record double pulse interferograms for the test disk while in resonance. This plan was agreed to by the UTRC, AEDC, and ISRL test engineers.

5.2 AEDC NSMS EVALUATION TESTS - SECOND TEST SERIES

The second test series was required for the following reasons: (a) sequential double-pulse or triple-pulse holograms recorded on the first test series were unacceptable for Karl Stetson of UTRC due to Moire type fringes in interferograms (b) AEDC NSMS data analysis had produced unsatisfactory results for two out of the three disk response modes and (c) the occurrence of abrupt collapse of the disk response modes without gradual phase change muddled the UTRC single degree of freedom analysis method.

For this second test series, the linear dynamic characteristics of the test disk had been improved by installing a 2.25-inch-diameter x 0.11-inch-thick stiffener on each side of
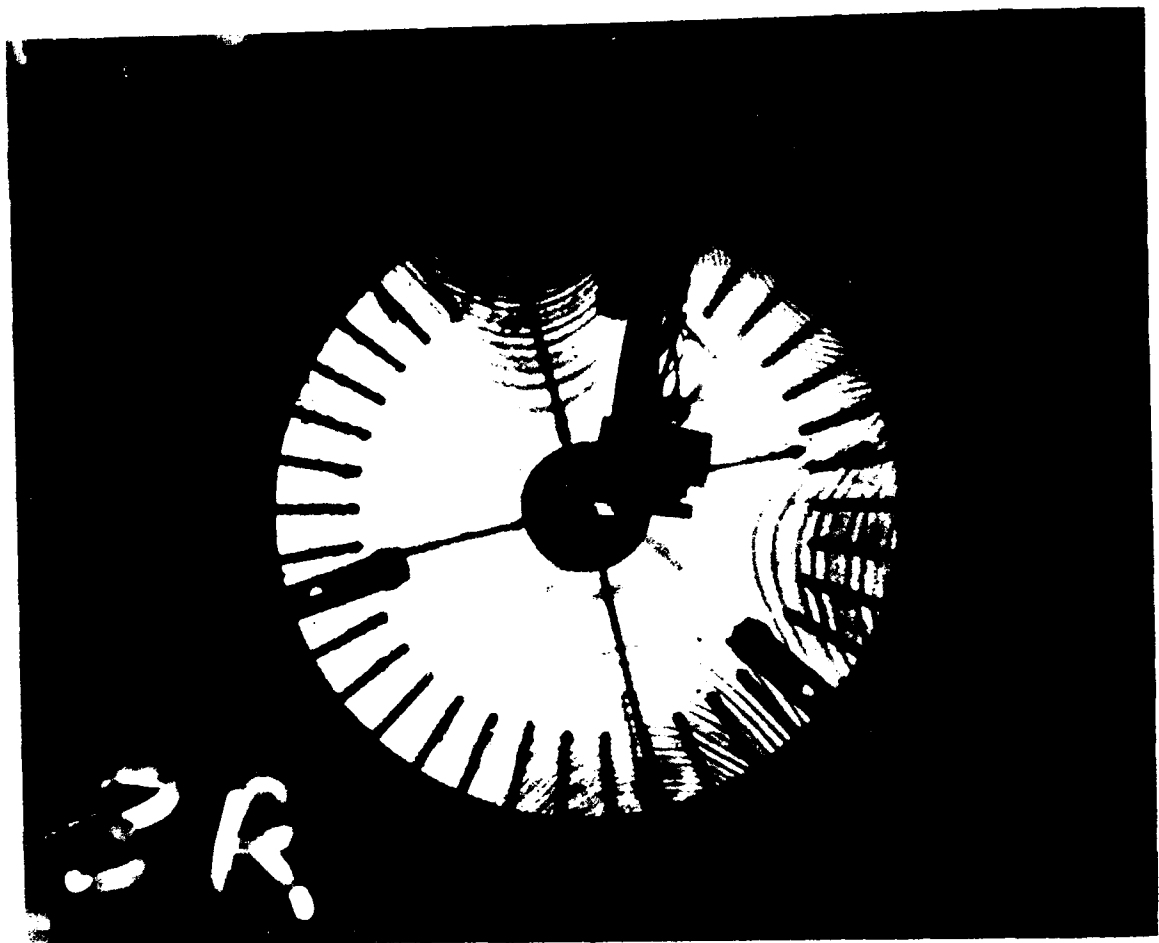
Figure 31. Triple Pulse Interferogram of the Disk
with Split Fringes.

the disk in the hub area. Also wider spacing was used between the disk and the excitation magnets.

Test matrix objectives and test conditions for this second series remained the same - excitation magnets were positioned on alternate sides of the disk on circles of 3.75-inch radius to excite a specific mode, and ISRL optical probes were positioned with angular spacings of 60, 40, and 30 degrees to measure the 2D, 3D, and 4D mode responses, respectively.

Test dates with run numbers and test conditions are provided in Table 6.

The first test in this series was with magnet gap spacing of 5/8 inch from the disk and with 25 μs for triple-pulse separation. Interferograms corresponding to Runs 1B and 2B contained an unresolvable number of fringes, indicating large displacements. The gap was increased to 3/4 inch in Runs 3B and 4B. AEDC NSMS on site data analysis by UTRC yielded no useful data because of high noise to signal ratios in the optical probe data. Threshold levels for their trigger device was altered, blade tips were refurbished, and the Argon laser output was trimmed. The subsequent test runs (5B, 6B) made on July 29 were useful. Triple-pulse holography was being pursued up to July 29. On that date, we decided to discontinue triple-pulse efforts and record double-pulse holograms at resonance, before resonance, and after resonance. The off-resonance holograms would provide qualitative phase information as the disk transited through resonance.

Double pulse holograms were made for 4D (Runs 7B through 10B and 17B and 18B), for 3D (Runs 11B through 16B), and for 2D (Runs 19B through 22B) with a variety of exciter spacings and pulse separation times. Two data sets for every test condition, one at resonance and the other without resonance (usually at 3,000 rpm for ISRL and resonance speed without magnets for UTRC) were acquired. Tests were conducted at various magnet gap spacings

60

TABLE 6

AEDC NSMS EVALUATION TESTS - SECOND TEST SERIES
ISRL DATA RECORDS
JULY 27 - AUGUST 5, 1988

Date	Run #	Mode	Magnet Gap (Inch)	RPM	Data Type	Remarks
7/27	1B	4D	5/8	3648	Resonance Speed	ISRL Data OK
	2B	4D		3000	Reference Speed	AEDC-No Data Holograms bad
7/28	3B	4D	3/4	3646	Resonance Speed	ISRL Data OK
	4B	4D		3000	Reference Speed	AEDC-No Data Holograms bad
7/29	5B	4D	3/4	3640	Resonance Speed	ISRL Data OK
	6B	4D		3000	Reference Speed	AEDC Data OK Holograms bad
8/1	7B	4D	5/8	3644	Resonance Speed	Good Data
	8B	4D		3000	Reference Speed	
8/2	9B	4D	5/8	3636	Lower Half Power Point Speed	Good Data
	10B	4D		3648	Upper Half Power Point Speed	
8/3	11B	3D	5/8	3642	Resonance Speed	
	12B	3D		3632	Lower Half Power Point Speed	Good Data
	13B	3D		3646	Upper Half Power Point Speed	
	14B	3D		3000	Reference Speed	
8/4	15B	3D	3/4	3633	Resonance Speed	Good Data
	16B	3D		3000	Reference Speed	
8/4	17B	4D	9/16	3642	Resonance Speed	Good Data
	18B	4D		3000	Reference Speed	
8/5	19B	2D	15/16	4063	Resonance Speed	Good Data
	20B	2D	15/16	4058	Near Resonance Speed	
	21B	2D		3000	Reference Speed	
	22B	2D		4058	Reference Speed Without Magnets	

61

from 9/16 to 15/16 inch to meet AEDC NSMS data range requirements.

5.2.1 AEDC Disk Spin Up and Spin Down Test

At the end of the standard test series that acquired response of the disk in its resonance modes, spin up and spin down tests were conducted for the AEDC NSMS one sensor method. Response amplitude of a disk accelerometer was monitored while the disk transited through resonance. Amplitude changes due to speed change in steps of 1 rpm on either side of resonance were recorded for the 2D, 3D and 4D modes. Phase change while the disk went through resonant speed was observed by monitoring the accelerometer output signal as triggered by the 1PPR signal. A smooth phase change of nearly 90 degrees was observed for the 4D mode when the magnet gaps were 3/4 inch. This data set was not acquired during the first test series due to nonlinear behavior of the disk.

5.3 UNEVEN PROBE POSITION TESTS: THIRD TEST SERIES

These tests were requested by the AEDC to verify the accuracy of an algorithm used by UTRC for uneven probe positions around the circumference of the bladed disk. Since large displacements were the prime concern, large excitation forces were achieved by placing the excitation magnets close to the disk.

After the test setup and data acquisition systems were prepared on August 23, eleven test runs as detailed in Table 7 were made on the following day. For each test, both the magnet and AEDC probe settings were changed to desired positions, and the test disk was quickly spun up to its resonance. Data were concurrently recorded by the ISRL NSMS with its probes at 60, 40 and 30 degrees for the 2D, 3D and 4D modes, respectively.

Holographic images for this test series were not recorded due to the film transport shutter malfunctioning.

TABLE 7

AEDC NSMS EVALUATION TESTS - THIRD TEST SERIES
UNEVEN PROBE POSITIONS
AUGUST 24, 1988

Date	Run #	Mode	Magnet Gap (Inch)	RPM	Data Type	Remarks
8/24	1C	4D	9/16	3648	Resonance Speed	ISRL and AEDC
8/24	2C	4D	9/16	3000	Reference Speed	Data Acquisition
8/24	3C	4D	9/16	3631	Resonance Speed	OK on ISRL
8/24	4C	3D	7/16	3600	Resonance Speed	No Data on AEDC
8/24	5C	3D	7/16	3000	Reference Speed 1	
8/24	6C	3D	No Magnets	3600	Reference Speed 2	
8/24	7C	4D	No Magnets	3631	Reference Speed 2 for Run 2C	
8/24	8C	2D	1/2	3000	Reference Speed 1	
8/24	9C	2D	1/2	4019	Resonance Speed 1	
8/24	10C	2D	1/2	4044	Resonance Speed 2	
8/24	11C	2D	No Magnets	4019	Reference Speed for Run 9C	

SECTION 6
NSMS DATA ANALYSIS PROCEDURE

6.1 DATA REDUCTION AND DATA ANALYSIS

The data reduction and analysis system used for the ISRL NSMS data of this effort is documented fully in (Ref. 15) UDR-TR-89-31, "Data Analysis Guide for the Noncontacting Blade Deflection Measurement System," by Thomas W. Held. This document is expected to be issued in the near future as an AFWAL Test Report. The data processing procedures are described briefly in the subparagraphs that follow.

6.1.1 NSMS Data Reduction Procedures for Stationary Wave Analysis

UDRI NSMS data reduction software was designed to run on a VAX computer. To perform data reduction analysis, the user stores test NSMS data on magnetic tape. The tape was then read on the UDRI VAX, and the data from the recorded runs were sorted and cataloged onto disk.

The user then processed these data for analysis and results-plotting. Terminal access to the VAX for these purposes was made through dialup connections from WPAFB or direct terminal connections at UDRI.

When a test disk was excited in a stationary wave mode on the disk, the NSMS system collected data for blade deflections at each of three plane-of-light detectors. These detectors were normally connected to NSMS system channels 2, 3, and 4. If each channel was working correctly, the user would get an independently complete set of data on each of the three channels, and he needed to process only one of these to analyze the specimen response.

For this type of test, the data reduction software first would read in the channel data and perform a statistical analysis of the data. The program then corrected the channel data for shaft speed variations and repeated the statistical

64

analysis. The correction was based on the following linear speed correction equation, developed by UDRI:

$$V_{Bik} = (R_{Bik} - M_{Bi}) - (R_{SLik} - M_{SLi})$$

$$+ F_i * [(R_{SLik} - M_{SLi}) - (R_{SHik} - M_{SHi})] \qquad (22)$$

Here:

V_{Bik} = Corrected data value for Blade i, at rev k.

R_{Bik} = Recorded reading for Blade i, at rev k.

M_{Bi} = Mean value for Blade i over all good recorded revs.

R_{SLik} = Recorded reading, at rev k, for the 16 ppr shaft encoder position immediately preceding Blade i.

M_{SLi} = Mean value over all good revs for the 16 ppr shaft encoder position immediately preceding Blade i.

R_{SHik} = Recorded reading, at rev k, for the 16 ppr shaft encoder position immediately following or coincident with Blade i.

M_{SHi} = Mean value over all good revs for the 16 ppr shaft encoder position immediately following or coincident with Blade i.

$F_i \quad = \dfrac{M_{Bi} - M_{SLi}}{M_{SHi} - M_{SLi}}$ = interpolation factor for Blade i.

The shaft encoder data were stored using the NSMS system channel 1.

6.1.2   <u>Time and Frequency Analysis</u>

After the preliminary reduction was completed, a printable report of the statistical analysis was generated. The program then created a time series for each of channels 2, 3, and 4 using the corrected data and then performed a frequency analysis.

The frequency analysis consisted of a Fourier analysis of the time series generated previously for one of the data channels. The program used an FFT routine from the ISML library to perform the Fourier analysis. The ISML library is a commercial mathematics and statistics software package and is available on both the UDRI VAX and the ASD SEWS ADA VAX.

As a final step, the data reduction software program writes to disk any requested time series data and results of the frequency analyses. These disk files can be used for plotting time series or frequency spectrum data.

6.1.3   UDRI NSMS Data Reduction Procedure for Traveling Wave Analysis

When a test disk is excited in a traveling wave mode on the disk, the NSMS system again collects data for blade deflections at each of the three plane-of-light detectors. For this test mode, however, the user needs results from each of the three NSMS data channels to generate an appropriate time series for the vibration analysis. Also, an additional low-response test run is required to generate a nonvibrating reference data set for the specimen's magnet-transducer configuration. The remaining system channel is used, as before, to collect the 16 ppr shaft speed variation correction data.

For the traveling wave test, the nonvib data set is first analyzed and processed as described previously. The data is corrected for shaft speed variations, and for channels 2, 3, and 4, the scaled mean of each blade's passage time count is stored. That is, the mean of a blade's passage time reading over all good recorded revs is divided by the mean 1 pulse per rev count value (1PPR) for the nonvib run. Since the nonvib run and its corresponding vibration run are made at different shaft speeds, the mean 1PPR values will be different between the two data sets and their ratio can be used to predict the nonvib reference value of each blade at the test condition rpm of each rev.

66

In the next step, the traveling wave data reduction software reads in each channel's data from the vib data set. The program performs a statistical analysis of the raw data. The program then corrects channel data for shaft speed variations and repeats the statistical analysis. The corrected data for each of the three data channels then is referenced to the nonvib data mean for each blade as adjusted for the rev speed difference. These corrected differential time of arrival values are converted to deflection values and then are incorporated into time history data sequences for the FFT frequency analysis procedure, as in the stationary wave analysis.

## 6.2 APPLICATION OF UDRI SOFTWARE FOR AEDC TEST SERIES

6.2.1 ISRL NSMS Data Analysis for the First Test Series

During the test runs for evaluation of the AEDC NSMS, data was recorded after the test disk had stabilized in resonance in the excited 2D, 3D, or 4D mode.

At the time (mid-April) that the data were recorded for the AEDC NSMS evaluation, UDRI was using a mathematical library subroutine which used an FFT analysis to calculate the PSD of the recorded data set. This subroutine produced frequency spectrums of the data signals that were nearly identical to those seen on the screen of the spectrum analyzer but containing scaling errors in the spectrum (blade deflection) amplitudes. During late April and early May, UDRI wrote a data reduction program to generate the Fourier coefficients of the blade deflection response spectrum, also based on the FFT algorithm.

The first 200 raw data input readings (blade deflections readings corrected for rotational speed variations) for two gaps are shown in Figures 32 and 33 for the 3D mode. The spectral plots generated by the new data reduction program for the time-series data listed in Table 5 are shown in Figures 34 and 35. Each complete data set consists of 9 readings per rev for 500 revs of data, with the remainder of the data set looking

Run 03A, 3-D, 12-Apr-88
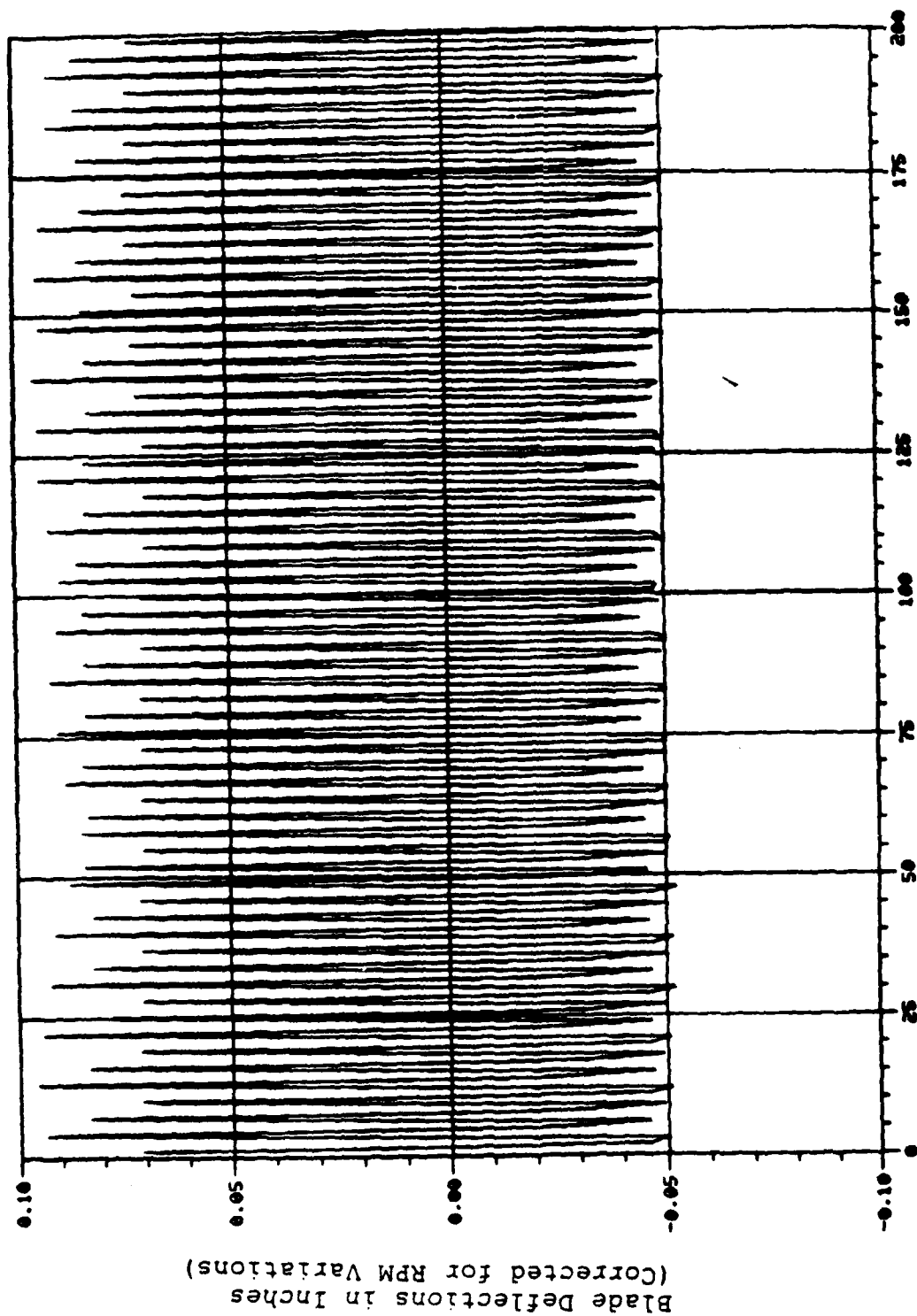
Time Series of 200 Data Readings

Figure 32. Corrected Time Series Data for 3D Mode - 5/16-in. Gap - First Test Series.

68

Figure 33.   Corrected Time Series Data for 2S Mode –
7/16-in. Gap – First Test Series.
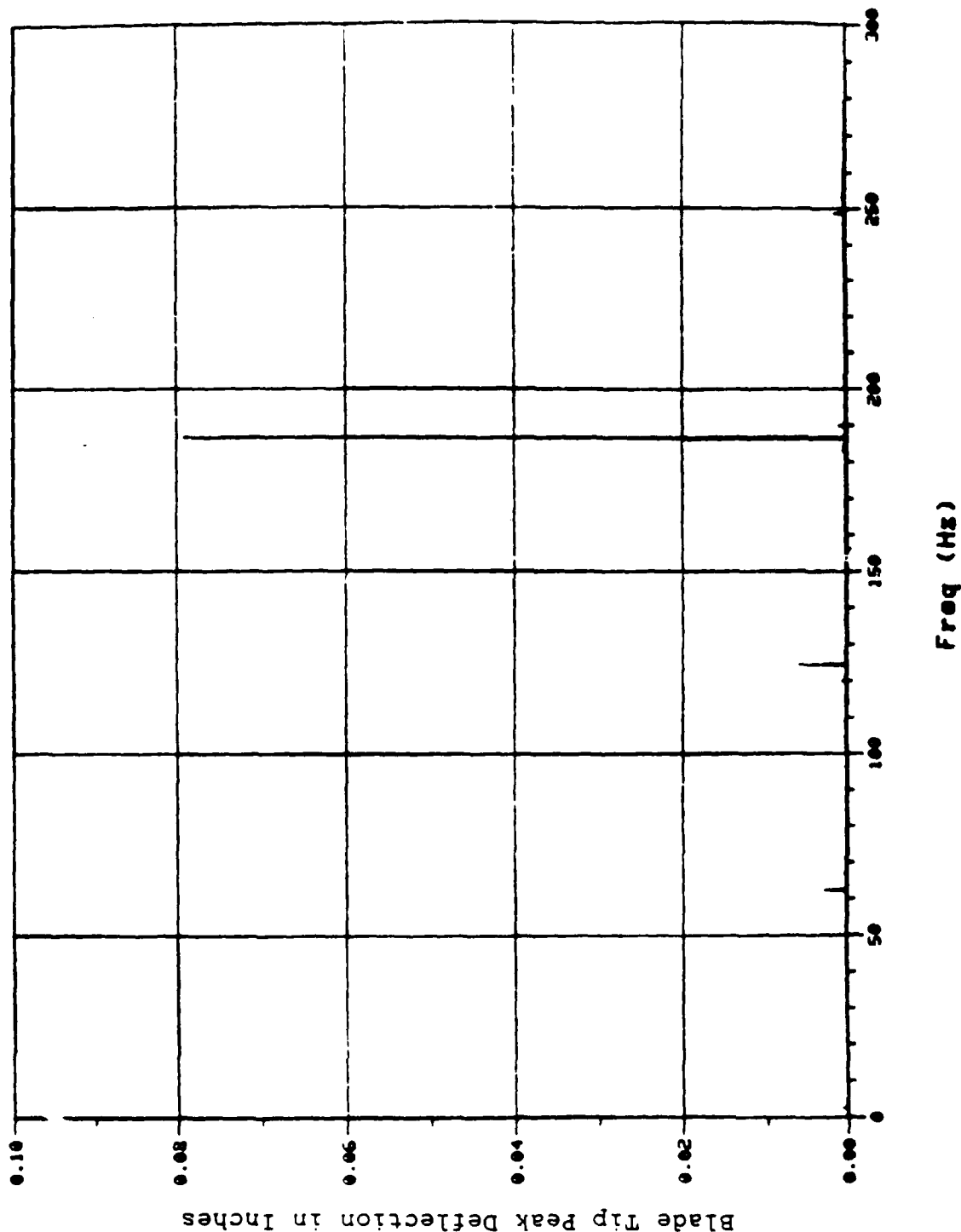
Figure 34. Fourier Components for the 3D Corrected Data Set – 7/16-in. Gap – First Test Series.
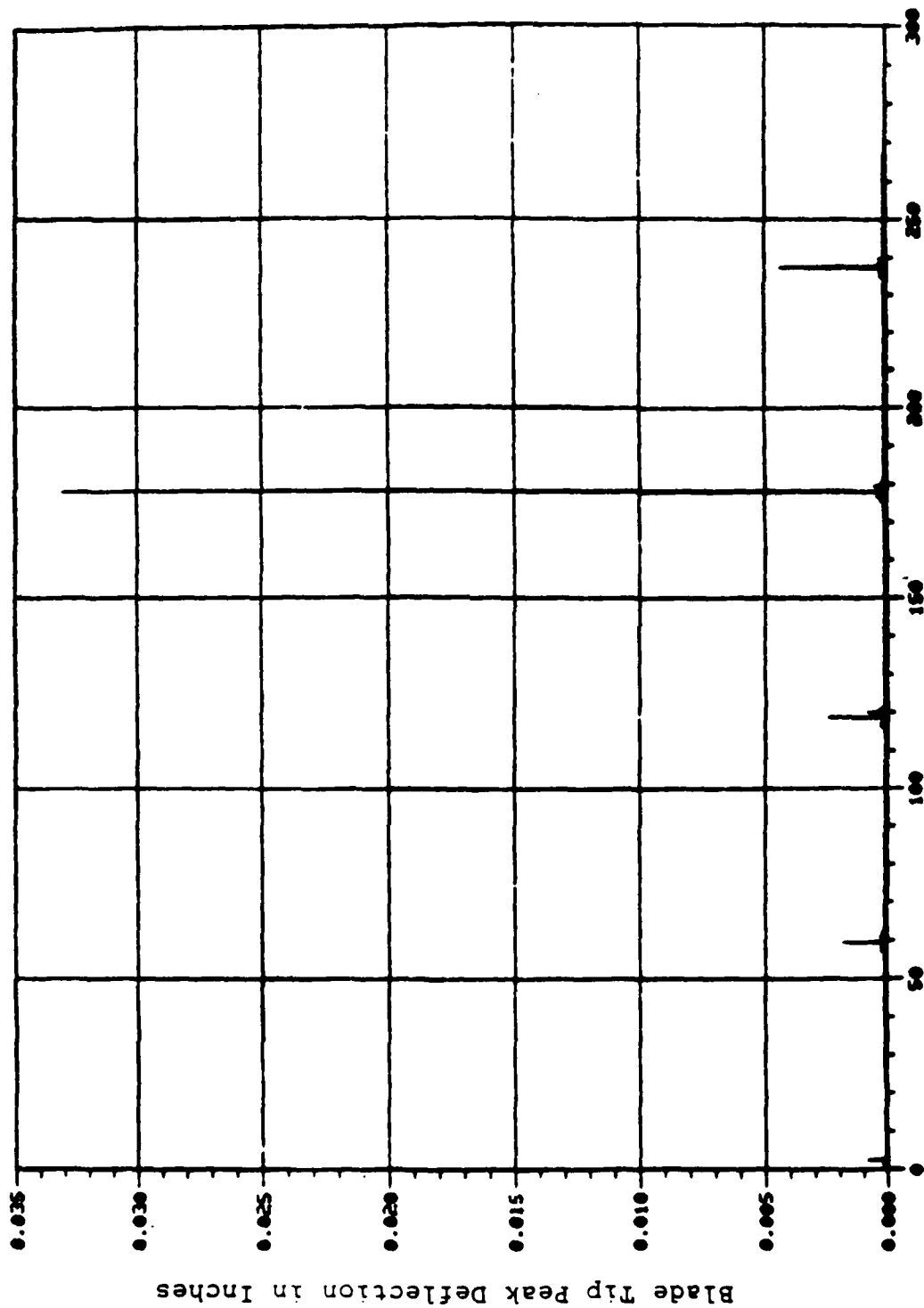
Figure 35. Fourier Component for the 3D Corrected Data Set –
5/16-in. Gap – First Test Series.

71

almost exactly like the first 200 readings. By comparing Figure 32 with Figure 34 and Figure 33 with Figure 35, the peak blade amplitudes agree very well in the two data sets at the predominant 3D mode. Note that the zero amplitude in the input data sets (Figures 32 and 33) is the statistical mean of the data, and the apparent data peak-to-peak offset is due only to the location (phasing) of the three optical plane-of-light transducers with respect to the fixed response mode in space (backward traveling wave on the disk) produced by the permanent magnet excitation system. This phasing is immaterial to the data reduction algorithm, and the half-amplitude spectrum peak in the 3D mode data of Figures 34 and 35 agrees very well with the blade input data positive amplitude peaks, which are obviously produced by data reading taken very near in phase to blade peak deflections. The variation in blade to blade amplitudes and in rev to rev amplitudes for each blade are the major sources of the minor data peaks shown in Figures 34 and 35 at the other integral modes of the test disk. These variations also are the likely cause of the nonlinear response of the disk indicated by the spreading of the resonance peaks over a fairly wide disk speed range until the resonance collapses abruptly when the highest resonance frequency is exceeded. This mistuning of the disk is likely very high because of the mass and stiffness variations around the disk due to the on-disk instrument installations.

6.2.2. ISRL NSMS Data Analysis for the Second Test Series

The ISRL NSMS recorded data for each of the test conditions in this test series. Resonance data for 500 revs at resonance rpm followed by reference data at 3,000 rpm were recorded for all test runs, and for the run 20B/22B an additional 2D resonance data set at 4,058 rpm also was recorded with a reference data set recorded at 4,058 rpm after removal of the excitation magnets. Data reduction programs were used to determine the Fourier coefficients of blade deflection time histories for the 500 rev data records and typical spectral plots

for half amplitude of response are shown in Figures 36 through 38 for Run 10B. Speed-corrected blade deflection times series data for the first 200 data points of this test are shown also in Figures 39 through 41.

In the present data reduction efforts, four sets of blade arrays were analyzed for each test run and produced nearly identical response spectrums. Data differences are attributed to mistuning of the disk. Blade peak deflection levels seen in the time series data of Figures 39 through 41 are nearly the same as those found at the resonance frequencies of the spectrums (Figures 36 through 38).

6.2.3   ISRL NSMS Data Analysis for the Third Test Series

The ISRL NSMS data were analyzed for these test runs. Data reduction programs were used to determine the Fourier components of blade deflections. Four sets (nearly symmetrically located blades) were considered in the analysis to determine the peak modal displacement of blade tips. The results from the ISRL analysis, presented in Table 12, showed less peak-to-peak amplitude of vibration than was expected for the imposed excitation forces. We believe this anomaly is because the disk had not stabilized in resonance. Previous experience had demonstrated that the disk required several small speed increments to reach stable resonance speed. A quick 1-day attempt to complete all 11 test runs yielded less than peak resonance values for the modal displacements because that procedure was not followed. The spectral components of displacements for these test runs can be seen in Figures 42 through 44.

6.3   INTERFEROGRAM FRINGE ANALYSIS

Double exposure interference fringes were interpreted to yield net whole field displacements of the resonating disk, following the calculation method described in Section 4.5.

73
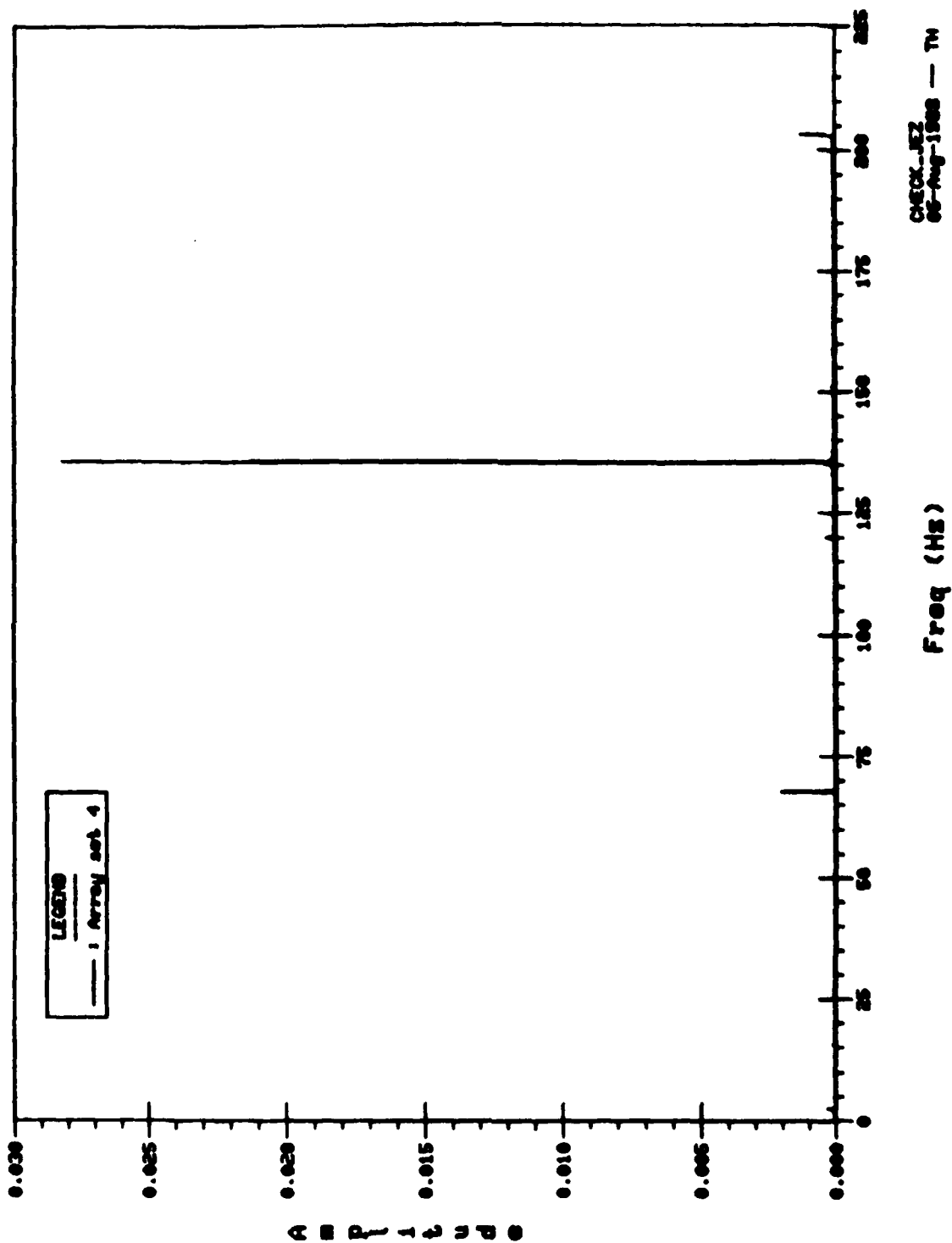
Figure 36. Fourier Components for the 2D Mode - Second Test Series.

74
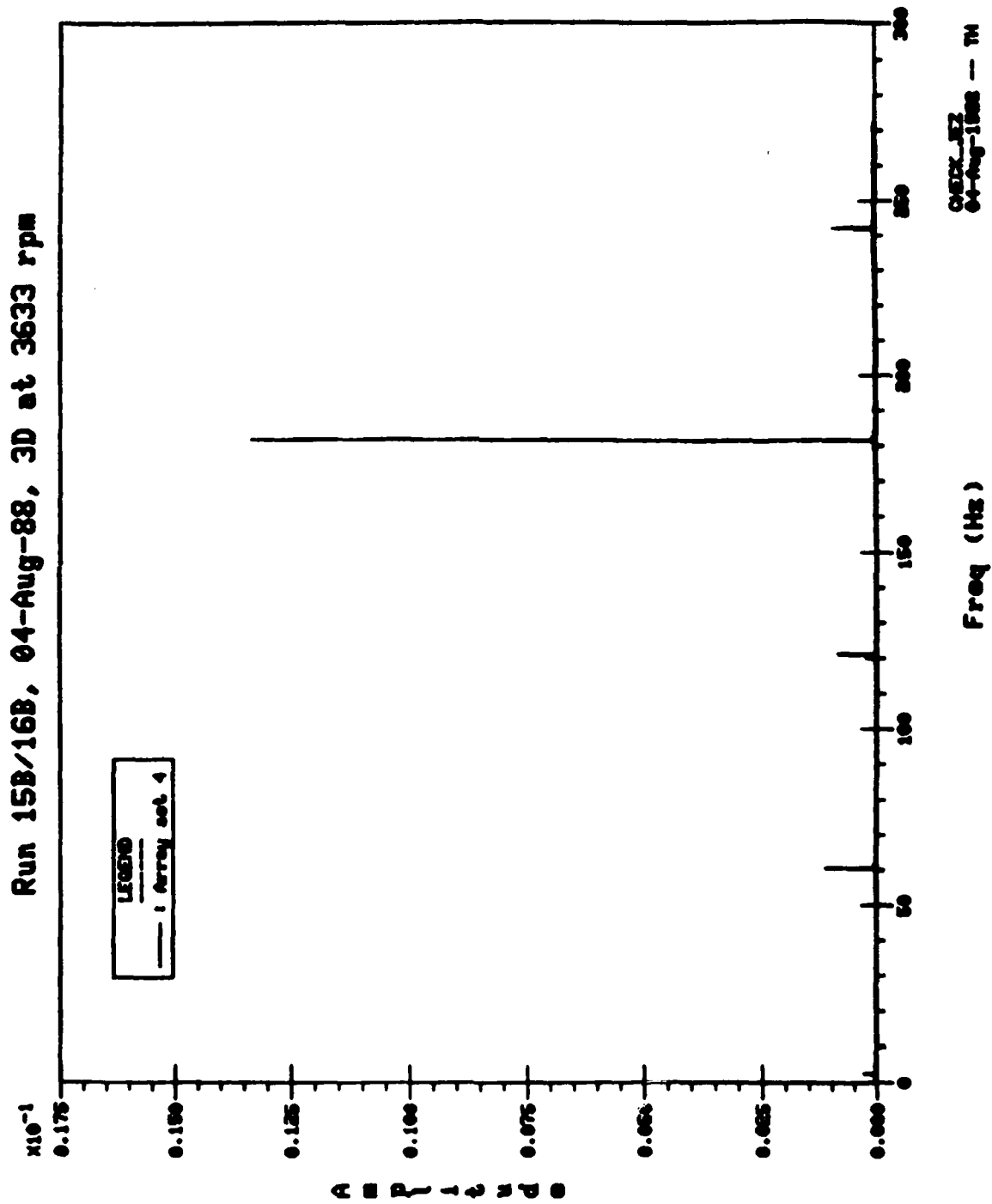
Figure 37. Fourier Components for the 3D Mode - Second Test Series.
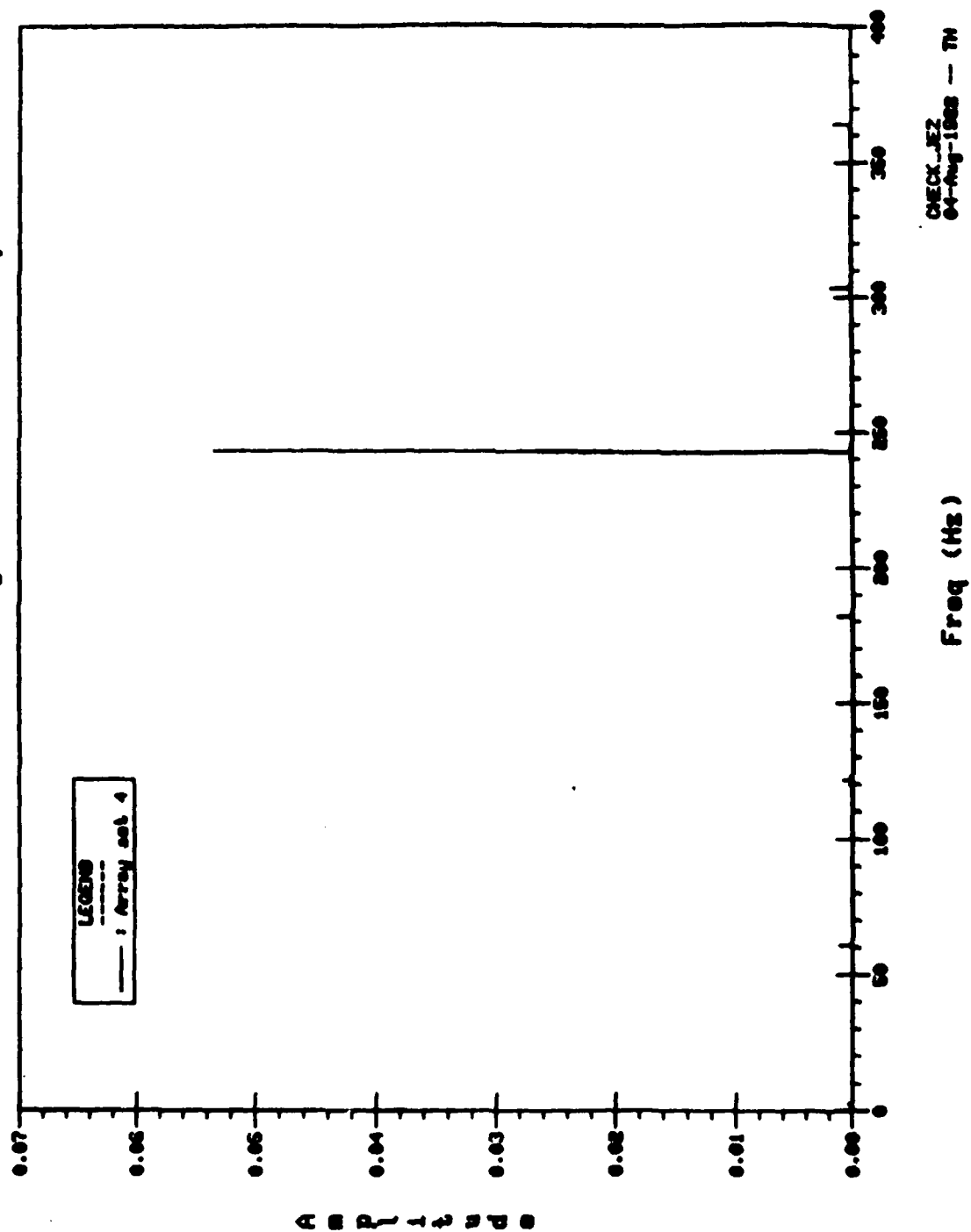
Figure 38. Fourier Components for the 4D Mode - Second Test Series.
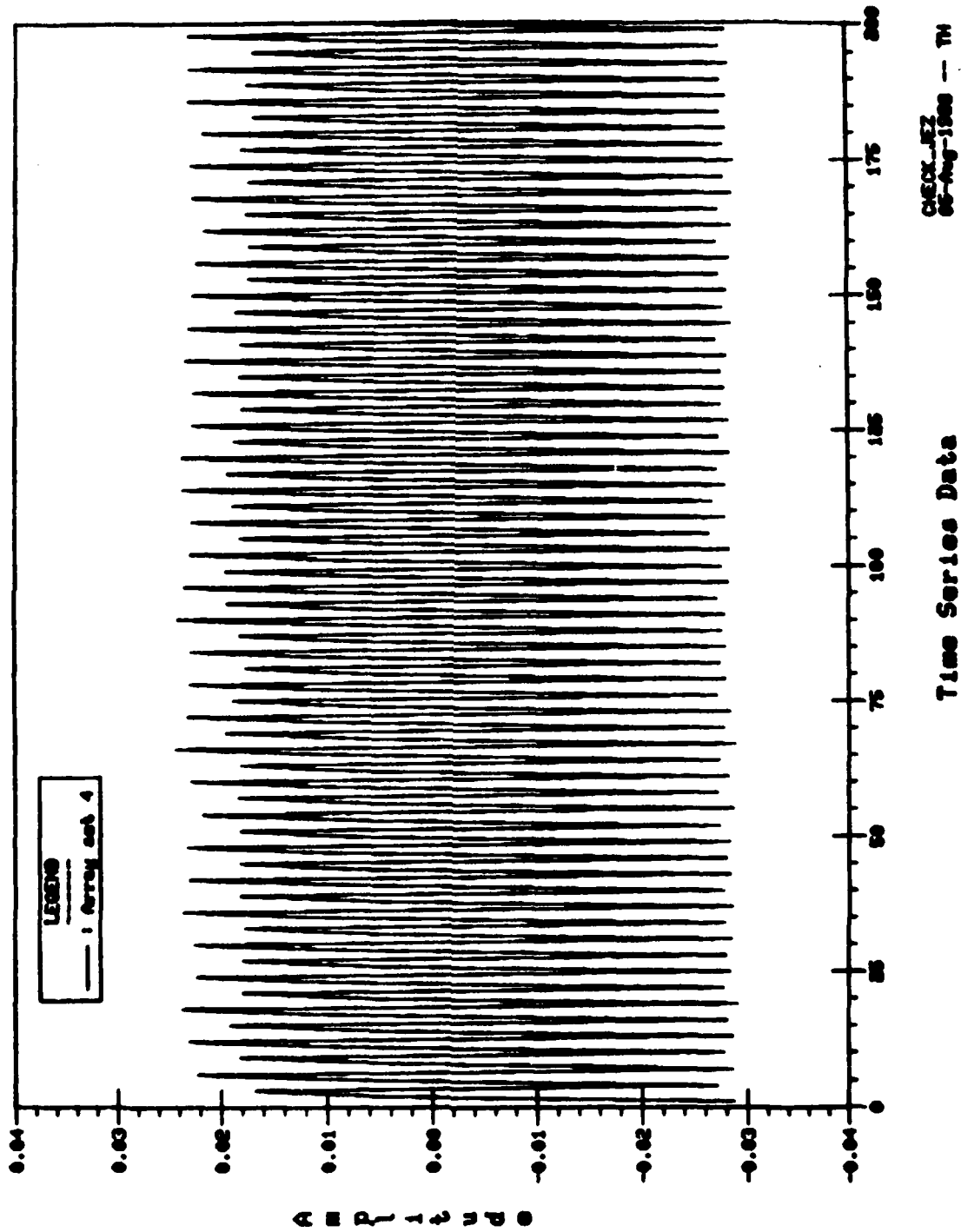
Figure 39.   Time-Series Data for the 2D Mode - Second Test Series.

77

Figure 40. Time-Series Data for the 3D Mode - Second Test Series.
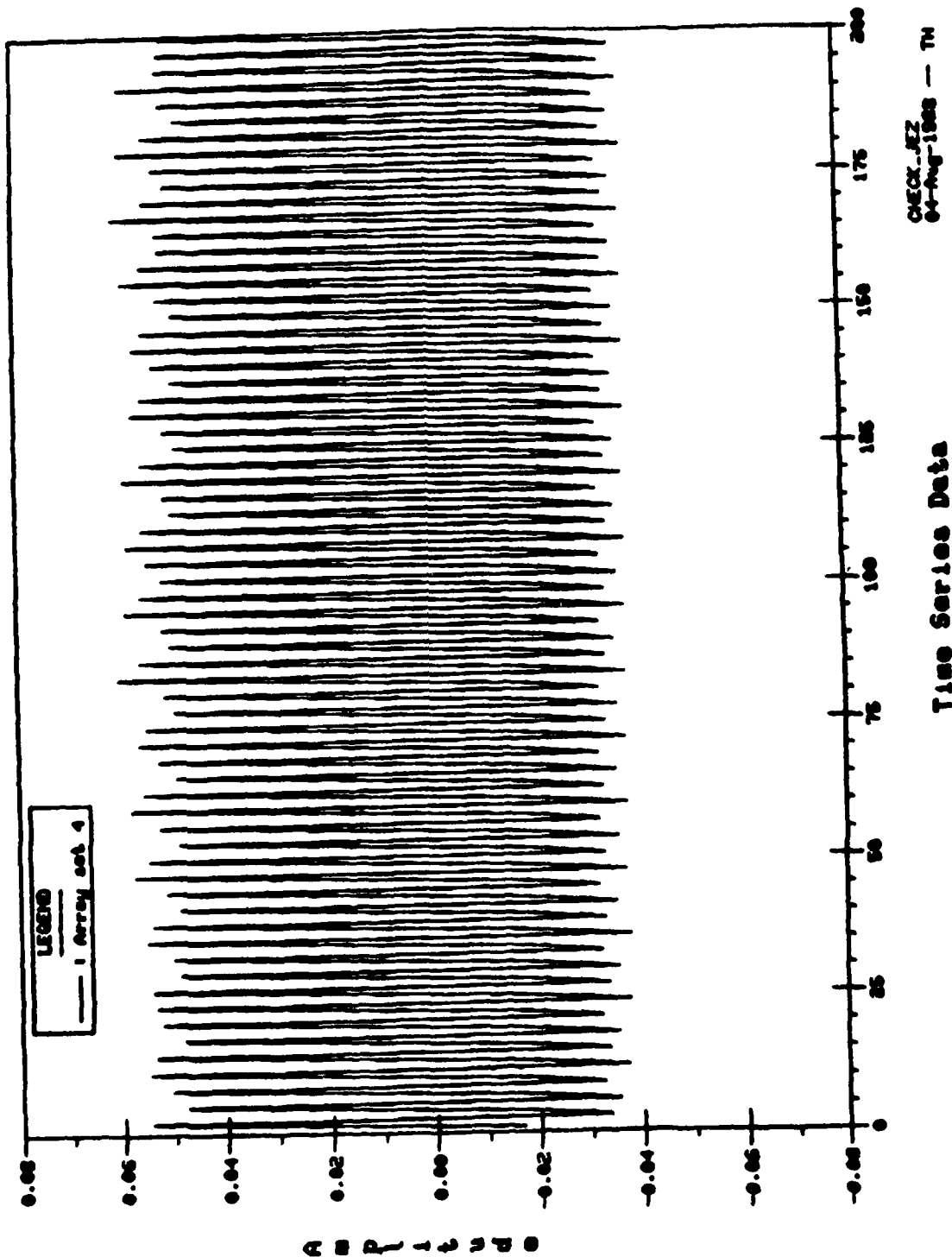
Figure 41. Time-Series Data for the 4D Mode - Second Test Series.
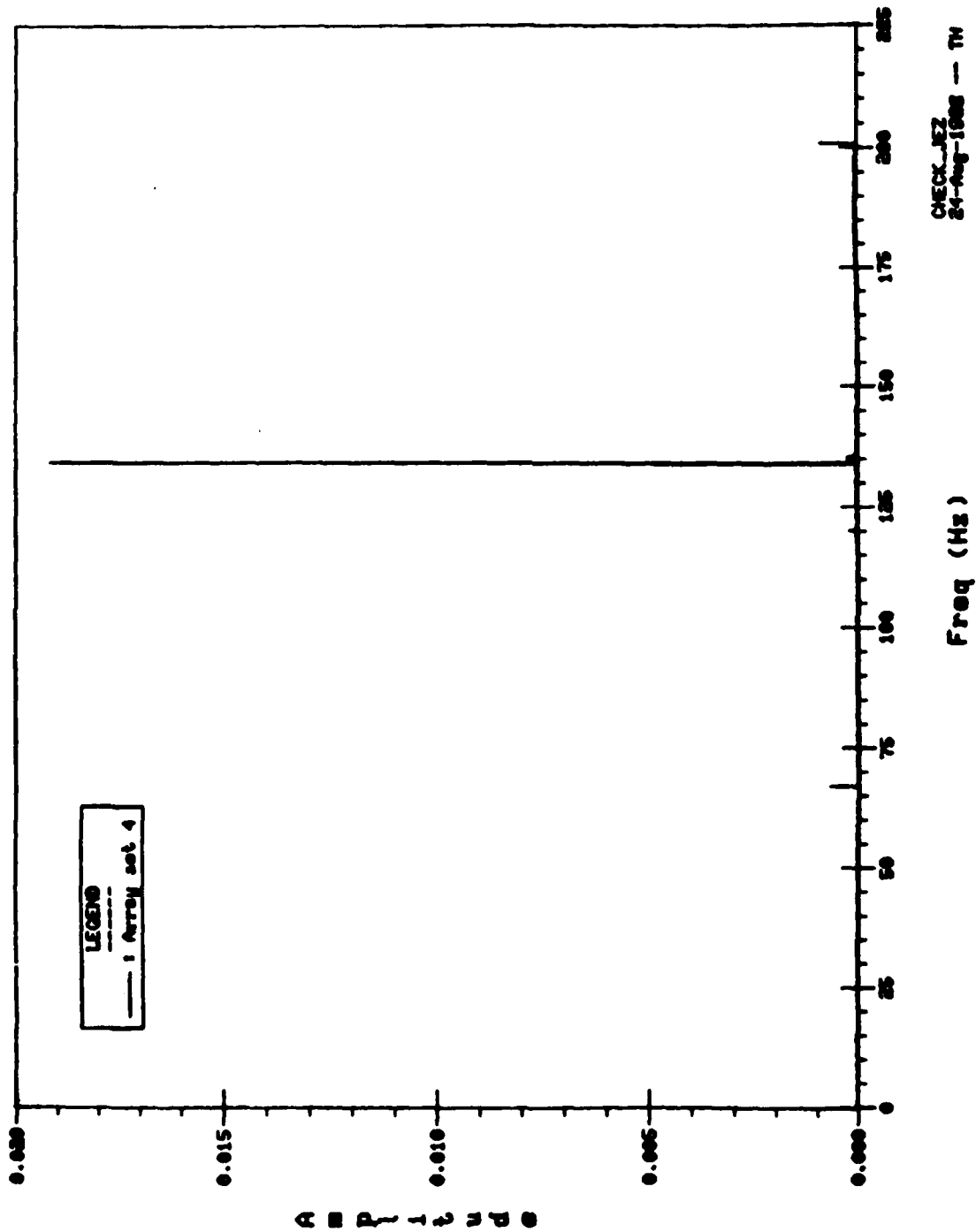
Figure 42. Fourier Components for the 2D Mode – Third Test Series.
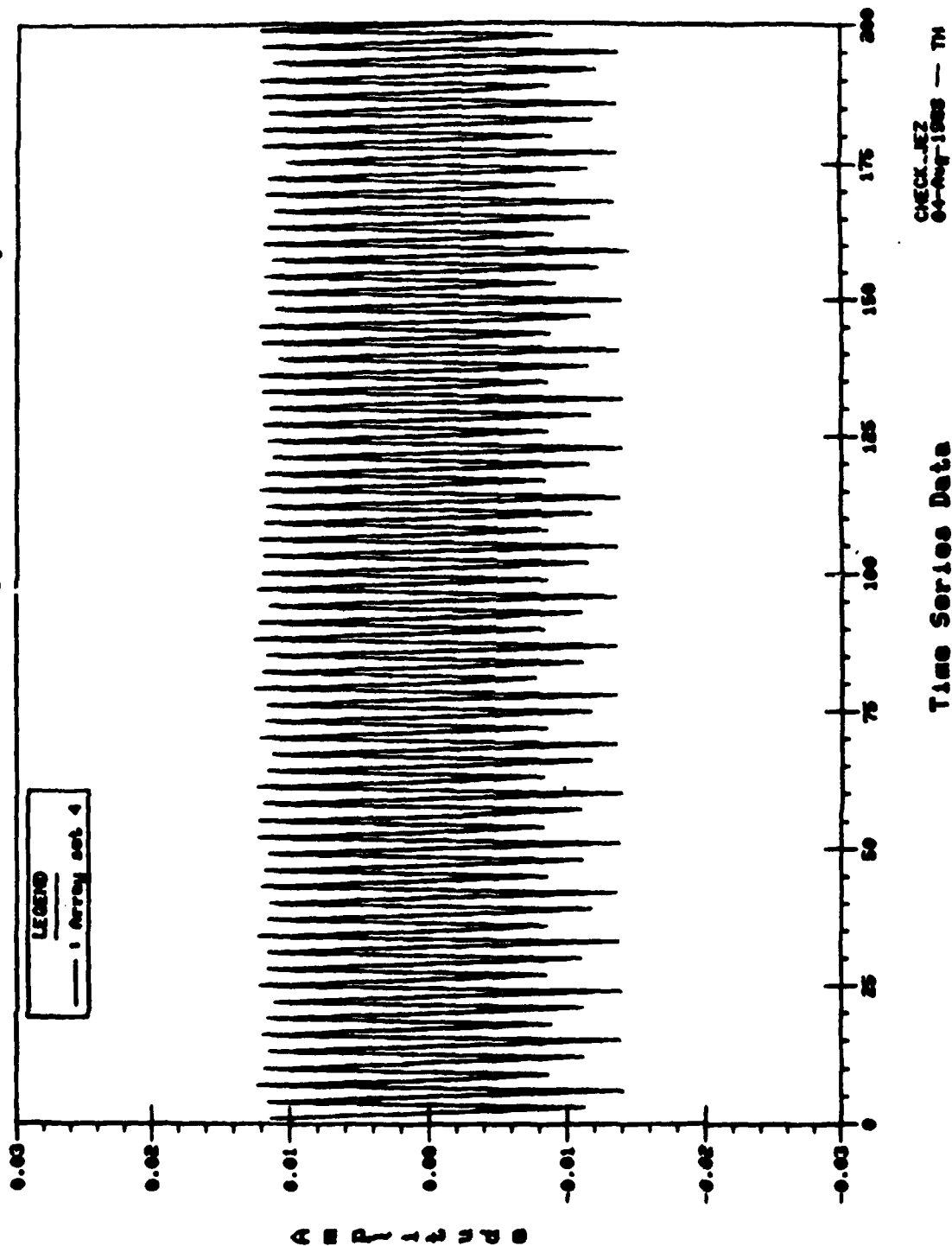
Run 04C/05C, 24-Aug-88, 3D at 3600/3000 rpm
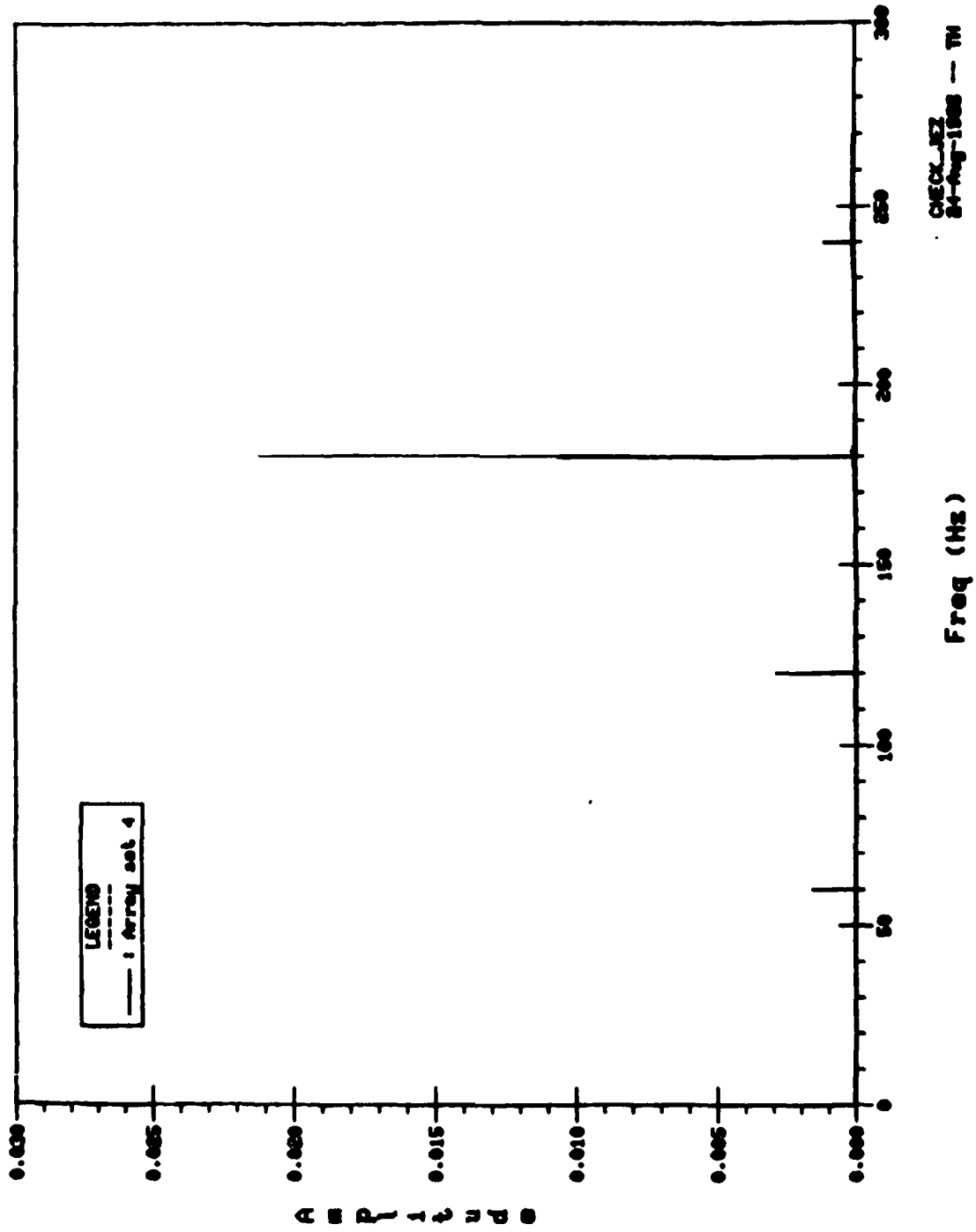
Figure 43. Fourier Components for the 3D Mode - Third Test Series.

81
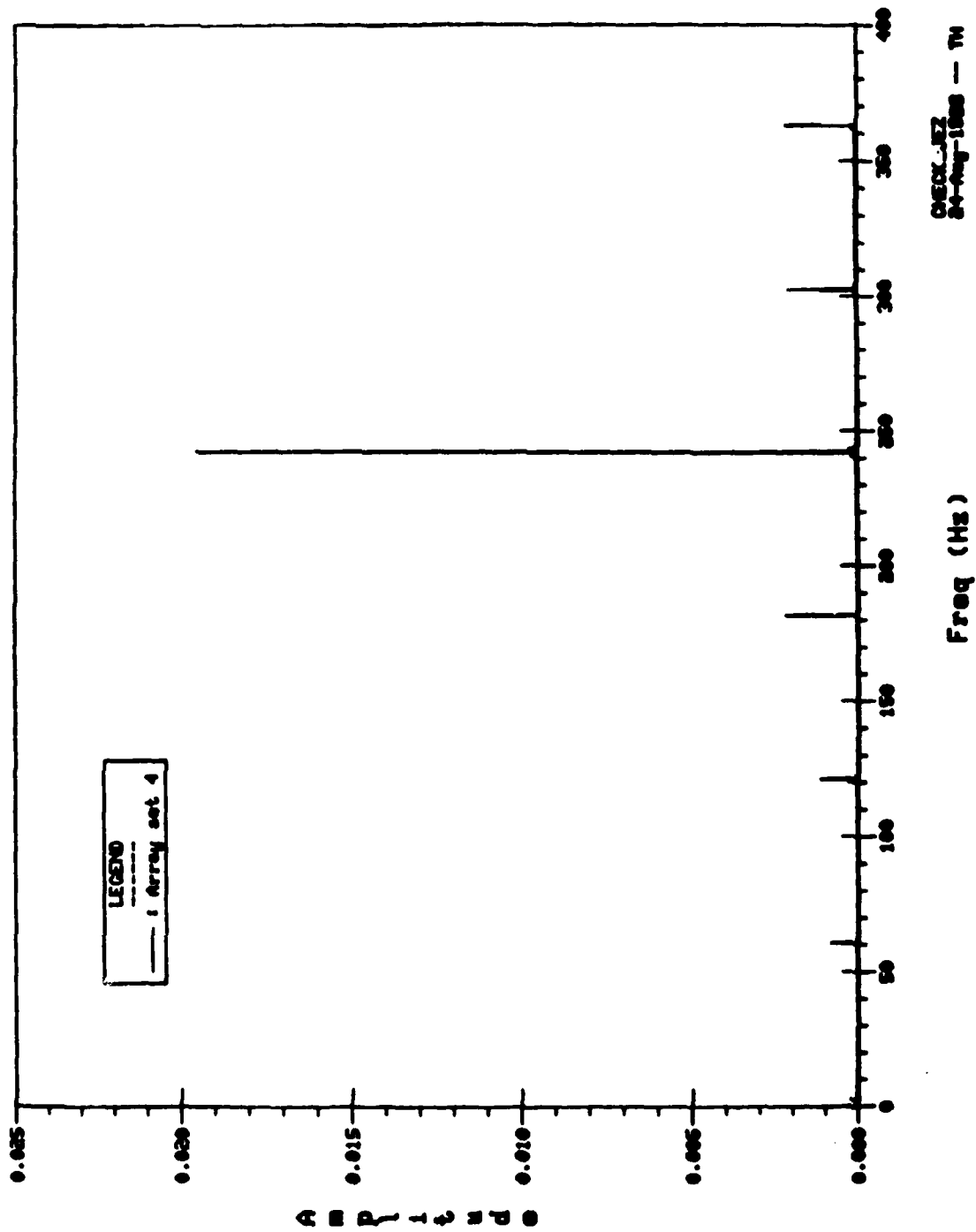
Figure 44. Fourier Components for the 4D Mode - Third Test Series.

Sample calculations of peak-to-peak out-of-plane displacement are provided here for illustration.

Peak-to-peak amplitude of vibration, 2A is

$$2A_{iD} = \frac{(2n-1)\lambda}{2 \sin 2\pi \, f_{iD}(\Delta t) \; \cos \alpha} \qquad , \; i = 2, \, 3, \, 4 \; .$$

In our experiment, $\qquad \lambda = 694 \times 10^{-9}\,m$

$$\Delta t = 10 \; \mu seconds$$

$$\alpha = 34.92°$$

$$f_{2D} = 135.4 \; Hz$$

$$f_{3D} = 182.0 \; Hz$$

$$f_{4D} = 243.0 \; Hz$$

Then $\qquad\qquad 2A_{2D} = 3.9025 \; \frac{2n-1}{2} \; mils$

$$2A_{3D} = 2.9138 \; \frac{2n-1}{2} \; mils$$

$$2A_{4D} = 2.1823 \; \frac{2n-1}{2} \; mils$$

The above equations present the scaling factors to be used for conversion of interference fringes to maximum deflection in mils for the cases when hologram pulse interval time was 10 μseconds. They were calculated assuming the sine equal to the angle in radians for these small angles. They can be scaled to other pulse intervals by dividing the scaling constant by 0.1 x Δt in μseconds for any of the three modal vibration patterns used in the test series.

Some selected double pulse interferometry results are presented for comparison with UTRC and ISRL NSMS results in Table 16.

SECTION 7
RESULTS AND DISCUSSIONS

This test program was designed to evaluate noninterference vibration measurement systems for defining the modal characteristics of an 11-inch-diameter 50-mil-thick test disk while the disk was excited in its diametral modes.

7.1 COMPARISON OF NATURAL MODES OF THE STATIC DISK

The zero speed normal mode data were first determined from static bench tests and were compared with the normal mode analysis data from the NASTRAN finite element method. Comparing the experimental and analytical results presented in Table 8, we would notice that the experimental frequencies were lower than the analytical values for all diametral modes considered. This discrepancy varied from 4 to 8%, and the errors in modal frequencies are essentially due to (1) the simplistic analytical assumption of infinite rigidity for the multi-channel

TABLE 8

COMPARISON OF ANALYTICAL AND EXPERIMENTAL FREQUENCIES (HZ)
OF 11-IN.-DIA. AND 50-MIL-THICK STATIC TEST DISK
WITH AND WITHOUT 2.0-INCH-DIA. HUB SLIP RING

| Mode | Without Slip Ring | | With Slip Ring* | |
	Analysis	Experiment	Analysis	Experiment
1D	58.2	58.0	80.5	-
UC	69.6	64.5	83.9	.
2D	84.4	82.0	100.4	95
3D	161.8	147.0	165.1	148
4D	244.0	219.0	244.6	215

*And with 0.1 inch thick hub stiffner

slip ring assembly over the 2 inch diameter hub surface area, and (2) large concentrated mass near the disk rotational axis. These two parameters were not modeled in the analysis. The slip ring unit and its mass effect contributed to lowering the natural frequencies of the static disk.

Mode shapes of the stationary disk have been recorded by the time-averaged holographic method and good correlation between the predicted and measured modes is shown by Figures 45 a-d. With increase of excitation force, we observed fringe increase and its travel toward the center of disk. This effect indicated the sensitivity of disk flexibility to excitation force and its effect became more apparent in rotating tests.

7.2 COMPARISON OF THE TEST DISK CRITICAL SPEEDS

Spin tests were conducted to establish the disk critical speeds. As explained in Section 5, these speeds were observed to be dependent on the excitation force magnitudes. A comparison for these speeds was provided only when the disk exhibited elastic response. Linear response of the disk was achieved with the excitation magnets installed with gaps from the disk surface of 9/16 inch or greater. The analysis and experimental results are summarized in Table 9. Measured critical frequencies for the second and third diametral modes provided excellent agreement

TABLE 9

NATURAL FREQUENCIES (HZ) OF 38 BLADED DISK WITH 2.0-INCH-DIA. HUB SLIP RING AT ZERO RPM AND AT CRITICAL SPEED

Mode	Zero Speed		Critical Frequencies (Speeds) in RPM	
	Analytical	Experimental	Analytical	Experimental
2D	100.4	95	132 (3950)	135 (4058)
3D	165.1	148	185 (3640)	184 (3670)
4D	244.6	215	246 (3700)	251 (3760)

85
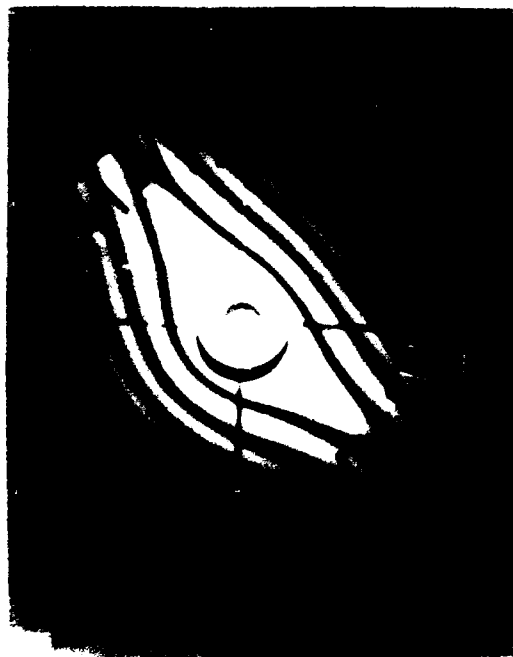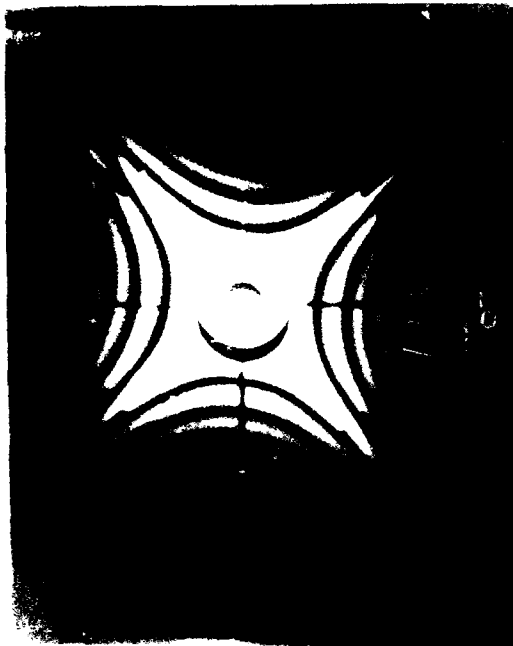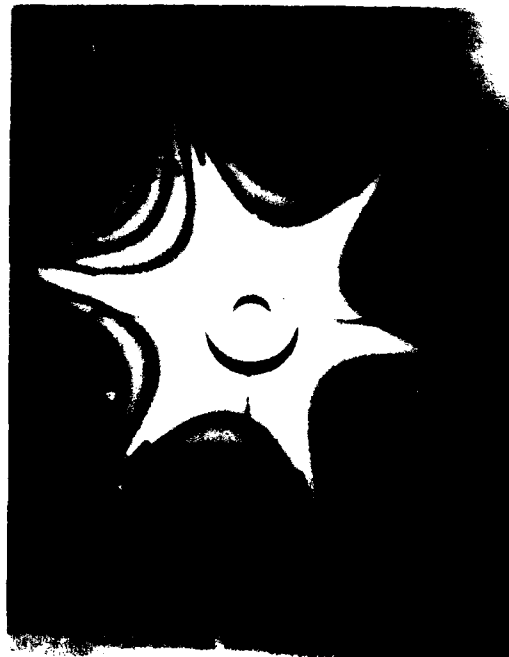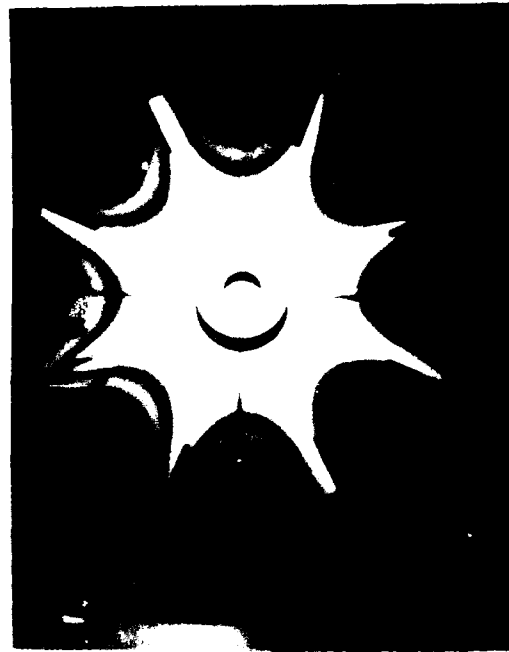
Figure 45. Analytical and Experimental Mode Shapes
of the Static Test Disk.

2D Mode – 87 Hz

4D Mode – 216 Hz

1D Mode – 65 Hz

3D Mode – 150 Hz

between the prediction and measurement. An error of 1.5% was noticed. An error of 5.5 % for the fourth mode was present. Measured frequencies were lower than the analytical frequencies and the error was possibly due to the over-estimation of centrifugal force effects for the disk with the rigid mass at the hub. Critical speed for the 1D mode was not measured because the lower branch of the traveling wave would intersect the speed axis much farther to the right, yielding very high critical speed. We decided not to run the tests at this high rotational speed.

7.3 MODE SHAPE ANALYSIS

For mode shape definition of the rotating disk, double pulse interferograms were made when the disk was in resonance. Figure 46 shows typical patterns for the 2, 3, and 4 diametral modes of the test disk for two excitation cases. These deflection patterns were recorded for 15- and 10-μs pulse separations. The recorded vibration had occurred in these time intervals of the harmonic wave. The increase in the number of fringes for a longer time-duration was evident, and typical interferograms for 10 and 15μs pulse separations are shown in Figure 47.

7.4 BLADE TIP DEFLECTIONS

Maximum deflections at the blade tips were determined from (a) point-wise measurements from AEDC and UDRI NSMS-Systems, and (b) wholefield interferogram data recorded when the disk had stabilized in resonance.

A summary of results analyzed by the UDRI NSMS data analysis software for the first, second, and third test series is provided in Tables 10, 11, and 12 respectively. In our analysis procedure, symmetrical arrays of blades were considered for 3 probe data. Software constructed time series data and FFT components of the data series yielded nearly identical peak-to-peak amplitude of vibrations for blade tips of the resonating test disk. Two, 3, and 4D modes for all excitation test conditions were analyzed.
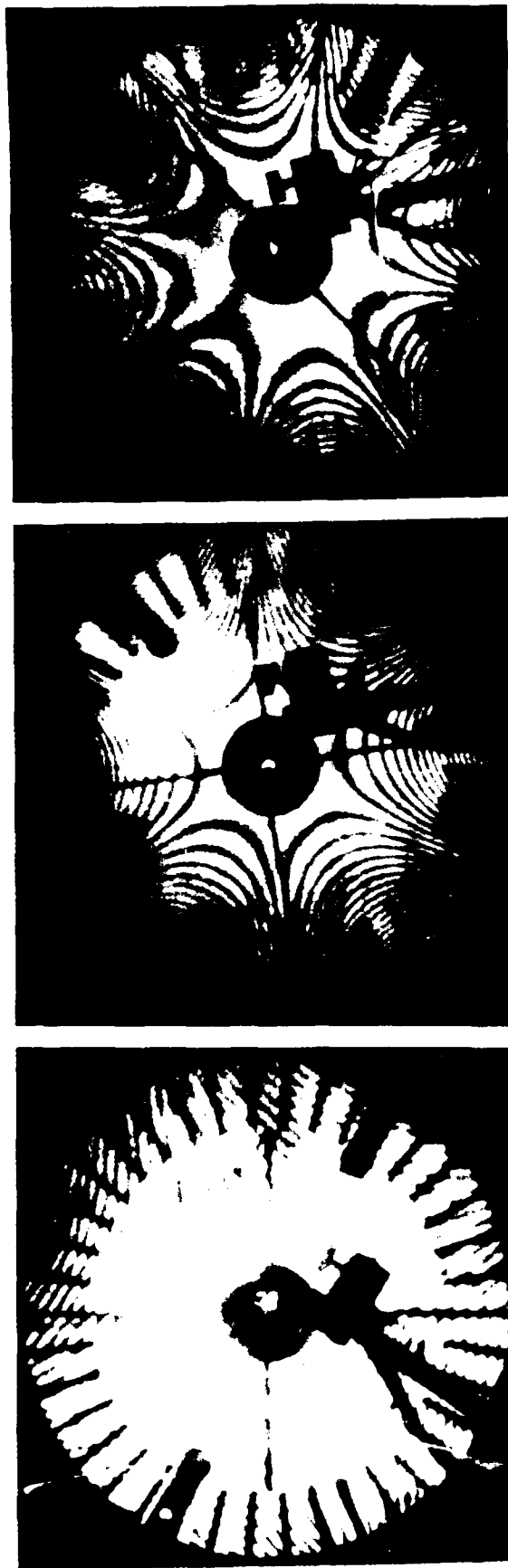
n	2D	3D	4D
N	4058	3642	3647
a	15/16	5/8	5/8
t	15	10	10

n = Mode   N = Critical Speed (RPM)
a = Magnet Gap (inch)   t = Pulse Separation (microseconds)

Figure 46. Interferograms for 2, 3, and 4D Modes of the Rotating Disk.

15μs
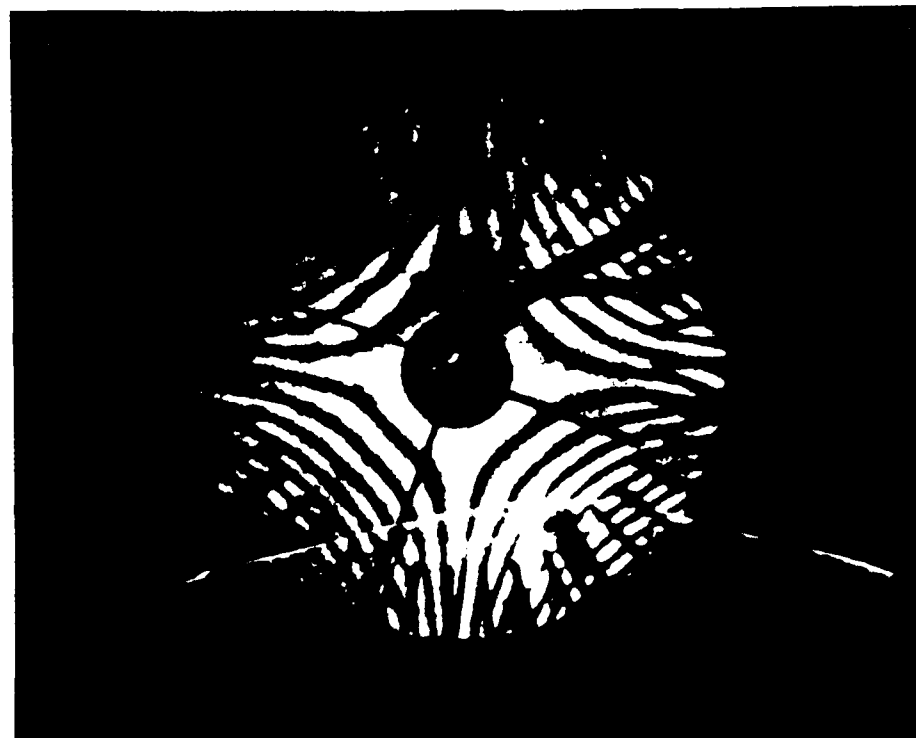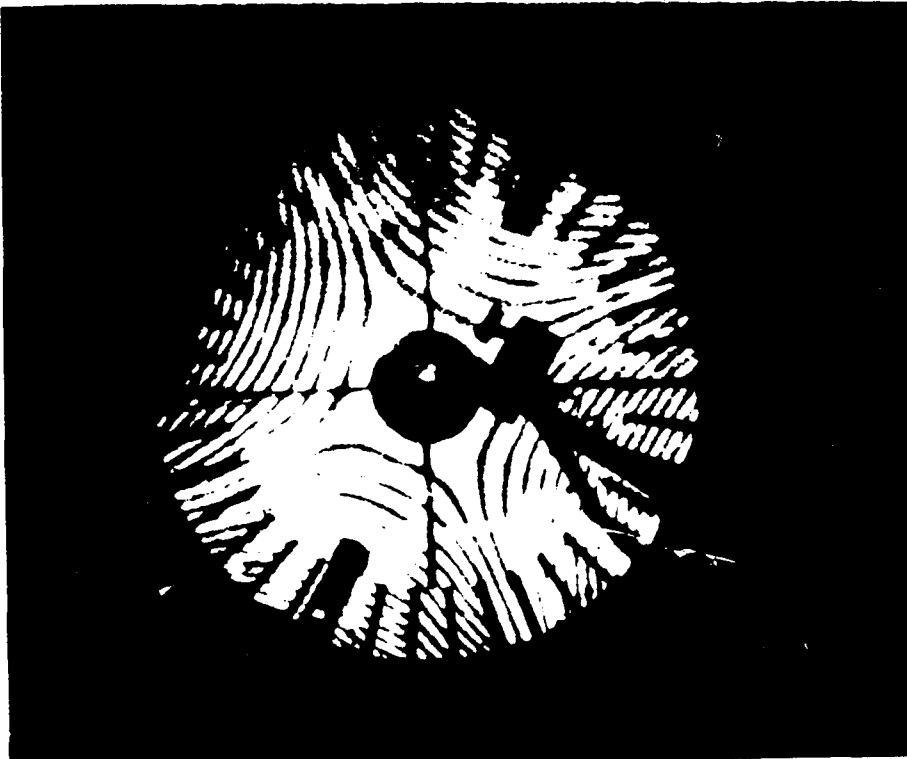
10μs

Figure 47. Interferograms for 2D Mode of the Rotating Disk
for 10 and 15 μs Pulse Seperation.

TABLE 10

BLADE TIP DEFLECTIONS (P-P)
CALCULATED FROM ISRL NSMS DATA
FOR THE FIRST TEST SERIES

Mode	Gap (in.)	Speed (rpm)	UDRI (p-p in mils)
3D	7/16	3720	110±2
3D	7/16	3560	52±2
3D	5/16	3732	160±4
2D	5/16	3970	No Data
2D	7/16	3780	176±5
4D	7/16	3630	62±2

AEDC analysis yielded results only for the first and second test series, and a summary of test conditions and results are provided in Tables 13 and 14. No results were obtained for the third test series because of a malfunction in the AEDC data acquisition system. The AEDC software computed blade tip deflections, and Tables 13 and 14 contain a range for blade tip deflections for each test condition. The first test series yielded large vibration amplitudes because the excitation magnets were located close to the test disk.

The wholefield deflection patterns for the test disk were recorded by double pulse interferograms and the interferogram fringes were interpreted to determine maximum displacements at blade tips. A calculation procedure described in Section 4 was used for this purpose. Peak-to-peak amplitudes were evaluated based on pulse width separation time compared to the disk response frequency. AEDC and UDRI independently calculated blade tip displacements from the recorded interferograms, and these

90

TABLE 11

BLADE TIP DEFLECTIONS (P-P)
CALCULATED FROM ISRL NSMS DATA
FOR THE SECOND TEST SERIES

Res/Ref. Data Record	Resonance RPM	Magnet Gap (Inch)	Mode	Mils Defl. - P-P*
1B/2B	3648	5/8	4D	25.5 ± 3.1
3B/4B	3646	3/4	4D	15.1 ± 2.7
5B/6B	3640	3/4	4D	19.5 ± 1.3
7B/8B	3644	5/8	4D	22.4 ± 2.1
9B/8B	3636	5/8	4D	18.0 ± 3.7
10B/8B	3648	5/8	4D	25.5 ± 2.0
11B/14B	3642	5/8	3D	44.5 ± 2.6
12B/14B	3632	5/8	3D	34.7 ± 2.5
13B/14B	3646	5/8	3D	45.9 ± 2.5
15B/16B	3633	3/4	3D	27.8 ± 1.8
18B/17B	3642	9/16	4D	108.3 ± 2.3
19B/21B	4063	15/16	2D	53.1 ± 3.1
19B/22B	4063	15/16	2D	51.7 ± 1.6
20B/21B	4058	15/16	2D	33.3 ± 2.0
20B/22B	4058	15/16	2D	30.2 ± 1.9

*Deflection Values are the Mean and the Dispersion of Results from Four Data Reduction Runs Using Different Blade Array Sets for the Input Time History Data.

TABLE 12

BLADE TIP DEFLECTIONS CALCULATED FROM ISRL NSMS DATA FOR THE THIRD TEST SERIES

Mode	Resonance Speed(rpm)	Gap (inch)	Peak-Peak Amplitude (mils)
4D	3631	9/16	30 ± 2
3D	3600	7/16	50 ± 3.0
2D	4019	1/2	38.3 ± 1.5
2D	4044	1/2	41.5 ± 0.5

results are included in Tables 14 and 16. A comparison of these results for selected test runs is provided in Tables 15 and 16. A range for blade deflections was defined by counting the number of fringes in different sectors of the 2, 3 and 4D integral order mode shapes. Reasonable agreement was found between AEDC and UDRI interferometric fringe analysis and between the interferometric and NSMS deflection data.

7.5 TRAVELING WAVE MODE SHAPE CHARACTERISTICS

For mode shape definition, holograms of the resonating disk were made. Figure 46 shows three such modal patterns corresponding to 2, 3, and 4 diametral modes. Two additional holograms, one at a lower speed and the other at a higher than critical speed were recorded to show the variation of the traveling wave position and amplitude with speed. Such changes in a 4D wave are shown in Figure 48.

From the off-resonance records, a stationary displacement wave of the shape A cos $n\theta$ can easily be seen. The location of the nodal diameter with respect to the static magnets at speeds below and above resonance indicates the lead and lag phase angles

Magnet

Nodal line

Magnet

Nodal line

Magnet

Nodal line

Before Resonance at 3640 RPM
Accelerometer Reading 0.049 V

At Resonance at 3647 RPM
Accelerometer Reading 0.072 V

After Resonance at 3652 RPM
Accelerometer Reading 0.043 V
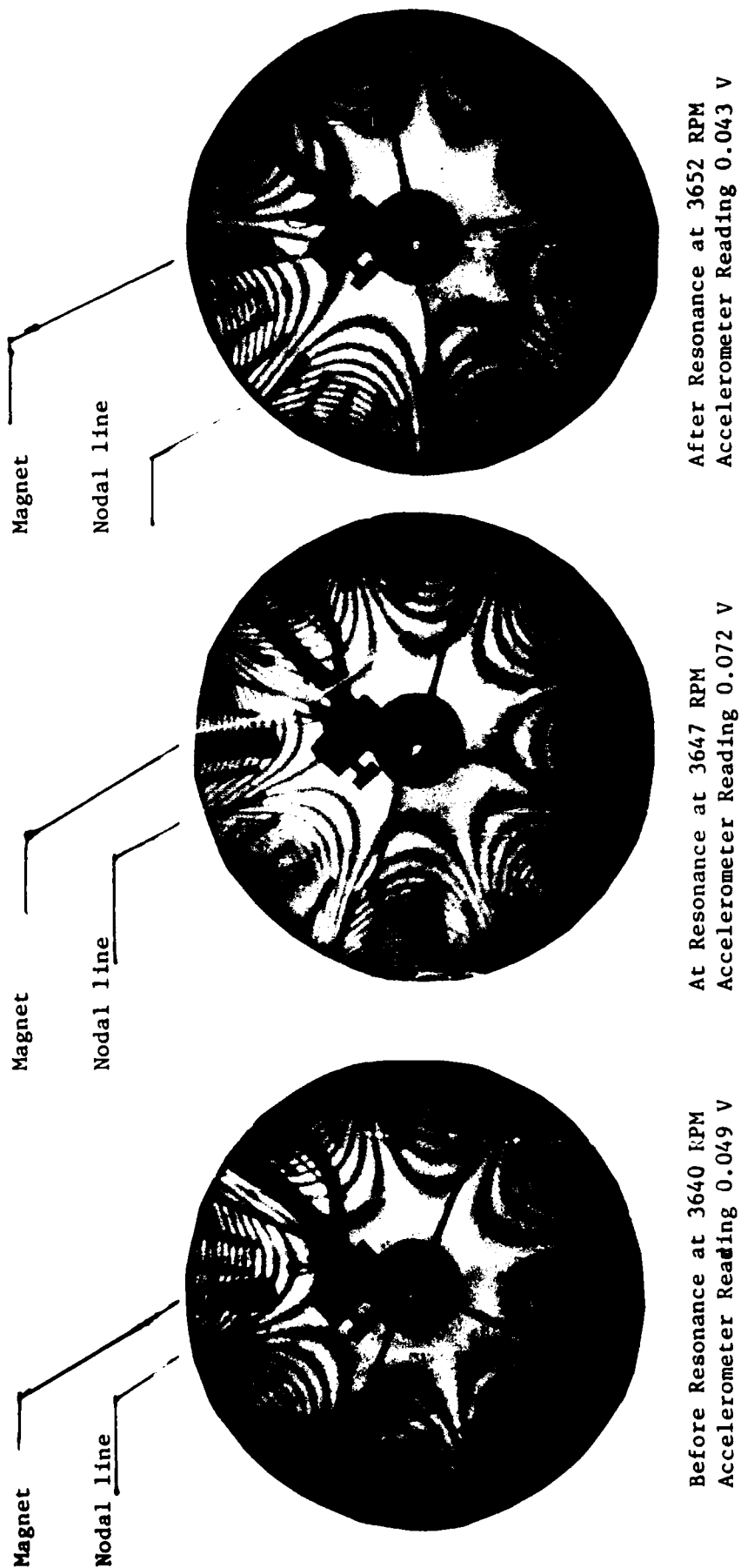
Figure 48. Traveling Wave Position At, Before, and After Resonance.

93

TABLE 13

TRC NSMS FOUR-SENSOR ANALYSIS RESULTS - FIRST TEST SERIES

	TEST CONFIGURATION				RESULTS			
Mux No.	Rotor Speed (rpm)	Excita- tion (E/O)	Magnet Gap (in.)	Sensor Spacing (deg)	Mode Order	Frequency (Hz)	Amplitude (mils p-p)	Phase Lag (deg)
2	3720	3	5/16	36.36.36	3	186.0	110	31
3					3	186.0	108	32
4					3	186.0	110	30
2	3720	3	5/16	36.36.36	3	186.0	110	31
3					3	186.0	112	
4					3	186.0	112	
2	3970	2	5/16	36.36.36	2	132.4	198	28
3					2	132.3	196	
4					2	132.4	200	
2	3970	2	5/16	36.36.36	2	132.3	196	29
3					2	132.4	196	
4					2	132.3	198	
2	3780	2	7/16	54.54.54	2	126.0	140	41
3					2	126.0	140	
4					2	126.0	160	
2	3780	2	7/16	54.54.54	2	126.0	130	41
3					2	126.0	138	
4					2	126.0	140	
2	3630	4	7/16	36.18.18	4	242.0	50	27
3					4	242.0	44	
4					4	242.0	50	
2	3630	4	7/16	38.18.18	4	242.0	50	27
3					4	242.0	50	
4					4	242.0	50	

94

TABLE 14

COMPARISON OF INTEGRAL ORDER TEST RESULTS - SECOND TEST SERIES

RUN NUMBER	TEST CONDITIONS SENSOR SPACING (deg)	ROTOR SPEED (rpm)	E/O - M/GAP EXCITATION (*-inch)	RELATIVE DISP FROM ACCEL	HOLOGRAM RESULTS CASE No	ENGINE ORDER	AMPLITUDE (mils p-p)	PHASE LAG (deg)	NSMS RESULTS ANALYSIS TYPE	ENGINE ORDER	FREQUENCY (Hz)	AMPLITUDE (mils p-p)	PHASE LAG (deg)
19.5-19.21	54,54,54	4000-4080	2-15/16	0.83	NH				SDOF	2	135.1 R	29	5)
19.2	54,54,54	4069	2-15/16	0.77	4/5	2	23-28/41-46	125/111	4-SENSOR	2	135.6 R	26-36	42
19.3	54,54,54	4063	2-15/16	0.65					4-SENSOR	ND	ND	ND	ND
19.4	54,54,54	4058	2-15/16	0.71	1	2	30-32	100	4-SENSOR	ND	ND	ND	ND
19.8	54,54,54	4048	2-15/16	0.68	2	2	26-30	28	4-SENSOR	ND	ND	ND	ND
19.17	54,54,54	4060	2-15/16	0.56	3	2	19-24	133	4-SENSOR	ND	ND	ND	ND
15.1	36,36,36	3642	3-5/8	1.00	14	3	48-50	67	4-SENSOR	3	182.1 R	30-50	100
15.2	36,36,36	3642	3-5/8	0.98	NH				4-SENSOR	3	182.1 R	30-50	93
15.3	36,36,36	3532	3-5/8	0.61	15	3	31-34	25	4-SENSOR	3	181.60/R	20-36	72
15.4	36,36,36	3649	3-5/8	0.58	NH				4-SENSOR	3	182.40/R	34-54	111
15.5	36,36,36	3646	3-5/8	0.81	16	3	48-52	79	4-SENSOR	3	182.30/R	34-52	109
16.1-16.15	36,36,36	3600-3660	3-3/4	0.62	6	3	24-26	31	SDOF	3	181.9 R	32	117
16.3	36,36,36	3625	3-3/4	0.40	7	3	29-31	65	4-SENSOR	3	181.30/R	8-21	67
16.6	36,36,36	3633	3-3/4	0.60	8	3	29-33	85	4-SENSOR	3	181.7 R	18-34	92
16.9	36,36,36	3637	3-3/4	0.60					4-SENSOR	3	181.90/R	20-36	98
107-11.16	36,18,18	3500-3800	4-3/4	0.32	NH	4			SDOF	4	242.8 R	28	108
12.1	36,18,18	3644	4-5/8	0.60	17	4	30-34	95	4-SENSOR	4	243.0 R	36-54	108
12.2	36,18,18	3636	4-5/8	0.37	18	4	25-29	46	4-SENSOR	ND	ND	ND	ND
12.3	36,18,18	3648	4-5/8	0.36	19	4	13-25	143	4-SENSOR	ND	ND	ND	ND
13.1-13.15	36,18,18	3500-3680	4-5/8	0.48	NH	4			SDOF	4	243.0 R	43	108
17.3	36,18,18	3642	4-9/16	0.47	9/10	4	29-36/25-31	98/94	4-SENSOR	4	242.8 R	34-48	118
18.1-16.16	36,18,18	3500-3700	4-9/16	0.47	NH	4			SDOF	4	242.7 R	47	100
18.4	36,18,18	3630	4-9/16	0.37	11	4	26-31	62	4-SENSOR	4	242.00/R	30	107
18.10	36,18,18	3643	4-9/16	0.28	12	4	13-23	150	4-SENSOR	4	242.90/R	24-34	140

ND - No Data, NH - No Hologram, R - Resonance, O/R - Off Resonance

95

TABLE 15

NSMS BLADE TIP DEFLECTION COMPARISON - FIRST TEST SERIES
(PEAK-TO-PEAK DEFLECTIONS IN MILS)

Mode	Gap (in)	Speed (rpm)	UDRI	UTRC
2D	5/16	3790	No Data	198-200
2D	7/16	3780	176 ± 5	130-160
3D	5/16	3732	160 ± 4	No Data
3D	7/16	3720	110 ± 2	110-112
4D	7/16	3630	62 ± 2	44-50

TABLE 16

NSMS AND LASER INTERFEROMETRY BLADE TIP DEFLECTION COMPARISONS:
SECOND TEST SERIES

(Peak-to-Peak Deflections in mils)

Mode	Gap (in)	Speed (rpm)	UTRC Interfe-rometry	UTRC NSMS	UDRI Interfe-rometry	UDRI NSMS
2D	15/16	4063	23-28			
			30-32	No Data	24.8	51.7
	15/16		26-30		31.3	30.2
3D	5/8	3642	48-50	30-50		
	5/8		31-34	20-36	50.4	44.5
	5/8		48-52	34-54		
3D	3/4	3633	24-26	32		
			29-31	18-34	29.9	27.8
			29-33	20-36		
4D	5/8	3644	30-34	36-54		22.4
			25-29	No Data	33.2	
			13-25	No Data		
4D	9/16	3642	29-36	34-38	34.9	27.6
			25-31			

97

of the force-wave relative to the response wave. When the disk
is in resonance, the peak of the response wave is at $\pi/2$ relative
to the excitation force.

Near resonance amplitude changes of the traveling wave with
speed are illustrated in Figure 49. The wave build-up and
decline effects are evident from the varying number of fringes in
holographic mode shapes when the disk is below, at, and above the
resonant speed. Fewer fringes are present in holograms made at
the lower and upper half-power points of the resonance curve.
Maximum number of fringes at the resonant speed of 4,058 rpm
indicates maximum dynamic displacement for the disk. Also,
maximum deflection occurred when the traveling wave node
coincided with the excitation force location. The holographic
mode shape records in Figures 46 through 49 seem to indicate the
opposite, but that is because the double pulse holographic
technique records nodes of the actual mode as antinodes in the
image and vice versa.

Fringe number differences in different sectors of a specific
modal pattern are attributed to imperfection in the disk, that
is, mistuning. Such asymmetric displacement patterns for the 2,
3, and 4D modes were recorded in our experiments. A typical
modal asymmetric fringe pattern for 4D is shown in Figure 50.
The offset effect seen in recorded mode shapes was due to the
back and forth switching between two closely spaced resonant
frequencies for different sectors of the disk. This is likely
due to the variable stiffness and mass distributions of the
instrumentation system installed to this very light disk.

7.6 NONLINEAR DYNAMICS

Tests were also conducted with various magnet spacings
ranging from 1/2 to 1 inch to study the effect of excitation
force on the dynamic response of the bladed disk. Amplitude
changes due to speed increments in steps of 1 rpm on either side
of resonance were recorded for the 2D, 3D, and 4D modes. A phase
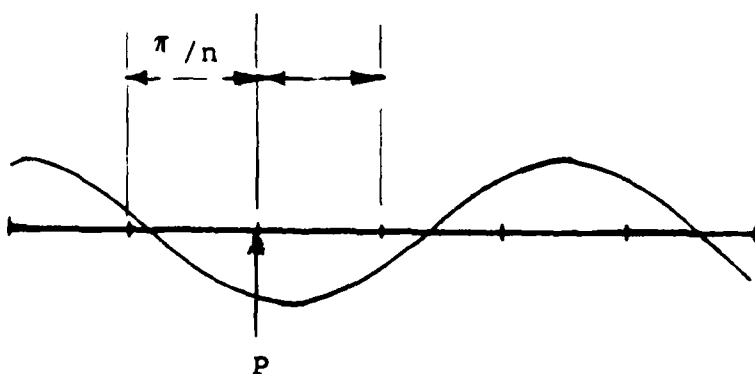change of nearly 90 degrees as the disk passed through resonance
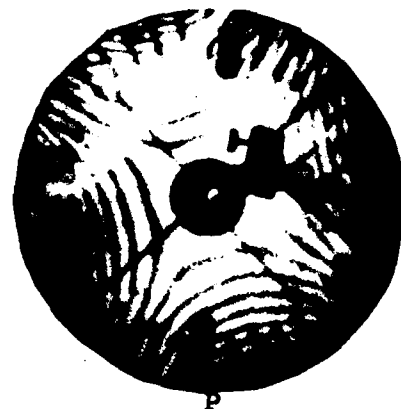
$\omega < \Omega$
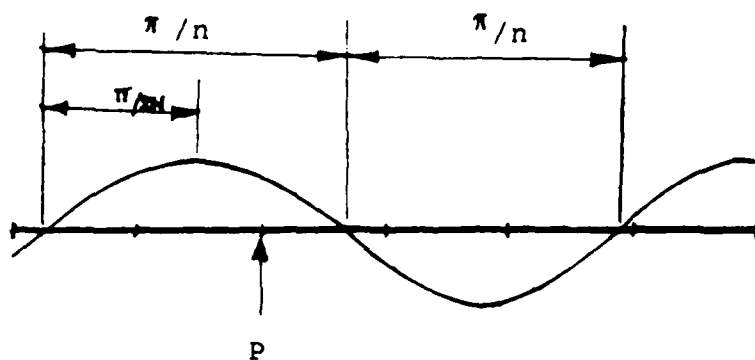
4,056 rpm, Amp = 12.5 fringes
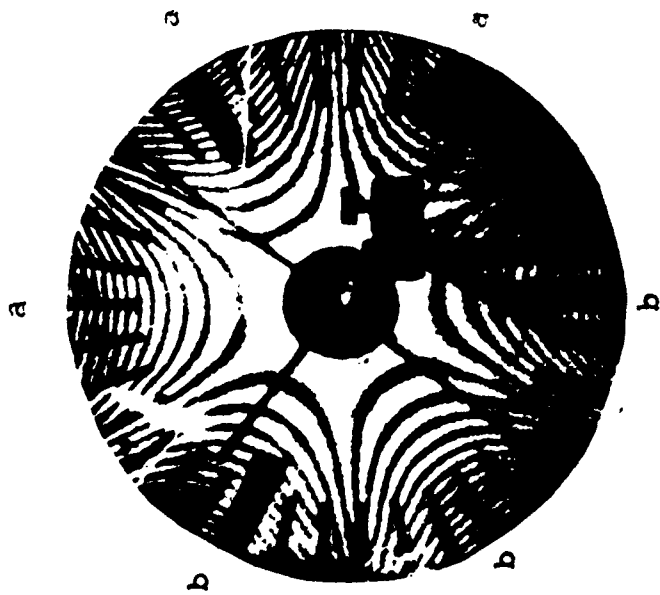
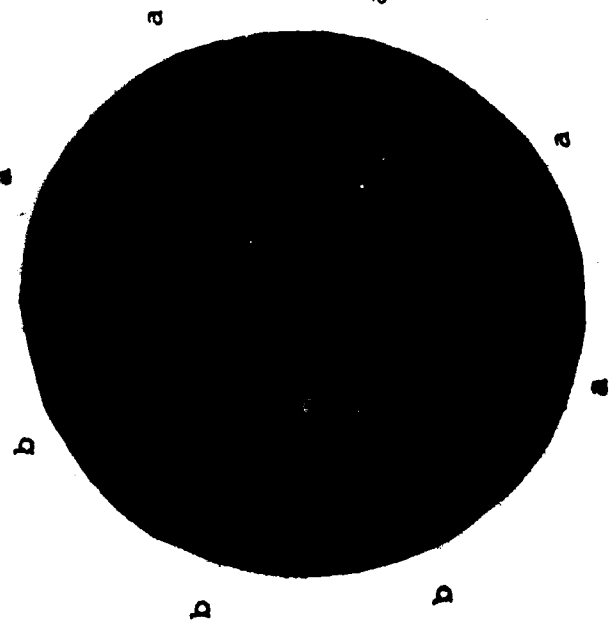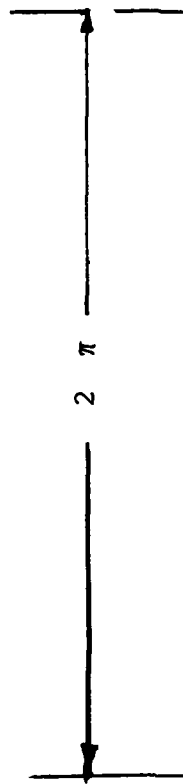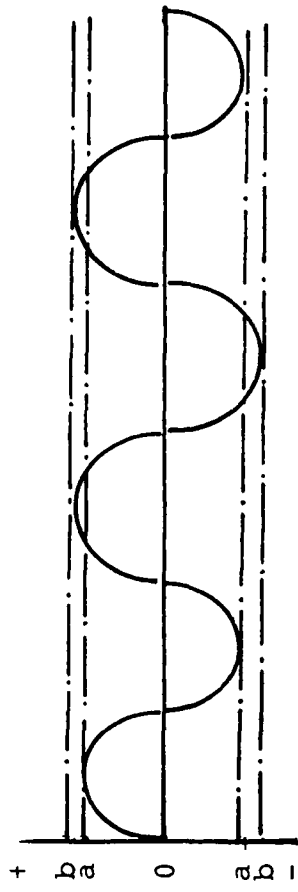$\omega = \Omega$
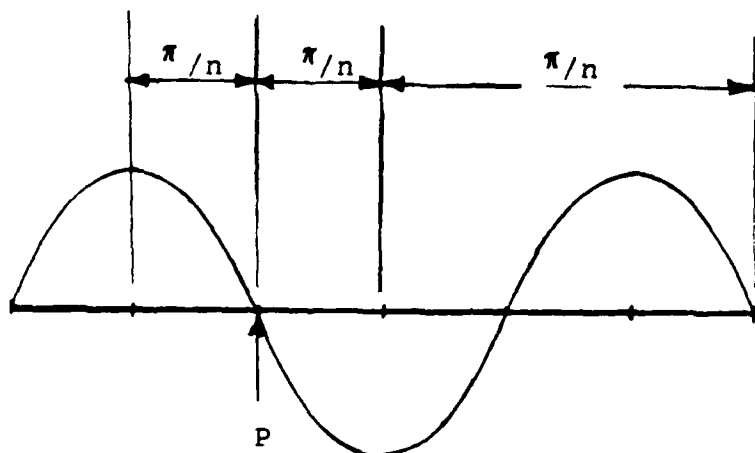
4,058 rpm, Amp = 14 fringes

$\omega > \Omega$

4,060 rpm, Amp = 9 fringes

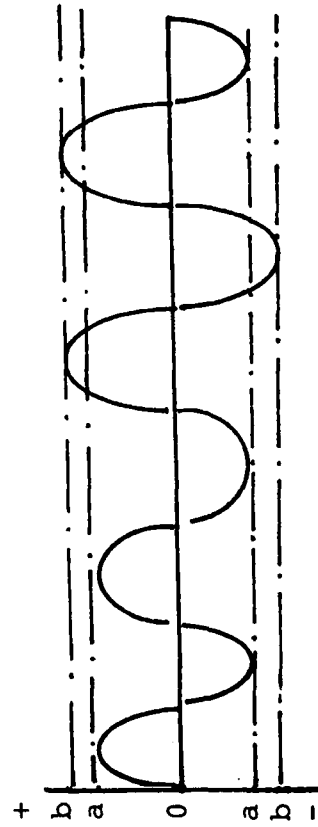Figure 49. Resonant Wave Build-Up with Speed.

99

Figure 50. Modal Asymmetry Due to Disk Imperfection.

is evident from Figures 51 and 52. A smooth phase change did not occur when the magnets were positioned closer than 9/16 inch. This was attributed to the nonlinearity of the disk. The nonlinear, hard spring response characteristic of the rotating bladed disk is presented in Figure 53. A sudden collapse of the amplitude of vibration and inability to follow the resonance curve are illustrated in Figure 54.
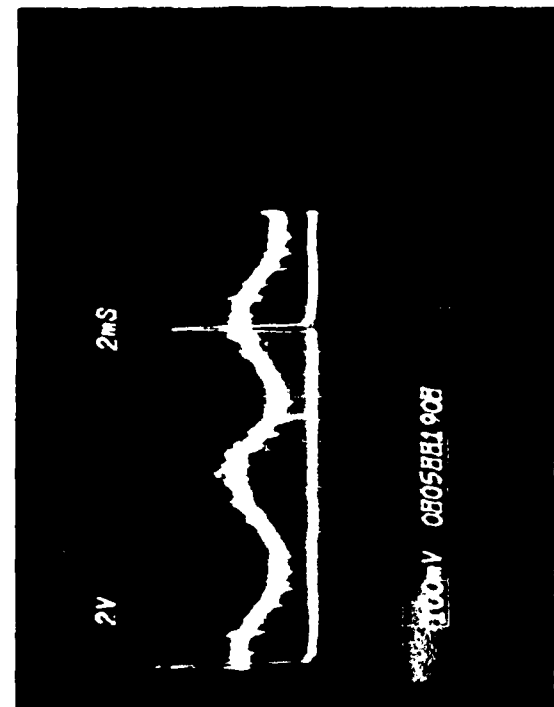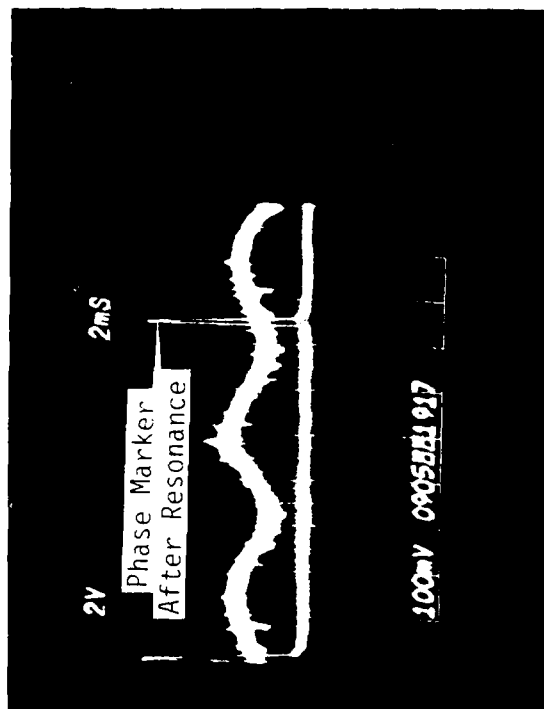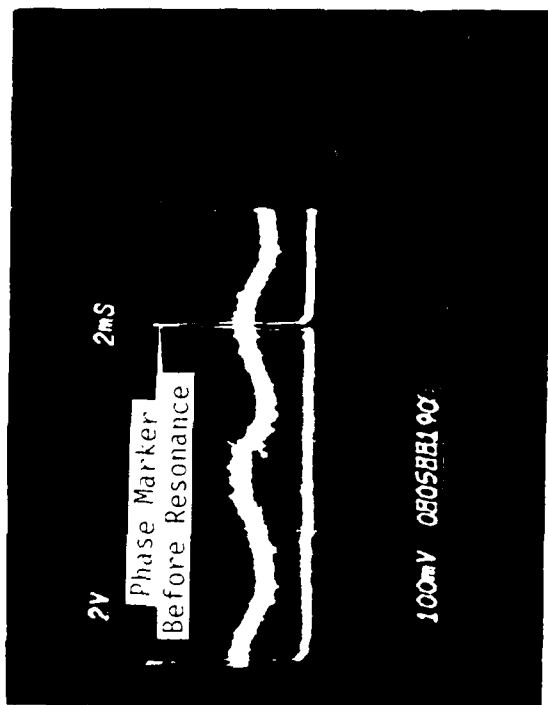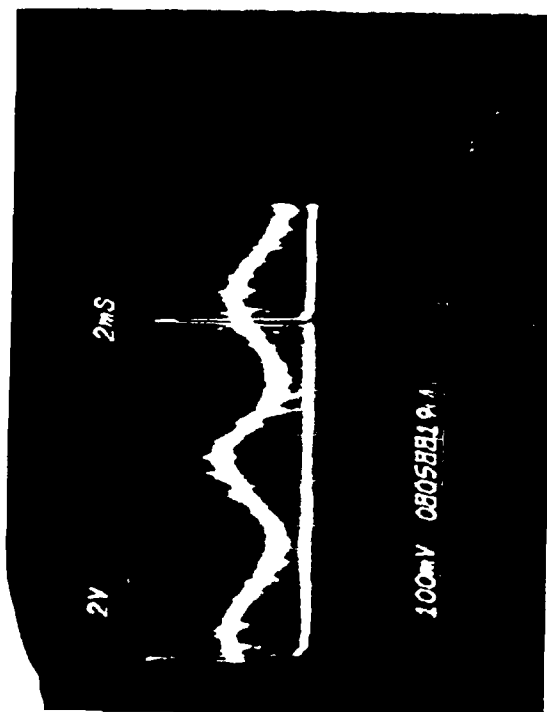
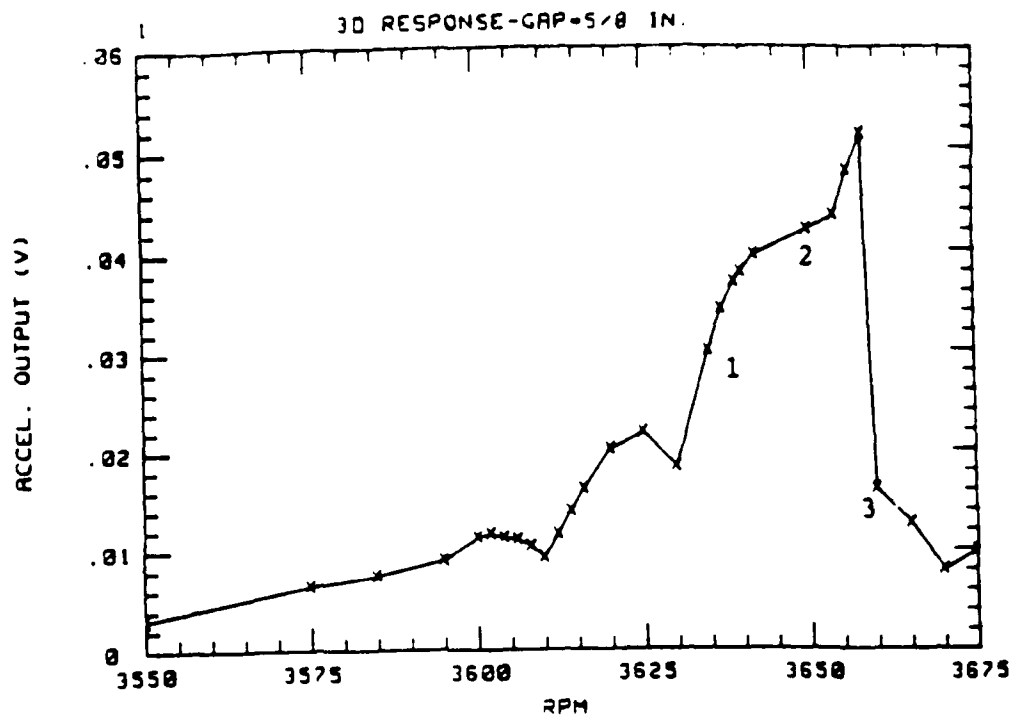Figure 51.   Phase Transition Diagram for 2D Mode.

3D RESPONSE-GAP=5/8 IN.

1. 3,635 rpm, Before Resonance
   Phase Marker on Trough of
   the Response Signal.

2. 3,650 rpm, Near Resonance
   Phase Marker Midway Between
   Trough and Crest of the
   Response Signal.
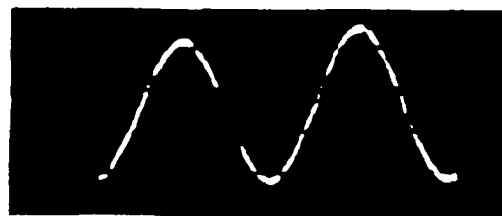
3. 3,660 rpm, After Resonance
   Phase Marker Near the
   Crest of the Response
   Signal.

Figure 52.   Phase Transition Diagram for 3D Mode.

103

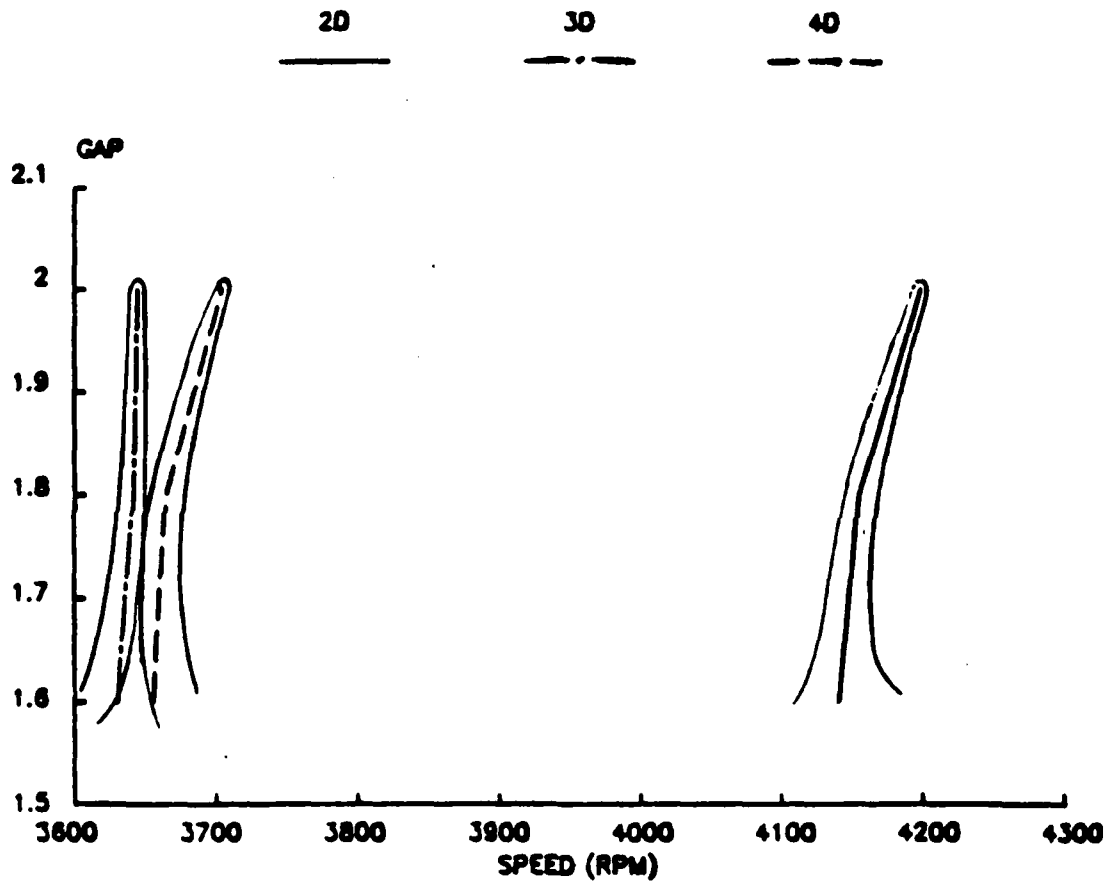# NONLINEAR DISK RESPONSE CHARACTERISTICS

Figure 53. Hard-Spring Characteristics of Rotating
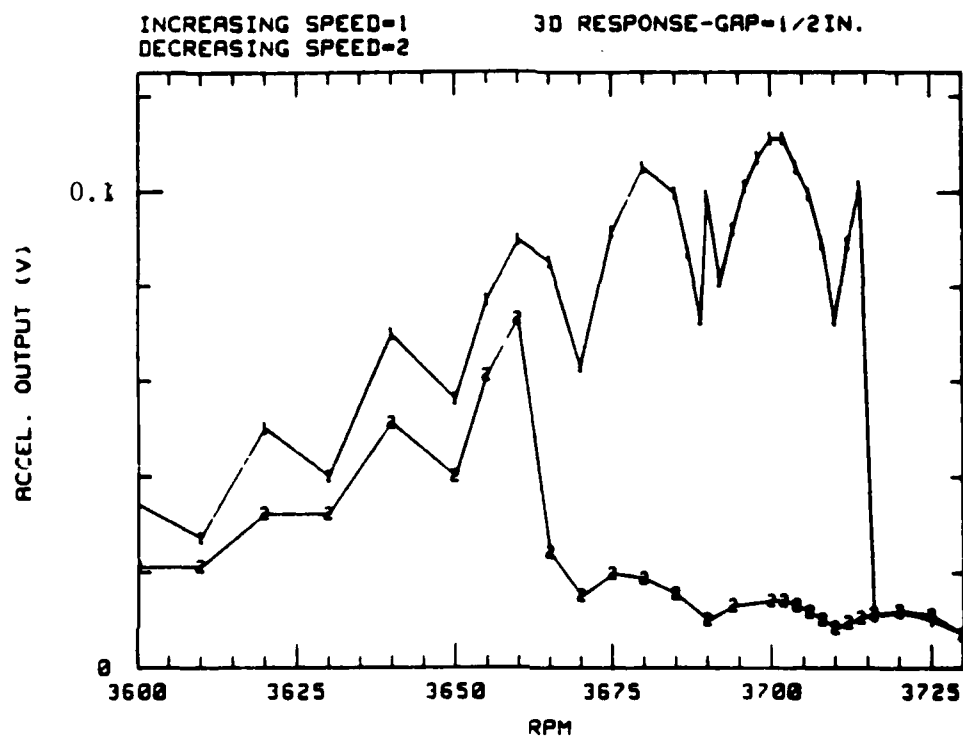Flexible Disk Under Static Force Field.

Figure 54. Amplitude Collapse of Nonlinear Disk.

105

SECTION 8
CONCLUSIONS AND RECOMMENDATIONS

A 38 bladed disk with modal frequencies within the frequency range, 100-250 Hz was designed and tested for resonant response in the 2, 3, and 4 diametral modes. Stationary static force fields due to a system of permanent magnets were used to excite backward traveling waves integral with disk speed. Excitation magnets were configured to selectively excite a specific mode.

Critical speed response could be sustained for speed variations of 100-200 rpm in the range 3,500 to 4,100 rpm. This effect was believed due to mistuning of the disk.

AEDC four probe, UDRI three probe and double pulse laser interferometric methods were concurrently used to measure blade-tip deflections of the resonating disk. Three test series - two series with AEDC probes at equal angular spacings and one series with probes at unequal positions were conducted. Amplitude and phase changes of the spinning disk in a critical speed range were monitored by disk-mounted accelerometers. Qualitative phase changes near disk resonance conditions were defined and correlated with excitation force locations. Data snowed negligible phase lead or lag angles due to disk modal damping.

ISRL NSMS data were processed off-line. Software constructed time series were speed corrected and analyzed for displacement spectral components. Vibrations in time and frequency domains, in some test cases produced low level spectral components of other frequencies signifying noise in the optical data. This was attributed to mistuning effects since responses of several blades were used to make up the time series data. UDRI NSMS analysis was performed overnight on Air Force mainframe computers, and the results at hand often provided clues to select appropriate excitation magnet and laser pulse settings for the next test.

106

For double pulse interferometry records, pulse separation times were selected to provide resolvable fringe numbers for the recorded modal patterns. Correlation between the nodal positions with respect to excitation force and also between vibration amplitude and critical frequency were established for the disk during its critical response. Interferometry data analysis yielded vibration amplitudes that compared well to NSMS values for most test cases. UDRI and UTRC fringe analysis showed good agreement. Mode shapes showed circumferential asymmetry of response (mistuning) in the disk.

The present investigation concentrated on the determination of one mode (cosine or sine wave) response of a bladed disk. It is recommended that the twin mode critical speed response investigation of a rotating disk be investigated so that the disk modal interpretation could be applicable to practical turbine disks. As the present experiments were conducted on the disk within a specific frequency range, this constraint resulted in the use of a very flexible disk and nonlinear behavior was easily triggered. A stiff disk would be more stable over its entire critical speed range. Stability characteristics of twin modes of vibrating disk under a stationary system of forces are worth pursuing to define disk critical speeds. Modal definition when the disk is near its resonance-speeds should be investigated in detail. Investigation on a realistic disk having both axial and tangential blade motions is needed to evaluate the measurement capability of NSMS methods in these circumstances. The extension of the NSMS test methods to actual compressor and turbine disks would be very desirable.

REFERENCES

1. Tobias, S. A., and Arnold, R. N., "The Influence of Dynamical Imperfection on the Vibration of Rotating Disks," Proceedings of the Institution of Mechanical Engineers, Vol. 171, 1957, pp. 669-690.

2. Ewins, D. J., "The Effects of Detuning Upon the Forced Vibrations of Bladed Disks," Journal of Sound and Vibration, Vol. 9, No. 1, 1969, pp. 65-79.

3. Stetson, K. A., "The Use of an Image Derotator in Hologram Interferometry and Speckle Photography of Rotating Objects," Experimental Mechanics, Vol. 18, 1978, pp. 66-73.

4. MacBain, J. C., Horner, J. E., Stange, W. A., and Ogg, J. S., "Vibration Analysis of a Spinning Disk Using Image-Derotated Holographic Interferometry," Experimental Mechanics, Vol. 19, 1979, pp. 17-22.

5. Stange, W. A., and MacBain, J. C., "An Investigation of Dual Mode Phenomena in a Mistuned Bladed Disk," ASME Paper No. 81-DET-133, ASME Design Engineering Technical Conference, Hartford, CT, September 20-23, 1981.

6. Hohenberg,, Rudolph, "Detection and Study of Compressor Blade Vibration," Experimental Mechanics, June 1967, pp. 19A-24A.

7. Zablofskiy, I.Ye, et al., "Contactless Measuring of Vibrations in the Rotor Blades of Turbines," Technical Translation FTD-4T-23-673-74, April 1974.

8. Nieberding , W. C., and Pollack, J. L., "Optical Detection of Blade Flutter," NASA Technical Memorandum 73573, March 1977.

9. McCarty, P. E., and Thompson, Jr., J. W., "Development of a Noninterference Technique for Measurement of Turbine Engine Compressor Blade Stress," Arnold Engineering Development Center Technical Report, AEDC-TR-79-78, June 1980.

10. Roth, H., "Vibration Measurements on Turbomachine Rotor Blades with Optical Probes," Proc. The Joint Fluids Engineering Gas Turbine Conference and Products Show, New Orleans, LA, March 10-13, 1980.

11. Endoh, M., et al., "Noncontact Technique for Measurement of Rotating Blades," Proc. 9th Annual Meeting of the Gas Turbine Society of Japan, 1981, pp. 111-116.

12. Chi, R. M., et al., "Conceptual Design of a Noninterference Stress Measurement System for Gas Turbine Engines," AEDC-TR-84-12, May 1984.

13. Jones, H. T., "Development of a Noninterference Technique for Measuring Engine Rotor Blade Stress, AIAA Paper, 85-1472, AIAA/SAE/ASME/ASEE 21st Joint Propulsion Conference, Monterey, CA, July 8-10, 1985.

14. Jones, H. T., "Performance Evaluation of a Noninterference Technique for Measuring Integral Order Vibrations of Turbine Engine Compressor Blades," AEDC Report, AEDC-TR-84-21, June 1984.

15. Held. T. W., "Data Analysis Guide for the Noncontacting Blade Deflection Measurement System," UDR-TR-89-31, March 1989 (to be reissued as an AFWAL TR).